Union College
Union | Digital Works

Honors Theses   Student Work

6-2017

Provenance of and Age of Granitoid and Sandstone Clasts in Conglomerates of the Paleocene to Upper Cretaceous Yakutat Group, Russell Fjord, Alaska

Alexander Dolcimascolo
Union College - Schenectady, NY

Follow this and additional works at: https://digitalworks.union.edu/theses
Part of the Geology Commons, and the Paleobiology Commons

Recommended Citation

Provenance of and Age of Granitoid and Sandstone Clasts in Conglomerates of
the Paleocene to Upper Cretaceous Yakutat Group, Russell Fjord, Alaska

by

Alexander Ryan Dolcimascolo

****

ABSTRACT

DOLCIMASCOLO, ALEXANDER RYAN. Provenance of and Age of Granitoid and Sandstone Clasts in Conglomerates of the Paleocene to Upper Cretaceous Yakutat Group, Russell Fjord, Alaska. Department of Geology, Union College, Schenectady, New York, April 2017.

The Paleocene to Upper Cretaceous Yakutat Group consists of a flysch facies. A conglomerate occurs in two places in Russell Fjord, and the composition and age of clasts bears on tectonic reconstructions. One site (#23) occurs in what is mapped as flysch and one in the mélange (#25), but the conglomerates are essentially identical. They contain clasts of sandstone, greenstone, limestone, marble, chert, and plutonic rocks that are clast supported, and interbedded with sandstones that contain coalified plant fragments. The maximum depositional age (MDA) of the U/Pb-dated zircons from the sandstone is 65.9 ± 1.8 Ma and 65.6 ± 2.2 Ma for the two samples, indicating deposition was Maastrichtian or younger. Grain-age distributions for these two samples yield populations at 69-74 Ma, 92-94 Ma,157-183 Ma, 1365 Ma, and 1710 Ma. The Jurassic population, which is subordinate, may be resolved into component populations at 154 Ma and 182 Ma. Clasts of sandstones and plutonic rocks were dated and analyzed. A well-rounded sandstone clast from the conglomerate at site #25 was dated and has an MDA of 71.7 ± 2.4 Ma, and the overall grain-age distribution is identical to sandstone elsewhere in the mélange. The similarity in MDAs and lithology of the sandstone clast and host mélange sandstone suggests that parts of the mélange may have been reworked. Three plutonic clasts from site #23 were analyzed for geochemistry in addition to two plutonic samples from tectonic slices (knockers) in the mélange. Based upon the geochemistry, the clasts are granite, trondhjemite, and tonalite, and both knockers are tonalite, and all plot as volcanic arc granites on discrimination diagrams. Two clasts and both knockers were U/Pb zircon dated. One clast has a date of 167.2 ± 2.3 Ma and the other has two zircon populations with modes at 156.2 ± 2.7 Ma and 179.5 ± 2.6 Ma. The bimodal age distribution is unexplained, but might be due to lead loss, mixing magma, or contamination. The granitic knockers are tectonic slices that have U/Pb dates of 174.9 ± 2.0 Ma and 173.8 ± 2.1 Ma. εHf(t) values on the 167 Ma clast and 175 Ma knocker range from +10.0 to +14.3 and +9.8 to +12.0, respectively. Thus, these data suggest that the source region for the granitoid clast and knocker are isotopically homogenous and juvenile. Potential provenances include the Jurassic Bonanza and Talkeetna arcs on Vancouver Island and Wrangellia, respectively. Geochemistry analysis on the plutonic rocks also show a correlation to fragments of similar lithology and age in the Western Mélange Belt (WA).

DEDICATION

I would like to dedicate this thesis to my family for all their support and guidance towards my personal development. They have always believed in me and encouraged me to do what I love and to follow my passions in science and geology. I would also like to thank the faculty of the Geology Department for their dedication to my education and giving me the opportunity to be a part of a research team as an undergraduate, especially John Garver, my research advisor.

ACKNOWLEDGEMENTS

TABLE OF CONTENTS

LIST OF FIGURES

LIST OF APPENDICES

INTRODUCTION

The southern margin of Alaska is the site of subduction between the Pacific and North American Plates and the modern setting is built on a collage of accreted terranes (Garver and Davidson, 2015). The Border Ranges fault separates this region's most distinctive terrane, the Insular superterrane, which consists of the Peninsular, Wrangellia, and Alexander terranes from one of the thickest accretionary complexes in the world, the Chugach and Prince William (CPW) composite terrane (Cowan et al., 1997; Plafker et al., 1994; Garver and Davidson, 2015). The CPW terrane is mainly Upper Cretaceous (Valdez Group) to Paleocene-Eocene (Orca Group) and extends from Border Ranges fault as the northern boundary to Baranof Island as the southern boundary (Plafker et al., 1994). Outboard of the CPW in the southeast lies a collision zone in which the Yakutat terrane is actively subducting underneath the CPW (Plafker et al., 1994). The nature of part of the Yakutat Group is the subject of this thesis.

The Yakutat microplate currently has two basement rock units: 1) Eocene basalts; and 2) Cretaceous flysch and mélange. It is hypothesized that the basement configuration may be due to a collision and juxtaposition of the two units at around 50 Ma (Worthington et al., 2012). After the collision, the basement units were blanketed by Tertiary sediments (Kultieth and Poul Creek formations), which are an overlap and thus, uniting the basement units in a single composite terrane (Plafker et al., 1994).

The Yakutat Bay and Russell Fjord area geology consists of three distinctive fault-bounded blocks, one of which is clearly related to the Yakutat terrane. The Outer block (block one) sits to the west of the Boundary fault, mainly in Yakutat Bay and these rocks are Campanian and Maastrichtian and mélange of the Yakutat Group (Plafker et al., 1994). The mélange in the Yakutat Group is inferred to be correlated with the mélange of the Chugach terrane, which is mid Cretaceous and older (Plafker et al., 1994). The lithology of the mélange assemblage typically consists of disrupted and variably metamorphosed broken formation with inclusions or knockers of basalts, metavolcanic rocks, chert, greenish-gray greywacke, pebble-cobble conglomerate, green tuff and argillite, and carbonates (Plafker et al., 1994). The Mélange has inclusions or blocks that are interpreted to be related to the units in Wrangellia and Vancouver Island (Plafker et al., 1994), but no quantitative dating has been done to test this hypothesis.

Next to the Yakutat Mélange is the Boundary Block (Block Two), which lies east of the Boundary fault and west of the Fairweather-Queen Charlotte fault. The facies in this block consist of the schist of Nunatak Fjord that are dominated by meta turbidites intruded by granites, granodiorites, and tonalities (Sisson et al., 2003).

East of the Boundary Block (Block Three), which includes rocks that lie east of the Fairweather-Queen Charlotte fault (towards Wrangellia) and together form a sliver of high temperature/low pressure metamorphic rocks of the Chugach Metamorphic Complex (CMC). These rocks were metamorphosed and partially melted around 15-20 km where andalusite is stable in an abnormally high geothermal gradient (Plafker et al., 1994). Metasediments (turbidites) of Block Three were deposited at 54 to 51 Ma (Gasser et al., 2012) and the plutonic rocks have an affinity with the Sanak-Baranof Plutons, which occur to the southeast and to the west (Plafker et al., 1994).

Rocks of Wrangellia (Block Four) lay to the north and east of the Border Ranges fault system (Plafker et al., 1994). The Wrangellia composite terrane is considered to be part of the backstop of the Mesozoic accretionary complex (Wilson et al., 2005) (Figure 1). These rocks primarily consist of Triassic carbonate rocks above greenstone, and volcanogenic sandstone (Plafker et al., 1994). Wrangellia has a record of three magmatic-arc assemblages: (1) the latest Triassic and Early Jurassic Talkeetna arc of the Peninsular terrane; (2) a belt of calc-alkalic plutonic rocks of Middle and Late Jurassic age that include the Late Jurassic Chitina arc; and (3) the Late Jurassic and Early Cretaceous Chisana arc (Sisson et al., 2003). The Wrangellia block is important to understand because the history of the arc magmatism in Wrangellia provides insight into the source of clasts in adjacent units, here the Yakutat Mélange.

Previous work by Garver and Davidson (2015) hypothesize that according to detrital Precambrian Zircon grains from flysch facies, the southern extent of the CPW terrane has an affinity to a southern Laurentia source (Mojave Breach), which may also include the Yakutat Group. It is suggested that this translation to Alaska happened between 75 and 40 Ma (Garver and Davidson, 2015). This idea of northward translation is also supported by paleomagnetic data suggesting that the Wrangellia composite terrane was 3000 km south at 90 Ma and the most outboard unit of Wrangellia is the CPW (Cowan et al., 1997). The relationship between flysch of Wrangellia and CPW may not correlate before the Eocene and has a separate translation history (Garver and Davidson, 2015). This study further investigates the translation history along the western margin by focusing on the Yakutat Group, which is potentially distinct from the CPW and Wrangellia Composite Terrane (Garver and Davidson, 2015).
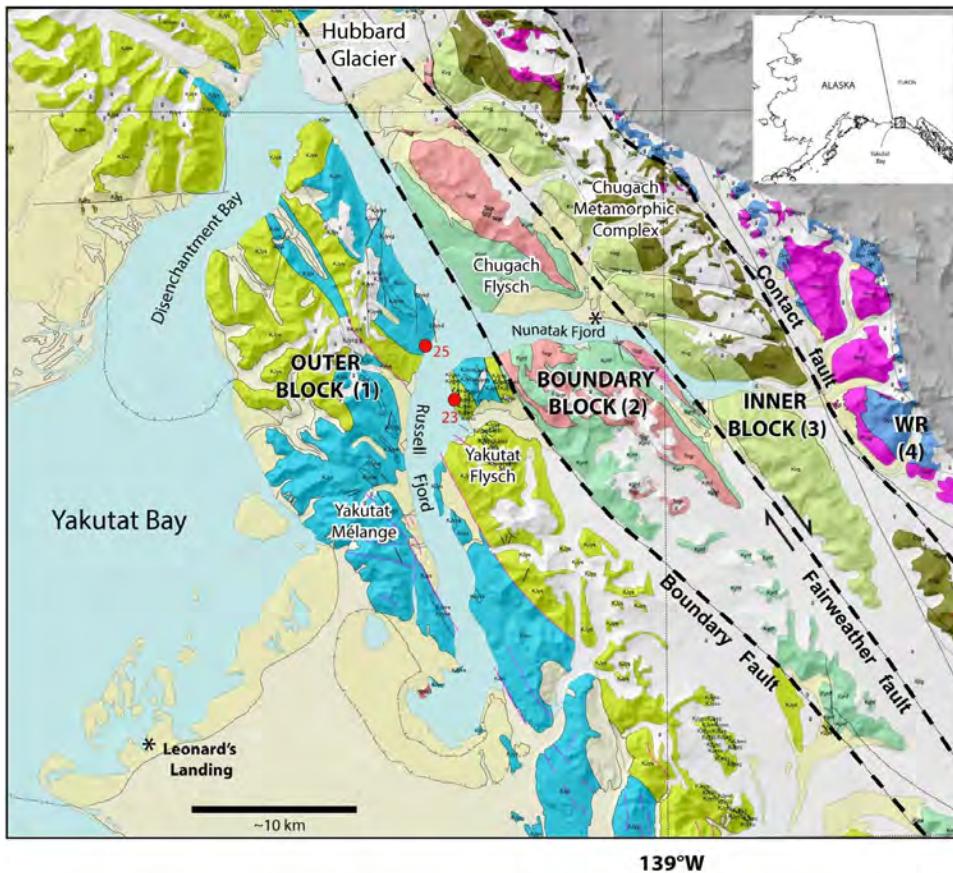
Figure 1: *Map of study area in southern Alaska showing sites RF16-23 and RF16-25. Spike Camp where most time was spent is shown by an astrix (* in Nunatak Fjord). Map modified from Wilson et al., 2005).*

Focus of Study and Details of Sample Sites

Our field team consists of John Garver (Union College), Julie Sophis (Union College), Cameron Davidson (Carleton College), Erin Arntson (Carleton College), and Eva Enkelmann (University of Cincinnati). Several projects emerged during the field sampling. Specifically, J. Sophis is focused on the provenance of the mélange sandstone units in the outer block (Block One), H. Olson examined the ages of flysch facies, including the schist of Nunatak Fjord, in the Boundary Block (Block Two) to compare the Boundary Block to the outer block (Block one), E. Arntson has studied the age and geochemistry of two plutons from a petrologic prospective in the Boundary Block (Block 2).

This project is focused on the source of conglomerates in the outer block (1) that are associated with the flysch, but also clearly mixed in the mélange. Site RF16-23 is located to the north of Seal Cove on the east side of Russell Fjord. This site is the location of a conglomerates and interbedded turbidites within the Yakutat Group flysch facies (Figure 2) and the conglomerates

have 5-50 cm clasts that are generally well-rounded, clast-supported, and have well organized. The cobbles have a variety of lithlogies including limestones, sandstones, greenstones, chert, and greenish porphyritic volcanics. RF16-23b.1-16 consists of 16 separate feldspar-rich granitoid clasts within the conglomerate, RF16-23c.1-8 consists of eight limestone clasts within the conglomerate, and RF16-23d represents one sandstone clast within the conglomerate.

Site RF16-25 is located on the west side of Russell Fjord across from the entrance of Nunatak Fjord and consists of a similar conglomerate. However, this conglomerate is a phacoid in what is mapped as the Yakutat Group mélange (Figure 3). This is a muscovite-rich sandstone and conglomerate contains similar lithologies as RF16-23. Three sandstone clasts were sampled from the conglomerate and three limestone clasts. The analyses of these clasts is important in understanding the nature of the source rocks, the timing of the tectonic processes in the outer block, and the age of the mélange in the Yakutat Block.

Figure 2: The conglomerate that will be analyzed and dated from site RF16-23 in the flysch facies of Russell Fjord, Yakutat, AK. The clasts studied in this project include granitoids (RF16-23b.1-16), limestones (R16-23c.1-8), and a sandstone (RF16-23d). The sandstone matrix is labeled RF16-23a.

The age of these conglomerates, the age of the clasts, and the chemistry of the clasts is important to determining the source region. These data will be used to evaluate hypotheses regarding movement of these rocks along the western margin of North America. Primarily, this study focuses on U/Pb and Lu/Hf dating on detrital zircons from individual clasts as well as geochemistry to investigate the origin of the sandstone. This thesis will outline the geology of

southeast Alaska, present the methodologies and data, and interpret these data in terms of potential regional tectonic reconstruction models.

Figure 3: The conglomerate phacoid that will be analyzed and dated from the mélange facies at site RF16-25 in Russell Fjord, Yakutat, AK. The clasts studied in this project include sandstones (RF16-25b.1-3) and limestones (RF16-25c.1-3). The sandstone matrix is labeled RF16-25a. Hammer for scale upper middle section.

GEOLOGIC BACKGROUND

Significance of the Mélange in the Yakutat Group

The Yakutat Group has a flysch facies and a mélange facies, and the age of the mélange is important for tectonic reconstruction. Originally, Plafker and others (1994) mapped the mélange facies as a unit older than the flysch facies, and this assignment suggests that the conglomerates would be older than Campanian-Maastrichtian because they occur as slices in this mélange.

Plafker and others (1994) originally mapped site RF16-23 as part of the **flysch facies** and RF16-25 as part of the **mélange facies** so an important question is how do the ages in these units compare because they are similar in the field. Plafker and Colleagues (1994) suggested that the mélange facies was mainly Lower Cretaceous and Upper Jurassic (~130-160 Ma) and was much older than the flysch facies (Campanian-Maastrichtian, based on ammonite fossils). This suggestion was very similar to previously published dates of the CPW mélange (Plafker et al.,

1994). The mélange was correlated to the Kelp Bay Group and McHugh Complex elsewhere in the CPW belt, while they correlated the flysch facies to the Orca Group and Valdez Group (Plafker et al., 1994, see Figure 7). Additional age data is crucial in determining the provenance of the conglomerate units through age correlations from other areas locally in Yakutat Bay or south along the edge of the Cordillera.

At site RF16-23 and RF16-25 (either side of Russell Fiord), a conglomerate unit is present, and both appear to be identical in the field despite being in different mapped units. It can be assumed the clasts are probably older than conglomerate deposition and clasts would get reworked into the mélange over time.

Does the Yakutat Group have an affinity with part of the Nanaimo Group, but have since been displaced to the North as suggested by Garver and Davidson, 2015? The Nanaimo Group sits on Wrangellia on southern and eastern Vancouver Island in British Columbia and the history of this block is currently controversial regarding transport (cf. Cowen et al., 1997 versus Mahoney et al., 1999). Paleomagnetic data from the Nanaimo suggests it was situated alongside California and northern Mexico (Housen and Beck, 1999).

Plafker et al., 1994 suggest that it is possible that the sandstone and granitoid clasts in the conglomerates within the Yakutat terrane came from the Kluane Arc of the Coast Plutonic Complex (CPC) (Plafker et al., 1994; and Haeussler et al., 2003). This complex is associated with Wrangellia and contains sandstone that is Upper Cretaceous in age that was intruded with plutons mainly between 100-90 Ma and 60-58 Ma (Haeussler et al., 2003).

Garver and Davidson (2015), suggest that there is a continuity of zircon grain ages across the CPW belt, but indicate that zircon from the Yakutat Group may be separate (Garver and Davidson, 2015). A northern Laurentia source as well as the Coast Plutonic Complex, has been suggested for the CPW rocks (Shumagins, Kodiak, Valdez, and Orca), but the Yakutut zircon are similar to a southern Laurentia source (Garver and Davidson, 2015). The positive εHf (t) values of Precambrian grains in the Yakutat Group are distinctive to southwestern Laurentia. Previous U/Pb Precambrian dates in the literature suggest that the Yakutat Group, which has age modes at around 1380 Ma, 1485 Ma, and 1722 Ma, relate to specific modes of anorogenic granites in southwestern Laurentia and also identical to the Yavapai-Mazatzal and Mojave provinces (1.6-1.8 Ga) and Granite-Rhyolite province (1.3-1.4 Ga) of southern Laurentia (Garver and Davidson, 2015). A possible source for the Yakutat Group may be the Sierran-Southern California-Peninsular Arc and it has been displaced ~3200 km (Garver and Davidson, 2015).

The mélange contains different sedimentary units and if younger than originally thought, it is possible that the conglomerates are related to the Orca Group, a conglomerate bearing unit of the CPW (Plafker et al., 1994). The Orca Group conglomerates in both the eastern and western Prince William Sound have similar sandstone clasts to the clasts in the mélange and flysch facies of Russell Fjord (Tysdal and Case, 1979).

Chugach and Prince William Terrane

The Chugach and the Prince William (CPW) terranes are suspect terranes in Alaska that are hypothesized to have formed in much more southern latitudes than its present position today in southern Alaska (Plafker et al., 1994; Cowan, 2003; Garver and Davidson, 2015). The CPW is a Maastrichtian to Paleocene accretionary complex that extends from the Shumagin Islands in the west to the Sitka Graywacke in the east (Garver and Davidson, 2015). Currently, the CPW is outboard of the Wrangellia composite terrane and inboard of the colliding Yakutat microplate on the southern Alaskan continental margin (Plafker et al., 1994; Enkelmann et al., 2010). The CPW terrane is primarily flysch that is Campanian to Eocene in age and is well-exposed for ~2200 km in southern Alaska (Plafker et al., 1994). Within the CPW terrane, the outboard flysch facies makes up >90% of the Chugach terrane and appears to be younger than the inboard mélange facies (Plafker et al., 1994).

The Yakutat terrane sedimentary cover rocks in southeastern Alaska and consists of Cretaceous clastic rocks and Paleogene oceanic crust (Plafker and other,1994). This terrane is fault bounded with the Boundary Fault to the south, the Queen Charlotte-Fairweather fault to the north, and the Contact Fault farther to the north separating this terrane from the Wrangellia terrane. Plafker and others (1994) suggest that along the northwest boundary the Yakutat terrane shallowly underthrusted the Prince William terrane (<15 km) for more than 200 km. Plafker and others (1994) has also mapped the area between the Queen Charlotte-Fairweather Fault and the Contact Fault as the Chugach Metamorphic Complex.

There is a continuity of crystallization ages of detrital zircon grains from CPW sandstones as well as consistencies in Hf isotopic ratios in Phanerozoic detrital zircons across the belt from the western localities, such as the Shumagin Islands, to the eastern localities, and the Yakutat terrane, suggesting that the Yakutat Group is part of the CPW terrane (Garver and Davidson, 2015). Garver and Davidson (2015) divide the Chugach terrane into many sub-terranes, identifying the Yakutat Group, despite being detached, as the southernmost fragment before the ~600 km strike-slip translation along the Queen Charlotte-Fairweather Fault during the late Tertiary.

The Contact fault is a fault that divides the Chugach and Prince William terranes between the inboard Upper Cretaceous Valdez Group (Chugach terrane) and the outboard Paleocene to Eocene Orca Group (Plafker et al., 1994). In the Kodiak area, there is the inboard Late Cretaceous Kodiak Formation on the northwest of the Contact fault, and the outboard Paleocene Ghost Rocks Formation on the southeast, (Plafker et al., 1994). The Ghost Rocks Formation is exposed in a belt about 10 km wide along the Kodiak Islands, and Sitkalidak Formations (Plafker et al., 1994).

The rocks of the Yakutat Group are distinctive and may have a unique provenance, and in fact may be a terrane independent from the CPW. Detrital zircons from sandstone samples of the CPW terrane indicate that the source region of the basement terrane comes from a volcanic arc lasting from the Late Cretaceous through the Paleocene with two distinctive histories (Garver and Davidson, 2015). The basement of the source produced Jura-Cretaceous zircons, with lesser Devonian and Precambrian grains (Garver and Davidson, 2015). However, differences in Precambrian zircon ages suggest two different source regions. To the west, in the Shumagin Islands, Kodiak Island, Prince William Sound, and Sitka all contain Precambrian zircons with isotopic compositions and ages that correlate to a northern Laurentian source (Precambrian grains mainly 1810 to 1870 Ma and 2520 to 2680 Ma), while zircon grains from rocks in the East (Yakutat) consist of isotopic compositions and ages that correlate to a southern Laurentian source (Precambrian grains approximately 1380 Ma, 1485 Ma, and 1722 Ma) that is potentially the Granite-Rhyolite province of the southwest United States (Garver and Davidson, 2015).

Paleomagnetic data suggest major northward translation of both the rocks in the east and west along the western margin of North America (Garver and Davidson, 2015). The rocks from the Resurrection Peninsula, which has an age of about 57 Ma, yield a mean paleolatitude value of 13 ± 9° south of its current location, indicating a northward translation of 1430 ± 990 km north (Bol et al., 1992). The paleolatitudes of the Ghost Rocks on Kodiak Island agree with this explanation of significant northward translation since 62 to 60 Ma (Plumley et al., 1982). The Kodiak rocks yield a mean paleolatitude value of 25 ± 7° which is about 2750 ± 770 km of northward translation (Plumley et al., 1982; Garver and Davidson, 2015). Paleolatitude analyses by Gallen (2008) and Housen and others (2008) also agree that the Ghost Rocks of Koidak Island underwent northward translation, indicating about 2500 ± 700 km of movement (Garver and Davidson, 2015). However, despite these studies, the idea of significant northward translation of these rocks is controversial due to the nature of structural corrections, primary remnant magnetization, possible remagnetization, and the movement on oceanic plates (Cowan, 2003 and Haeussler et al., 2003).

Displacement estimates based on detrital zircon comparisons suggest that the Sierran-Southern California-Peninsular Arc may have be a candidate source of the rocks in the Yakutat terrane (Garver and Davidson, 2015). One hypothesis by Garver and Davison (2015) suggests that the southern California arc collapsed along a narrow tectonic corridor as a result of the Mojave Breach, which allowed this southwestern source to spill out into the forearc basin, which may have included the Yakutat terrane. This hypothesis means that Yakutat flysch and the Franciscan Complex and may be similar. Thus, some of the flysch in the Yakutat flysch was deposited in the southwestern United States within close proximity to this source and then was transported up the western margin about 3200 km to Alaska since the Late Cretaceous (Garver and Davidson, 2015). To further support this hypothesis, the rocks within the Yakutat terrane need to be addressed. It is very possible that the Yakutat Block is independent of the CPW and has its own unique history.

Yakutat Terrane

The Yakutat microplate is a tectonic block that is currently colliding into the margin of southern Alaska. The terrane consists of basement units overlain by Tertiary stratigraphy. The basement units include: a extensive and thick Eocene basalt unit that is primarily offshore and underwater and a Cretaceous flysch/mélange unit of the Yakutat Group that is exposed in the Yakutat Bay area. The Eocene basalt unit maybe an oceanic plateau and may be related to rocks in the Pacific Northwest (Worthington et al., 2012). The Yakutat Group has zircons that may indicate transport as much as 3200 km (Garver and Davidson, 2015). The basement units are unconformably overlain by Tertiary strata. These cover strata consist of the Kulthieth, Poul Creek, Yakutaga Formations that blanketed the basement units after overthrusting at 50 Ma (Perry et al., 2009; Worthington et al., 2012).

Previous published U/Pb results suggest that the Yakutat Group mélange may be correlated to rocks of Baranof and Chicagof islands to the east, and the upper flysch facies in Yakutat Bay is correlative to the Sitka Graywacke to the east as well as the Valdez Group, Kodiak Formation, and Shumagin Formation to the west (Plafker et al., 1994; Garver and Davidson, 2015).

The thick sequence of Cenozoic clasitc sedimentary rocks has been displaced at least 600 km northwest along the Queen Charlotte-Fairweather transform fault during the late Cenozoic (Plafker et al., 1994). This block has also been underthrusted at a shallow depth (<15 km) on its northwest boundary for at least 200 km beneath the Prince William terrane (Plafker et al., 1994). The dextral oblique Transition fault system makes up the southern boundary of the Yakutat block, and the Pacific plate has underthrusted the terrane also at a low angle (Plafker et al., 1994).

Correlation of Yakutat and Chugach-Prince William Terranes

Many reconstructions have supported the hypothesis that the flysch/mélange of the Yakutat terrane may be the easternmost part of the CPW terrane (Plafker et al., 1994). However, the relationship of the Yakutat unit to the CPW, is poorly resolved. If the Yakutat terrane unit has any affinity to the CPW, the sandstones most likely share the same provenance. According to sandstone petrographic data in the eastern part of the Orca Group (same belt as CPW, but to the West), the composition of the sandstones are mainly volcanic lithic clasts. This composition would suggest that the provenance was a magmatic-arc, potentially from the Peninsular terrane, a Jurassic arc (Dumoulin, 1987). The Valdez and Orca Groups form a single flysch sequence that was a result of a Late Cretaceous and Paleogene source that was progressively unroofing (Dumoulin, 1987) and U/Pb dates on detrital zircon show that the source is dominated by a Late Cretaceous source area (Garver and Davidson, 2015).

The Orca Group, which has conglomerates, have young MDAs that are mainly between 61-55 Ma in eastern prince William Sound (Grimm, 2015) and 65 and 53 Ma in western Prince William Sound (Hilbert-Wolf, 2012). Conglomerates in the Orca Group contain about 50% of well-rounded pebbles, cobbles, and boulders of foreign felsic porphyry and locally granitic lithologies (Tysdal and Case, 1979). Orca conglomerates also include clasts of limestones, sandstones, volcanic rock fragments, (Tysdal and Case, 1979). Major minerals within these sandstone clasts are quartz, plagioclase and potassium feldspar grains as well as detrital biotite, detrital epidote, and detrital metamorphic rock fragments (Tysdal and Case, 1979). One hypothesis worth considering is a similar provenance between part of the Yakutat unit and the Orca Group so we need to evaluate the conglomerates in both the eastern and western Prince William Sound (Plafker et al., 1994).

Translation of the Chugach-Prince William Terrane

There has been a lot of controversy about the amount of tectonic translation processes of the terranes of southeastern Alaska (Cowan, 2003; Haussler et al., 2013; see Garver and Davidson, 2015 for summary). One hypothesis supports the idea of large northward translation, which is based on both geologic and paleomagnetic data (Cowan, 2003), while the second hypothesis does not (Haeussler et al., 2013). Other scenarios involve translation of terranes along with the mid-Cretaceous Coast Mountain orogen and that all have moved as much as ~3200 km relative to North America since 90 Ma (Cowan et al., 1997).

Cowan (2003) suggests that the CPW may have been translated ~1100 km since 50 Ma. This is known as the Baranof-Leech River hypothesis and is supported by paleomagnetic data from the

CPW belt. This hypothesis suggests that the Chugach terrane must be compatible with the tectonic event regarding a ridge intersecting a trench on the western margin of North America 50 Ma as well the plate motions allowing for northward coastwise displacement of the CPW terrane relative to North America (Cowan, 2003; Worthington et al., 2012). Cowan (2003), formulates this hypothesis by observing that the schists of the Chugach terrane located on Baranof Island possess a syn- kinematic, Buchan-type metamorphic mineral assemblages of andalusite, staurolite, and almandine garnet (Cowan, 2003). These rocks on Baranof island also yield a K/Ar date of 34.7 to 45.7 ± 1.4 Ma (Cowan, 2003). The K/Ar dates for the Leech River rocks are very similar being 36.7 ± 2.6 to 41.2 ± Ma and also closely resembles the very distinct metamorphism from the rocks on Baranof Island. Both units have twice-deformed biotite schist and phyllite derived from sandstone-mudstone flysch as well as chert and interbedded volcanic rocks (Cowan, 2003). Thus, Cowan (2003) suggests that Baranof Island was once contiguous with the Leech River complex. A strike-slip fault separates these two locations by 1100 km, however this concept of strike-slip translation supports the idea that they match and were once continuous (Cowan, 2003). However, the paleomagnetic data may have been reset and are therefore inaccurate and that there may be a plate missing in the reconstructions of northeastern Pacific Ocean in Paleocene-Eocene time (Haeussler et al., 2003).

This translation hypothesis relies on both the paleomagnetic data from outboard terranes as well as the petrology and geochronology of the different terranes. The paleomagnetic data of Paleocene rocks from the Resurrection ophiolite (57 Ma) demonstrate this significant northward translation as its paleomagnetic latitude indicates 13 ± 9° south of its current location (1430 ± 990 km) (Bol et al., 1992). The slightly older Ghost Rocks on Kodiak Island (60 to 62 Ma) indicate a mean value of 25 ± 7° of latitudinal displacement (~2750 ± 770 km) (Plumley et al., 1982; Garver and Davidson, 2015).

Translation of the Yakutat Microplate

The Yakutat Block is a composite continental and oceanic terrane is believed to have moved with the Pacific plate within the Pliocene and Quaternary and is currently colliding into the North American Plate in the Gulf of Alaska (Bruns, 1983; Worthington et al., 2012; Enkelmann et al., 2010, 2015). This block, which is currently situated in the northern Gulf of Alaska is fault-bounded between the Queen Charlotte-Fairweather Fault system (northeast), the Transition fault (south), and Chugach-Saint Elias thrust fault system (north), and the Kayak Island thrust faults (west); all of which are faults (Enkelmann et al., 2010, 2015). The Yakutat Block consists of two distinct basement elements: Eocene basalts (eYAK) and the Cretaceous Yakutat Group (kYAK), in addition to Tertiary *transport stratigraphy* that covers the basement units. This cover consists of Upper to Pleistocene strata of the Kulthieth, Poul Creek, Yakutaga Formations (Perry et al.,

2009). With respect to the question of origin of the Yakutat Block, these three units are distinct and need to be considered separately. These three elements, however, are complex and their origin have been debated for decades (Bruns, 1983; Davis and Plafker, 1986; Plafker et al., 1994; Perry et al., 2009; Garver and Davidson, 2015).

Bruns (1983) hypothesizes that the basaltic basement (eYAK) originated from the subduction of a plate boundary—the Kula-Farallon plate margin, located in California. In the Bruns (1983) model, the spreading center of the Kula-Farallon Plate (south option for this boundary) involved forming basaltic eruptions in a basin and that was adjacent to a more southerly spreading center. It is hypothesized that subduction of the northern spreading center occurred about 45 Ma, and during this process subduction cut off part of the western margin of North America, which subsequently connected to the Kula plate (Bruns, 1983). This event explains the initial northward movement of the Yakutat Block. Bruns (1983) hypothesized that a subduction origin for the Transition fault (southern margin of terrane) is unlikely as there is no observable accreted section along the fault, thus migration of the southern spreading center and subduction under North America about 25 Ma must have led to the truncation of the Yakutat block on the southern side and the Yakutat Block has since been moving northward with the Pacific plate towards Alaska. Keller and others (1984) observed the presence of warm-water microfossils in Yakutat strata (planktonic foraminifera) indicate that the Yakutat block was 30°±5° south of its present position in the early Eocene 50 Ma. However, these samples containing the microfossils were collected along the offshore shelf of the Yakutat Block, which makes the stratigraphic context of the samples unclear. Plafker and others (1994) suggest that the model of Keller and others (1984), which is based on limited foraminiferal data, is not compatible with other critical data (lithology, metamorphism of rocks, paleomagnetic data, etc) for the terrane source.

The Davis and Plafker (1986) hypothesis suggests that that the origin of the Yakutat Block relates to the Kula-Farallon plate boundary in the early to middle Eocene (about 48 Ma), however they suggest that the Kula triple junction was situated in the Pacific Northwest (north option for this boundary i.e. Breitsprecher et al., 2003). However, Bruns (1983) hypothesizes the southern option for this plate boundary, while Davis and Plafker (1986) argue for the northern option (i.e. Doubrovine and Tarduno, 2008). Their idea is based on the observation of trace element abundances in geochemically similar basalts, which occur in a linear belt from southern Vancouver Island to the southern Oregon Coast Range (Davis and Plafker, 1986). At 48 Ma, this model suggests that the Yakutat basalts were situated along the coast of either Washington or British Columbia and it was sliced off of and translated northward in the Neogene (Davis and Plafker, 1986). The northward translation occurred along the Queen Charlotte-Fairweather fault system (Davis and Plafker, 1986).

Later, Plafker and others (1994) suggest that the transport history of the Yakutat Block is shorter, and moved as part of the CPW. This idea is based on the offset of the Dangerous River fault, which is thought to be the offset equivalent of the Chatham Straight fault. The offset of the Dangerous River fault interpretation suggests that British Columbia or southeast Alaska is the original setting of the Yakutat Block and was the southern extension of the Chugach-Prince William (CPW) terrane. This hypothesis relies on a link between Yakutat and CPW. Similarities of the in age, lithology, structure, source directions, and plutons in the Yakutat mélange and flysch suggest correlation to the Kelp Bay Group and Sitka Graywacke in southeast Alaska. A hypothesis to explain its original position is that the Dangerous River fault zone in the Yakutat Block was a continuation of the Chatham Strait and therefore it has since experienced 600 km of dextral strike slip movement (Plafker et al., 1994).

The Plafker and others (1994) model has implications for the correlatives to the Yakutat mélange. They suggest that the exotic olistostromal blocks in the Yakutat Block mélange unit must have required a nearby Wrangellia terrane source in the Late Jurassic and Early Cretaceous, the assumed age of the mélange. This source may have been from the segment of Wrangellia currently exposed in the Queen Charlotte Islands and Vancouver Island (Plafker et al., 1994). There is no observed source terrane containing similar characteristics south of Vancouver Island, which suggests that the maximum relative motion of this exotic block is about 800 km (hypothesized to be the probable length of the exposed Wrangellia terrane that was exposed to the south of the Chatham Strait) (Plafker et al., 1994).

The Yakutat cover strata, mainly the Kultieth and Poul Creek fomations, may represent transport of the terrane past the BC Coast Ranges (Perry et al., 2009). Distinctive detrital zircon U/Pb and fission track analyses of the cover strata also suggest that the Yakutat Block could be related Coast Plutonic Complex (CPC) and the Kuiu-Etoilin belt, indicating that the Yakutat Block may have moved past central British Columbia in the Tertiary (Perry et al., 2009). These samples are from the Kulthieth Formation (Middle Eocene), the Poul Creek Formation (Lower Oligocene to Lower Miocene), and the Yakataga Formation (Miocene to Pleistocene); all of which cover basement units (Perry et al., 2009). The hypothesis that the CPC was the source to the Yakutat Block agrees with the depositional record of both the Kulthieth and Poul Creek formations. Both of these formations have a non-volcanic source terrain that crystallized at about 50 to 220 Ma and cooled from about 40 to 110 Ma (Perry et al., 2009). Therefore, this cooling process can most likely be correlated to the plutons of the northern CPC and Kuiu-Etoilin belt (Perry et al., 2009). The overall lack of volcanic zircons suggest that the Yakutat Block was in a northern position since the Late Eocene because very few volcanic rocks exist north of the Cascades. Although the

zircon data from the cover strata (Perry et al., 2009) suggest a northern setting, this hypothesis does not rule out a southern option for basement rocks including Yakutat Group rocks.

Zircon data from the Yakutat Group flysch (older basement unit) suggest similarity to southwestern Laurentia, only at the edge of the margin today in southern California. Garver and Davidson (2015) hypothesize that that the flysch of the Yakutat Group has a source in southwest Laurentia as it contains Precambrian detrital zircons with age modes of 1370 Ma and 1450-1475 Ma, and Hf isotopes that are also similar to those that occur in the modes of anorgenic granites in southwest Laurentia (Garver and Davidson, 2015). This idea is supported through U/Pb analysis, indicating that part of the basement may have been originated as far south as southern California (Garver and Davidson, 2015). In this scenario, the basalts indicate a different setting and they imply that the Yakutat Block was adjacent to the Eocene basalts of the Crescent terrane in Washington and Vancouver Island as well (Garver and Davison, 2015). Overall, there has been a considerable amount of northward translation regarding the Yakutat Block. Garver and Davidson (2015) hypothesize that this margin-parallel translation must be due to the terrane-bounding Border Ranges fault system as this would allow for slip between the flysch of the Chugach in addition to the more inbound terranes.

METHODS

Rocks were collected during a field expedition in the summer of 2016. The field team consisted of Professor John Garver from Union College, Professor Cameron Davidson from Carleton College, Professor Eva Enkelmann from the University of Cincinnati, Julie Sophis from Union College, Haley Olson from Carleton College, Erin Arntson from Carleton College, and myself from Union College. This project involved significant logistics, so just getting to the field site was a major undertaking. All of the equipment that would be used (tents, boats, etc.) was locked away in storage and we took out the boats beforehand, run them for a few days, and inspect everything to make sure that there would be no issues in the very remote field setting. Inventory was also important regarding our equipment for cooking and daily use. After successfully inspecting all of our materials, it was apparent that we bought enough food and additional equipment to last us 10 days in the field.

Getting into the field took a number of steps. To get to Yakutat, we packed up a cargo van and boarded the AMFS ferry that would transport us and all equipment to Yakutat overnight from Whittier. Once in Yakutat, we organized for sample collection in Yakutat Bay (from Yakutat town) and then in Russell Fiord (by spike camp). Sample collecting in Yakutat Bay lasted two days before we flew to our campsite on Nunatak Fjord where we would then collect samples on the interior of the bay in both the Russell and Nunatak Fjords. The field team collectively sampled six

different sites in Yakutat Bay (labeled as YB16-01-06) and an additional 33 sites (labeled as RF16-01-33) successfully within the Fjords throughout the entire field experience.

Sampling in the field consisted of remote access along shoreline exposures in two Zodiac® boats. Different sites were visited along Disenchantment Bay, Russell Fjord, and Nunatak Fjord (see Figure 1). At field sites, notes were taken of the location, bedding, mineralogy, and structural features. Finally, the team would identify coarse-grained sections of the bedrock (mainly sandstones) for extraction using rock hammers for further analysis in the laboratory for the recovery of zircons.

Laboratory Work

Zircon mineral separation and preparing the chips to make thin sections for each sample was done at Carleton College in Northfield, MN as well as Union College in Schenectady, NY. To obtain zircons, each sample was crushed and then ground until it reached a consistency similar to sand. A baseball to softball-sized amount of rock was removed for geochemistry. For preparing the clasts from the conglomerates for the crushing phase, it was important to remove any matrix rock from each of the clasts with a diamond saw to avoid contamination. After crushing and grinding, samples were sieved to the < 400 μm size fraction. Ideally, the less than 400 μm grains should fill about half to three-quarters of a gallon sized Ziploc® bag.

Following sieving, most samples (excluding granites) were separated on a Rodgers table® at Macalester College in Minneapolis, MN. In this step, the sample is concentrated by density using water and on a grooved, inclined surface (the effect is like a gold pan). Most samples (excluding granites) then were dropped down a vertical magnet to separate the unnecessary magnetic materials from the potential zircons. The drop-mag grains get put in a heavy liquid solution (TBE) and further separated by density. After TBE, the sample enters the Franz isodynamic separation phase. This phase consists of dropping the grains at progressively higher magnetisms starting at 0.1 Amp and folding each level of magnetic sediment into its own labeled pouch. The non-magnetic grains are primarily zircon and apatite. The final phase in the mineral separation process consists of repeating the heavy liquids phase, but this time with MI to separate the apatites from the zircons. Once the heavy sediment is dropped, the sample should mostly be zircons and the mineral separation process is complete.

The preparing of thin-section chips was very conservative to save as much as the hand sample as possible. The first step was to cut a small portion of one end using a diamond saw blade to get a flat cut side and next cut is done by flushing this cut side up against a straight block to cut another side parallel at the appropriate thickness. There is a groove on the diamond saw platform

that marks where to place this block. After making two parallel cuts, the piece was analyzed to see which is best and most representative of the sample. Areas with fractures were avoided. Once the side for the thin section is chosen, the next step is to draw an outline of a thin-section on the face of the chip in pencil. After outlining the chip, the outline was cut out with the saw and the finished product fit a thin-section glass. The last thing to do is label the side opposite of the good face for the thin-section in permanent marker so it does not get lost in the transfer process and so the right side appears on the thin-section. Thin sections were then made at Union College by Bill Neubeck. Both mineral separation and cutting chips for thin sections for sandstone samples were done during the summer at Carleton College. In the fall, the mineral separation process for all granite samples and some sandstone samples occurred at Union College. The granite samples, however, did not undergo the Rodgers table$^{®}$ or drop-mag steps as the fine fraction went right to TBE.

U/Pb Dating of Zircon

U/Pb isotope measurements were handled through standard methods at the University of Arizona Laserchron Center. About 100 to 300 grains were randomly selected for analysis in addition to some hand-selected with a certain shape and color distinctive to Precambrian grains. It was assumed that Precambrian grains are more likely to be well-rounded and display colors in the pink series due to longer exposure effects of radioactive decay over time (Garver and Kamp, 2002). Both the random and Precambrian picked grains for each sample were placed onto the same 1" epoxy mount in addition to standard zircon grains. After these grains are incorporated into a mount, each mount was polished down to a depth of ~20 µm so they can be polished, imaged, and cleaned. The U/Pb analysis was done by the laser ablation multicollector inductivity coupled plasma mass spectrometry (LA-MC-ICPMS) (Gehrels et al., 2006, 2008). The ablation process consists of ablating zircons with a Photon Machines Analyte G2 excimer laser with a spot diameter of 20 µm (Gehrels, 2010). This material is then carried in helium into the plasma source of a E2 ICPMS, which contains a flight tube that measures U, Th, and Pb isotopes simultaneously (Gehrels, 2010). These isotopes are measured in static mode by using Faraday detectors with 3×10^{11} ohm resistors for ^{238}U ^{232}Th ^{208}Pb ^{206}Pb in addition to dynode ion counters for ^{204}Pb and ^{202}Hg (Garver and Davidson, 2015). There is a 15-second integration period with the laser off (for background) and with the laser firing for each analysis (Gehrels, 2010). Also, there is a 30 second delay between each sample that the machine utilizes to prepare for the next analysis. About a 20-µm pit is left after the ablation process.

The concentrations of U and Th are correlated to the standard values. The errors for determining the ^{206}Pb/^{238}U and ^{206}Pb/^{204}Pb as well as ^{206}Pb/^{207}Pb and ^{206}Pb/^{204}Pb are ~1 to 2% at 2-sigma level. However, there is more precision for younger grains in the ^{206}Pb/^{238}U system and less

precision for younger grains in the ^{206}Pb/^{207}Pb system due to the intensity of the ^{207}Pb signal. The cross-over in precision between ^{206}Pb/^{238}U and ^{206}Pb/^{207}Pb occurs at around 1.0 Ga. Thus, the best for grains younger than 1000 Ma are from ^{206}Pb/^{238}U. Concordant ages are based upon the relationship between ^{206}Pb/^{238}U and ^{206}Pb/^{207}Pb. If this ratio is equal to 1 ± 10%, the age is concordant. On the concordia plot, if the sample yields an age below the concordia line, there is Pb loss. If the sample yields an age above the concordia plot, there is U loss. If there is horizontal translation to the right of the concordia line, it is assumed that the sample contains excess ^{204}Pb (common lead). An Hg correction is made and is sometimes significant when the Hg background is high. ^{204}Hg interferes with ^{204}Pb. This is corrected by measuring ^{202}Hg and the subtraction of ^{204}Hg according to the natural ^{202}Hg/^{204}Hg ratio is 4.35. A common lead correction must also be made. This is done by the means of using the Hg-corrected value of ^{204}Pb as well as assuming Stacey and Kramers' (1975) initial Pb composition with their uncertainties (1.5 for ^{206}Pb/^{204}Pb and 0.3 for ^{207}Pb/^{204}Pb) because there is variance in modern rocks.

Inter-element fractionation is corrected by ablating a grain with a known age, 563.5 ± 3.2 Ma, at about every fifth measurement. The resulting uncertainty for this correction is usually 1 to 2 percent (2-sigma). Pb/U fractionation is usually around 5% and apparent fractionation of Pb isotpes is generally <0.2 percent (Garver and Davidson, 2015).

εHf (t) on Clast and Knocker

Hf isotope measurements were handled through standard methods at the University of Arizona Laserchron Center. The depleted mantle curve on the εHf(t) verse U/Pb age plot is from Vervoort and Blichert-Toft (1999). The ^{176}Lu/^{177}Hf ratio is 0.0115, which allows the plotting of Hf crustal evolution curves (Vervoort and Patchett, 1996; Vervoort et al., 1999). Hf isotope analyses were measured with a Nu HR ICPMS, which was connected to a Photon Machines Analyte G2 excimer laser. The instrument settings must be established, which is done by analyzing 10 ppb solutions of JMC475 and a Spex Hf solution first, followed by additional analyses of 10 ppb solutions of Spex Hf, Yb, and Lu. All solutions need to yield ^{176}Hf/^{177}Hf of ~0.28216 for the most optimized laser ablation analyses. Seven independent standards were analyzed were are included with the samples on the same epoxy mounts. These include: Mud Tank, 91500, Temora, R33, FC52, Plesovice, and Sri Lanka. Unknowns do not get analyzed until these standards measure values of acceptable precision and accuracy. Each standard must also be measured and analyzed at least once for about every 20 unknowns. All standards and unknowns from the same session get processed and reduced together. The decay constant of ^{176}Lu (λ=1.867e^{-11}) can be used to determine the time of crystallization by looking at current ^{176}Hf/^{177}Hf. (Münker et al., 2001; Söderlund et al., 2004; Garver and Davidson, 2015).

The laser beam used for this laser ablation technique has a diameter of 40 µm. The Hf ablation pits are also in the same spots as the U-Pb ablation pits. The CL images must be used to make sure that the ablation pits did not overlap with any inclusions or multiple age domains (since this laser has a larger diameter than the laser from U/Pb laser ablation). There is a single 40 second integration for the background (no laser firing), which is followed by 60 one second integrations (laser firing). The typical laser fluence of ~5 J/cm^2 and pulse rate of 7 hz was used, which corresponds to about a 0.8 microns per second ablation rate. Isotopic fractionation is corrected using a method developed by Woodhead and others (2004). The βHf value (mass bias function) requires measuring ^{179}Hf/^{177}Hf and βYb requires measuring ^{173}Yb/^{171}Yb. The βLu is also assumed to be the same as βYb. The fractionation formula is corrected by an exponential formula (βHf= Ln (R^{obs}/R^{true}) / ΔM). To correct Yb and Lu, ^{176}Yb/^{171}Yb and ^{176}Lu/^{175}Lu are measured, respectively (Woodhead et al., 2004). The critical isotope ratios for ^{179}Hf/^{177}Hf, ^{173}Yb/^{171}Yb, ^{176}Yb/^{171}Yb and ^{176}Lu/^{175}Lu are also used for the correction and done line-by-line (Woodhead et al., 2004). If the Yb single is low, the βHf can be used for fractionation of Yb isotopes and the corrected ^{179}Hf/^{177}Hf filter out 2-sigma outliers.

Raman Spectroscopy

Raman measurements were made with a Bruker Optics Senterra® Spectrometer coupled to an Olympus® BX51 reflected light microscope at Union College. Raman spectroscopy was performed using a 633 nm external He-Ne laser. Analyses were done on polished mounts with internal surfaces of exposed zircons that had already been dated by Laser Ablation, and Raman measurements were made on either side of the ablation pit. The spectrometer includes a computer controlled three-grating turret with a spectral resolution up to 3 cm -1 and automatic laser and Raman frequency calibration. Samples were first located at 100x using bright field objectives, and the measurements were made with video camera and long working-distance dark field objectives at 500x. The signal was captured by a low noise 1024x256 pixel thermoelectric-cooled CCD detector. Measurements were made with a laser power of 20 mW, and an aperture of 25 x 1000 µm. An integration time of 10 to 60 s was used during acquisition of the Raman shift (longer for high-damaged grains), and automated collection was done for background and monochromatic wavelength. For samples with a very strong peak to background ratio, a simple rubberband background correction was made, but for those with a more elevated background or a background broadly concave (likely due to slight fluorescence), a concave rubberband background correction. We then used Fityk® for peak fitting and we concentrated our efforts on the $_{v1}$SiO$_4$ (~974 cm -1) symmetric stretching and the v$_3$SiO$_4$ (~1007 cm -1) antisymmetric stretching (i.e. Marsellos and Garver, 2010). We use a Lortenzian approximation using the Levenburge-Marquardt method. Each grain was measured twice in slightly different spot locations that tended to vary by less than 20 µm, and grains were oriented with c-axis in a N-S position.

The reported values for the Raman modes is the average of the two spot measurements. The average variation in measurements for the v_3SiO_4 mode is about ~0.2 cm-1.

Geochemistry of Plutonic Clasts and Knockers

Plutonic clasts: RF16-23B1, B2, and B7 and plutonic knockers RF16-16 and 26 were analyzed for major elements and some trace elements at Hamilton College by Julie Sophis (Union College). Initially, these samples were processed in at Carleton College by a Chipmunk Crusher to reduce the size of the sample. These chips were then removed and sent to Union College for additional preparations. Here, the sample chips were crushed in a RockLabs Hydraulic Crusher until the chips were under 6 mm. Next, approximately one tablespoon of sample was poured into a Specs® aluminum oxide grinding vessel. Most samples needed five minutes of grinding time within the RockLabs Shaker to achieve the necessary result (fine powder with the consistency of flour), while others needed longer required longer to achieve this. To ensure that there was no cross contamination, cleaning procedures took place between each sample. The final sample powder was split between two vials, with one to be analyzed for major element analysis and the other for trace element analysis.

At Hamilton College, dilithium tetraborate was mixed with the powdered rock sample in a 2:1 ratio (7.00 g and 3.500 g, respectively). Slight variations in measurement may have occurred, however it was crucial to ensure that the rock powder was exactly half of the tetraborate. Next, the measured samples were mixed in a shaker and then poured into graphite crucibles. These crucibles were placed on ceramic trays and then heated in an oven at 1000° C for 70 min. The samples remained in the oven for 70 min. The heating allows the powder samples to turn into glass beads. When the samples cooled, the sample beads were reground to ensure the sample is completely homogenous between the tetraborate and rock sample. Graphite is then scrubbed off of the bottom and sides of the beads to make the etching of the sample number easier. The sample needs to be powered for 30 s into a tungsten carbide bowl within a Rocklabs Shatterbox. A drop of ethanol is also mixed within this bowl to help eliminate possible moisture. Once ground, without inducing cross contamination, the powder is carefully poured back into the graphite crucible and is cleaned between samples. The samples then get heated for a second time at 1000° C for 70 min. If the sample is removed and contains air bubbles or cracks, it must be reheated. The sample number etched to the top of the beads with a diamond tipped Dremel once cooled.

Again, all graphite is removed from the bottom and sides of the beads through polish, which ensures a smooth surface. After polished, the beads were processed in a Thermo ARL Perform'X X-Ray Fluorescence spectrometer. Three additional duplicate beads were made to check

homogeneity and reproducibility of data. Discriminant diagrams using the geochemistry of major earth elements were analyzed to classify Plutonic clasts: RF16-23B1, B2, and B7 and plutonic knockers RF16-16 and 26. These diagrams were made in Microsoft Excel following templates published by Kurt Hollocher of Union College. Diagrams include LeBas and others (1986); Frost and others (2001); Barker (1979) and Pearce and others (1984).

Limestone Chemical Dissolution

The limestone clasts RF16-23C1, C2, C3, C4, C5, C6, C7, C8, RF16-25D, RF16-25C1, C2, C3, RF16-14A, and RF16-12B were prepped for chemical dissolution using adopted procedures by Collinson (1963). First, each sample was weighed before being crushed to the size of cm chips by the Chipmunk Crusher., and then weighed again (Appendix F). All samples were then weighed again to make sure no material has been lost. There were a few exceptions where there was too much mass, in which not all of it was used for dissolution. Each sample was then placed into a 2000 ml container. 200 ml of 99% Glacier Grade Acetic acid and 1800 ml of water was then mixed into the containers containing the limestone chips to create a 10% solution of acetic acid. These solutions were left to sit for 24 h, while stirring occasionally to dissolve the limestone. After 24 h, each container was carefully decanted and then wet sieved. Wet sieving consisted of using tap water and a small hose. The top sieve was 16 mesh and the lower was 100 mesh. It is necessary to keep everything that goes through the sieves for examination, however conodonts should be caught on the lower sieve. Each sieve should be thoroughly rinsed with fine-spray before the start of the wet sieve process for each sample.

Next, each sample was then placed into an oven on a dry hotplate to dry overnight. Once the samples are dried, the conodonts, which are part of the heavy fraction, will be able to separate into light and heavy functions by the means of TBE heavy liquids. The samples are then dried overnight. All excess material was stored and potential conodonts were then looked at under the microscope.

<div align="center">

RESULTS

</div>

Field Comparison

RF16-23 and RF16-25 are located at the north end of Russell Fjord (RF16-23 is to the north of Seal Cove and RF16-25 is across the fjord, just south of the knocker where Russell Fjord meets Nunatak Fjord). The strata of both sites are very similar to one another as both sites contain nearly identical conglomerate units (Figure 4). For example, both conglomerates facies contain sandstone, greenstone, granitoid, and chert clasts. RF16-23a is the matrix sample and is an arkosic sandstone containing plant fragments and ammonites. The clasts within this

conglomerate (#23) are 5-50 cm. They are generally well-rounded, clast-supported, and have well organized layering due to current flow during deposition. The conglomerate cobbles largely contain limestones, sandstones, greenstones, less than 10% chert, and greenish porphyritic volcanic sediments. Site RF16-25 appears to be a large phacoid in what the mélange facies. RF16-23 and 25a are both muscovite-rich arkosic sandstones in which each respective conglomerate is set in.

Figure 4: *Photos of two conglomerate units: A) RF16-23 and B) RF16-25. Both units look nearly identical in observation with varying types of clasts and sizes although on different sides Russell Fjord.*

For RF16-23a, the maximum depositional age (MDA) of the detrital zircons from the matrix sandstone is either 65.9 ± 1.8 Ma and 67.9 ± 0.9 Ma (n=3, n=10), depending on how many grains were used. Similarly, for RF16-25a, the maximum depositional age for the detrital zircons from the matrix sandstone is 65.6 ± 2.2 Ma and 67.2 ± 1.1 Ma (n=3, n=10). These ages are Maastrichtian (Upper Cretaceous), identical within error, and occur at the K-T Boundary.

Plutonic Clasts and Knocker age

Site RF16-23 contains the conglomerate unit in what is mapped as the Yakutat Flysch facies (Plafker et al., 1994). RF16-23b.1-16 consists of 16 separate feldspar-rich granitoid clasts, RF16-23c.1-8 consists of eight limestone clasts within the conglomerate, and RF16-23d represents one sandstone clast within the conglomerate. For site #23, in addition to the matrix sample, U/Pb analysis was done on RF16-23b.1 (here B1) and RF16-23b.2 (here B2). B1 gives a mixed date between 150 Ma and 180 Ma. B2 gives a date of 167.3 ± 1.8 Ma. The dates for B1 are complicated; (B1)) contains zircon grains that yield two main distribution ages with the first at 154.6 ± 2.3 Ma (Upper Jurassic) and the second at 179.5 ± 2.2 Ma (Lower Jurassic). Interestingly, the ~155 Ma population tends to have a uranium that is less than 200 ppm, while the ~180 population has a mixed uranium concentration. The zircon grains from the granitoid

clast, RF16-23B.2 (B2), has a single age distribution between the two main distribution ages of B1, and is 167.3 ± 1.8 Ma. Clast RF16-23B.7 was not U/Pb dated.

The mineralogy of clasts B1 and B2 is nearly identical. Clast B1 contains: quartz, plagioclase, K-feldspar, and chlorite (replacing biotite), sericite, and epidote (both partially replacing feldspar) secondary minerals. This sample also has a cataclastic vein. B2 contains: quartz (some phenocrysts), plagioclase, K-feldspar, and biotite with secondary chlorite and rutile replacing biotite as well as sericite and epidote partially replacing feldspar. Some of the quartz in this sample is subhedral and large and look like phenocrysts. Prehnite is present in a cross-cutting vein, and thus, these biotite granite clasts must have experienced low-grade metamorphism.

The Yakutat Mélange also has knockers of metaplutonic rocks. Sample RF16-16, located at 59.93722°,139.39713°, and RF16-26, located at 59.85071°,139.31404°, are granitic knockers and yield U/Pb ages of 174.9 ± 0.89 and 173.8 ± 1.0 Ma, respectively.

Whole Rock Geochemistry of Igneous Rocks within the Mélange

The geochemistry of the plutonic rocks within the Yakutat Group mélange: RF16-23B.1 (B1), RF16-23B.2 (B2), RF16-23B.7 (B7), RF16-16 (16), and RF16-26 (26) was analyzed at Hamilton College (NY) and then were plotted on discriminant diagrams to reveal their characteristics. These diagrams include a modified TAS diagram for plutonic rocks from LeBas et al., (1986) and a Granite classification diagram from Barker (1979) (Figures 5; Figure 6). The original TAS diagram is used to classify volcanic rocks, however the discriminant fields can be converted to be used for plutonic rocks.

According to the TAS diagram, which is used as a naming tool that classifies all of the solid and molten materials within the igneous pluton, the classification of the clasts range from granodiorite (B1) to granite (B2), to monzonite (B7), while the knockers range from monzodiroite (16) to gabbroic diorite (26) (Figure 1).

The granite classification diagram also shows additional classifications for these plutonic rocks. For example, that the clasts plot as trondjemite (B1), granite (B2), and granodiorite (B7), however both knocker samples are tonalities (16 and 26) (Figure 6). Thus, it can be loosely suggested that each clast may have come from different plutons, whereas the two sampled knockers may be from the same pluton.
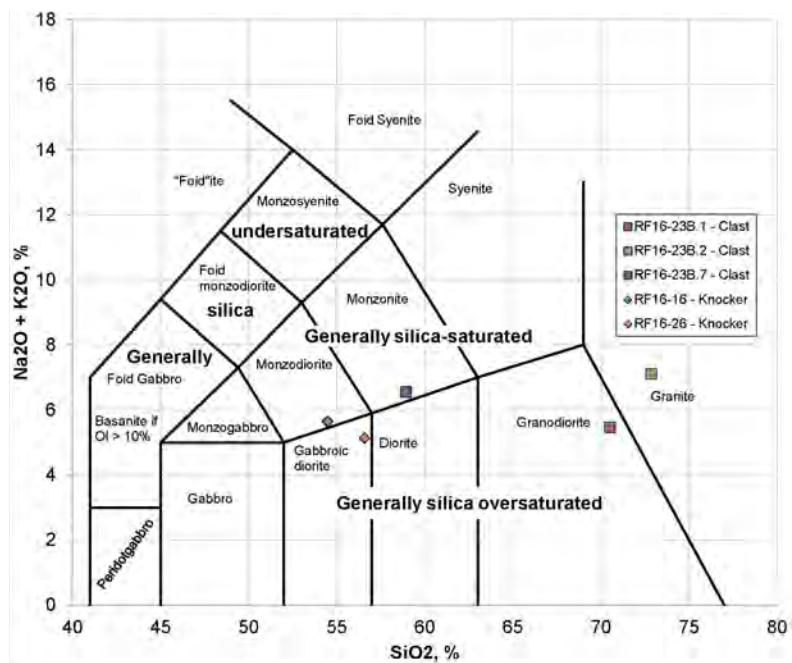
Figure 5 *Plutonic rocks (clasts and knockers) of the Yakutat mélange plotted on a modified TAS diagram for plutonic rocks from LeBas et al., (1986) (Middlemost, 1994). B1 plots as a granodiorite, B2 as a granite, and B7 as monzonite. Knockers: 16 plots as a monzodiorite, and 26 as a gabbroic diorite. The knockers are lower in silica than the clasts.*
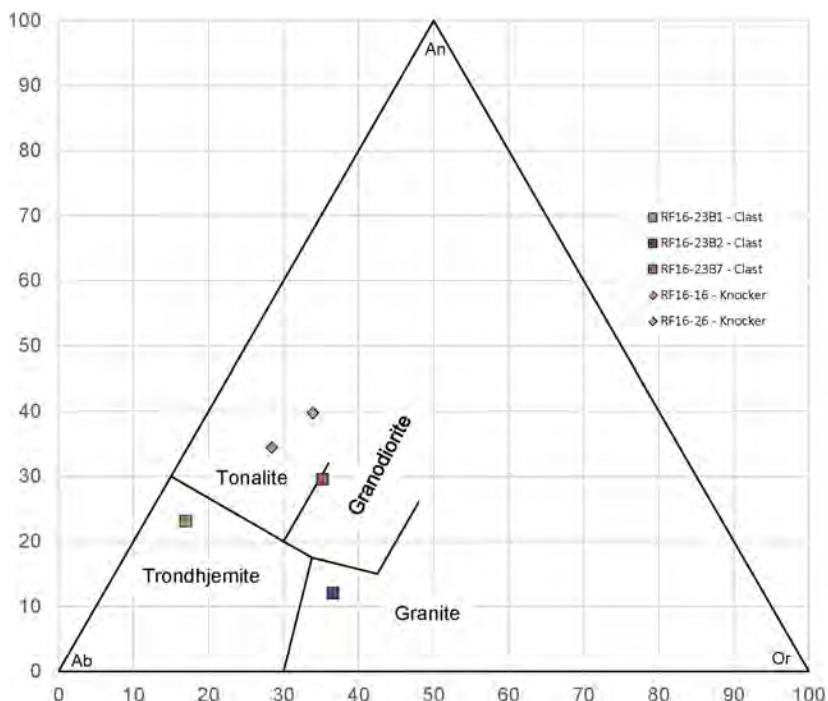
Figure 6: *Plutonic rocks of the Yakutat mélange plotted on a Granite classification diagram from Barker (1979). The clasts: B1 plots as a trondhjemite, B2 as a granite, and B7 as a granodiorite. The knockers: 16 and 26 both plot as a tonalite.*

εHf (t) Values

This study analyzed ^{176}Hf/^{177}Hf isotope ratios for 10 and 15 previously dated zircon grains from the plutonic clast RF16-23b.2 and plutonic knocker RF16-16, respectively. The ^{176}Hf/^{177}Hf isotopic ratios are used for understanding crustal evolution. ^{176}Hf/^{177}Hf isotopic ratios are normalized to the ^{176}Hf/^{177}Hf isotopic ratio of the undifferentiated mantle (chondritic uniform reservoir; CHUR) and are written in epsilon notation, εHf(t). Positive εHf(t) values indicate a juvenile crustal source during the evolutionary history for these zircon-bearing plutonic rocks, whereas negative εHf(t) values indicate an older and more evolved crustal source (Garver and Davidson, 2015).

The εHf(t) values for the ~167 Ma clast, RF16-23b.2, range from +10.0 to +14.3 (Figure 7). There is a single outlier zircon grain within this clast that plots above the depleted mantle line with an εHf(t) of +16.5, but it is suggested that this analysis was offset from the U/Pb laser ablated spot. The εHf(t) values of the similarly aged plutonic knocker (~175 Ma), RF16-16, range from +9.8 to +14.2 and no outliers (Figure 7).
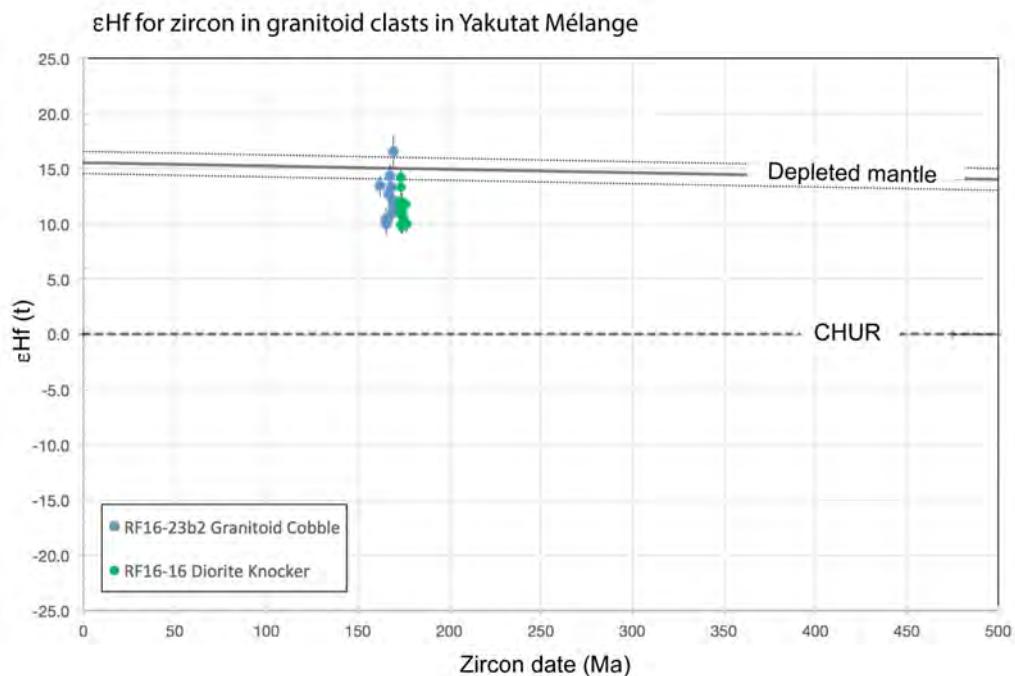
Figure 7: Plot displaying εHf(t) values for the plutonic clast, RF16-23b.2 and the plutonic knocker, RF16-16. Both the clast and knocker are very similar in age: 167 Ma clast and 175 Ma, respectively, and yield very similar εHf(t) values range from +10.0 to +14.3 (clast) and +9.8 to +12.0 (knocker). These εHf(t) values indicate that the plutonic clast and knockers are homogenous and juvenile.

U/Pb Ages of Zircon in Sandstone Clast

RF16-25b.1-3 contains three sandstone clasts from the conglomerate. U/Pb analysis was done on sample RF16-25b.2. Out of the three sandstone clasts from this site, this one was the coarsest and had considerable material. The maximum depositional age (MDA) of the detrital zircons from the sandstone clast is 71.7 ± 2.4 Ma and 72.3 ± 1.4 Ma (n=3, n=10 respectively). Thus, this sandstone clast is Campanian to Maastrichtian (Upper Cretaceous), and the MDA is about 6 Myr older than the matrix (if MDA approximates depositional age) (Figure 8). The relative probability versus age data for this sample also shows main age peaks at 73 and 91 Ma with little populations at 146 Ma and 183 Ma. There are also large Precambrian peaks at 1380 and 1740 Ma.
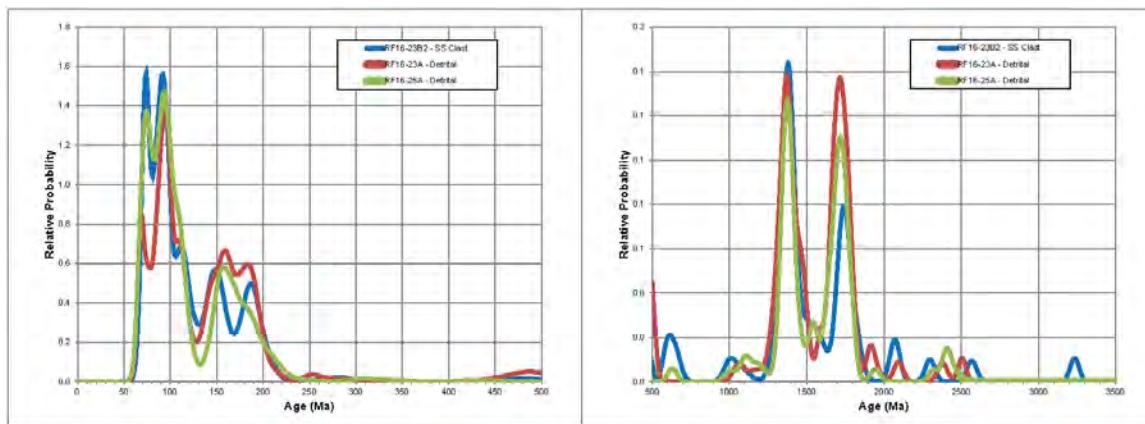
Figure 8: Plot displaying comparison between sandstone clast (RF16-25b.2) and detrital sandstone matrixes from RF16-23a and RF16-25a.

Limestone Clasts and Limestone Knockers

Of the samples completed: RF16-23C1, C2, C5, C7, C8, and RF16-25C1, all were barren of conodonts. This means they are either post-Triassic in age, or from an environment without conodonts.

DISCUSSION

Sandstones

Sandstone RF16-23a and RF16-25a have a PDF that show nearly identical ages. These ages are visually represented in Figure 1. From youngest to oldest, the major peaks occur at 69-74 Ma, 92-94 Ma,157-183 Ma, 1365 Ma, and 1710 Ma (Figure 9). The correlation of peak ages between the samples support the initial hypothesis in the field with respect to these sandstone matrixes being

part of the same unit. After comparing the normalized relative probability vs age (Ma) for both Precambrian and non-Precambrian grains of RF16-23a and RF16-25a, it seems likely these two units are the same.
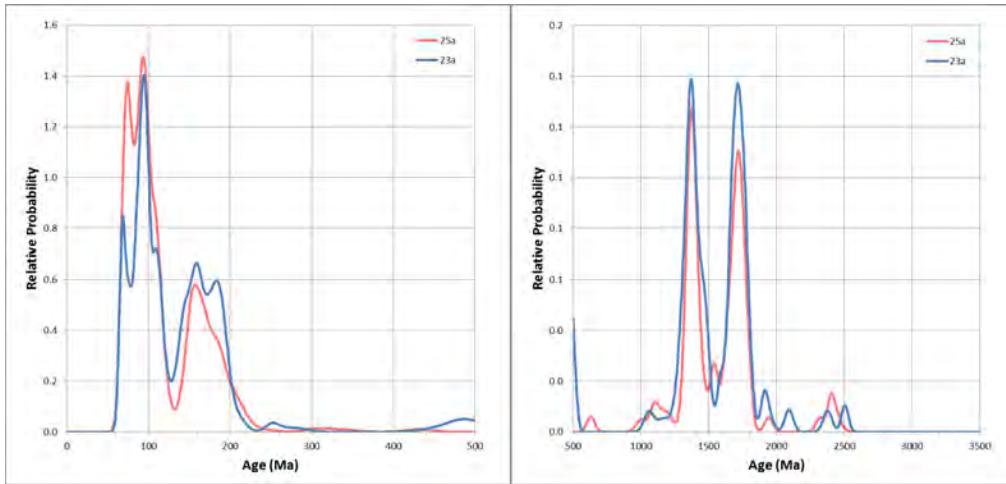
Figure 9: Comparison of normalized data of the relative probability for a specific age from RF16-23a and RF16-25a to one another (sandstone matrix samples). The graph of the left displays the ages of non-Precambrian zircons, while the graph on the right displays the Precambrian grains. The peaks for both the Precambrian and non-Precambrian grains for each sample appear to strongly correlate with one another, suggesting that they are the same unit.

Although the sandstone at sites RF16-23 and RF16-25 are mapped differently (flysch vs mélange) the U/Pb data suggest that they are the same unit (Wilson et al., 2005). All the types of clasts (sandstone, limestone, greenstone, granite, and chert) within the conglomerates are present at both sites and are also situated within the mélange unit. The sandstone clast (~72 Ma) is similar in age to the sandstone unit (69-74 Ma) within the mélange and has the same age populations. Thus, I hypothesize that part of the mélange was uplifted and then redeposited into itself, suggesting that sedimentation and mélange formation was occurring at the same time.

Raman Spectroscopy

Raman Spectroscopy was done on the Precambrian zircon grains from sample RF16-23a (conglomerate sandstone matrix) to understand zircon crystallinity values. To determine crystalline grains versus grains that are radiation damaged, the Raman wavenumber $v_3(SiO_4)$ (cm^{-1}) was plotted for each grain against its specific eU (effective Uranium) value (ppm), which was obtained through LA-ICPMS analysis.

A total of 69 Precambrian grains from RF16-23a were assessed in two different locations for crystallinity values using Raman Spectroscopy. The majority of these grains yielded strong

signals for both Raman analyses with similar values and low standard deviations; while a few grains yielded weak Raman signals. These grains were shot with a longer integration time to get a stronger single. However, if grains were still yielding a low signal, they were either refitted (3 grains), had one of the two analyses discarded due to an isolated low signal (2 grains), completely rejected due to both spots yielding a low signal (1 grain), or completely rejected due to super heterogeneous zoning in which the U values cannot be relied on (1 grain). Thus, 67 grains are included in the results of this analysis.

For the 67 analyzed Precambrian grains of RF16-23a, it appears that there is no correlation between eU and crystallinity versus radiation damage (Figure 10). For example, high eU (~1000 ppm) yields high Raman values (~1007.0+) as well as low Raman values (~1005.0), indicating both crystalline and damaged, respectively. The same result also occurs for all grains no matter what the eU value is (eU ranges from (3000-85 ppm) (Figure 10).

Previous published literature suggests that Raman Spectroscopy indicates the metamorphic history of these Precambrian grains (Garver and Davidson, 2015). Thus, published Precambrian grains from the CPW terrane are old as they have most likely accumulated radiation damage for 0.5 to 1.0 Gyr while the Precambrian grains from Yakutat Bay are young with little disorder and most likely only accumulated radiation damage for the past 100 Myr since the late Mesozoic (Figure 10) (Garver and Davidson, 2015). Interestingly, when RF16-23a is compared to the result of Garver and Davidson (2015) it appears this sample has a wide range of radiation in Precambrian grains as the data plot between these two arrays (Garver and Davidson, 2015) (Figure 10). This suggests that Precambrian grains from RF16-23a may either be annealing from the older array (0.5-1.0 Gyr) or experiencing slightly more disorder and radiation damage than the younger array (100 Myr). A third interpretation is that there may be a third field in between the two arrays determined from Garver and Davidson (2015).
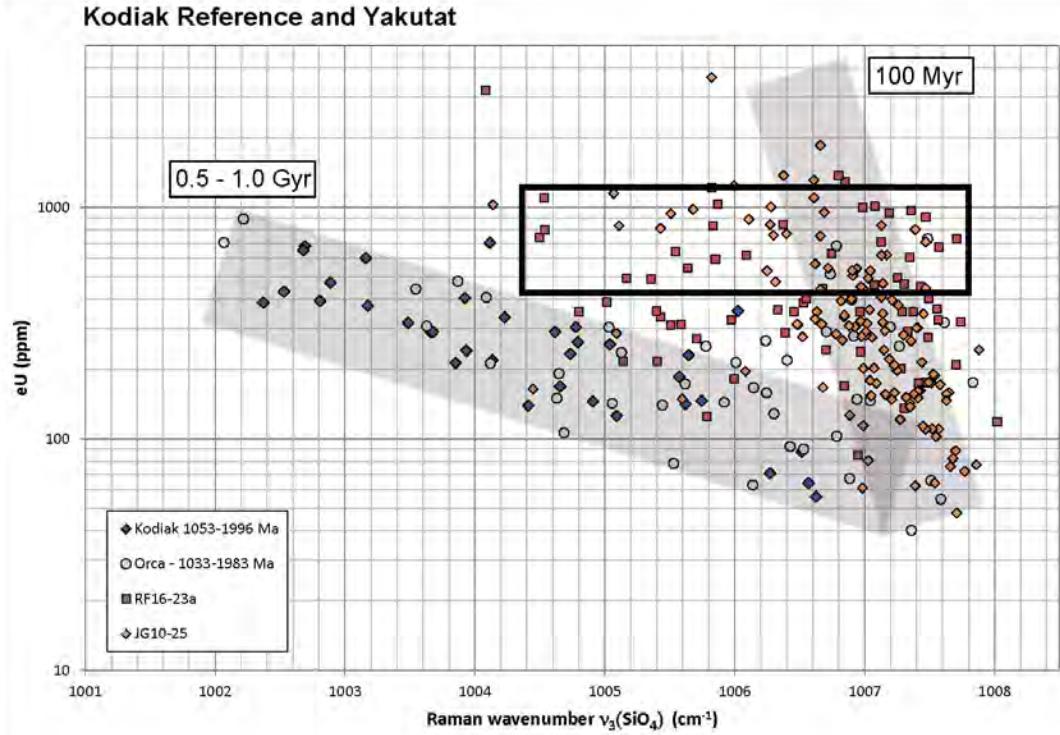
Figure 10: *Plot comparing Precambrian zircon crystallinity from sample RF16-23a (detrital sandstone) to previously published detrital sandstones within the literature from the Kodiak and Orca Groups as well as a sample from JG10-25 from Point la Touche in Yakutat Bay. RF16-23a plots in between the two previously published arrays of radiation damage (shaded regions) (Garver and Davidson, 2015) suggesting either a wide range of radiation damage, indicated by the black outlined box or potentially a third field.*

Plutonic Clasts

Due to inheritance, the granite clast (B2) from site #23 contains two main grain-age populations. There may have been a younger intrusion with lower U concentrations that were reworked during intrusion. Also, the 155 Ma population is tightly clustered (much more than the 180 peak). The grains that yield the 180 Ma population have both high and low uranium (>200 and <200 ppm), but are not as tightly clustered (Figure 11). There is one outlier (grain #32) that yielded a date of 139 Ma and another two (grains #17 and #28) that yielded Precambrian dates. The lower uranium grains that yield the 155 Ma population are generally irregularly zoned on the CL map (grains #7, #31, #35 are exceptions) as opposed to the standard zircon zoning pattern grains that yield the 180 Ma population (Figure 12). Hypotheses that could explain these two main peaks are potential mixing within the magma in which they crystallized, and introduction of foreign grains within the sedimentary system or possibly a laboratory error. Sample RF16-23b.2 yielded one main age population at ~167 Ma. The mean age of this sample is also ~167.2 ± 1.8 Ma, which is Middle Jurassic. Thus, we require Jurassic plutons in the source.
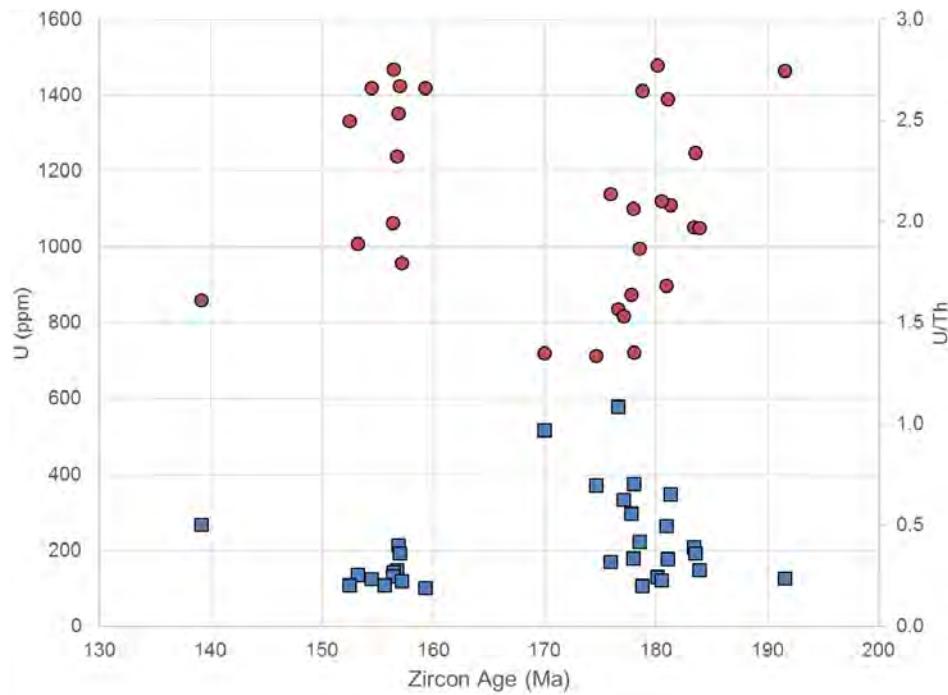
Figure 11: *This graph plots the uranium (ppm) and uranium/thorium versus zircon age for RF16-23b.1. The squares correspond to uranium concentration while the circles correspond to uranium/thorium. There are two distinct clusters for uranium (ppm) around 155 Ma (Upper Jurassic) and 180 Ma (Lower Jurassic) with the 155 Ma cluster being more consistent. The 155 Ma cluster also tends to have a uranium concentration under 200 ppm, while the 180 Ma cluster has some over 200 ppm and some under 200 ppm. The U/Th ratio for the 155 Ma population also appears to be more clustered than the 180 Ma population. Two zircons have Precambrian dates from this sample and do not appear on the graph.*

The source of the plutonic clasts may be very complicated because they can either be from the mélange or the source area. The main peaks from clast B1 were ~155 and 180 Ma and the main peak for clast B2 was ~167 Ma. This is similar to the plutonic rocks in the mélange, RF16-16 and RF16-26, which have ages of ~175 and 174 Ma respectively.
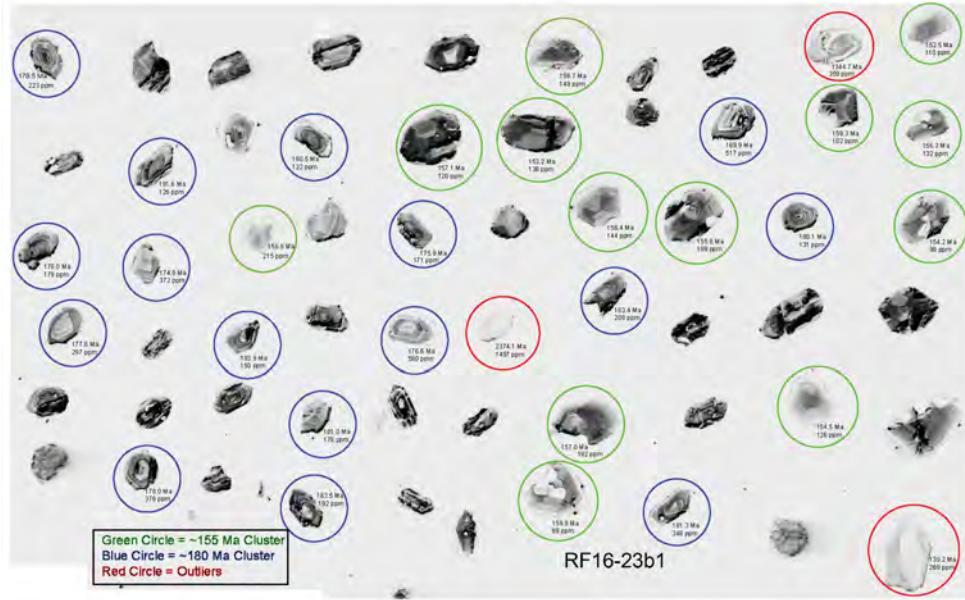
Figure 12: This is an inverted CL image of zircons for sample RF16-23b.1, a granite clast. The grains circled in blue yield the ~180 Ma date, the grains circled in green yield the ~155 Ma date, and the grains circled in red are outliers. The grains that have a uranium concentration of <200 ppm generally correlate to the 155 Ma. The grains that have a uranium concentration of >200 ppm generally correlate to the 180 Ma peak. There are exceptions for both cases. The grains that yield the 155 Ma peak are generally irregularly zoned (grains #7, #31, #35 are exceptions), while the grains that have standard oscillatory zircon zoning correspond to the 180 Ma peak.

Of interest is the Jurassic population of grain ages because they allow us to better understand the age of the granites in the context of the source area. To compare the granite ages (clasts and knockers) we combined similar detrital samples that had the same age spectra to enhance the Jurassic signal. We combined the normalized PDF plot for YB16-06 (n=104), RF16-23a (n=202), RF16-25a (n=294), RF16-25b.2 (n=294), and RF16-21 (n=299) (n=1193). In this we see more structure in the Jurassic peaks (kernel=1). There are populations at 158 and 187 Ma. Next, we plot the age of the granites on the same plot and can see that they belong to the same Jurassic peak (Figure 13). A conclusion is that an important part of the basement in the source terrane must be Jurassic granitic rocks and recall that they occur as both knockers in the mélange and clasts in the conglomerate. The granite clasts in the conglomerate must have come from the Jurassic basement or from the knockers of granite in the mélange itself.
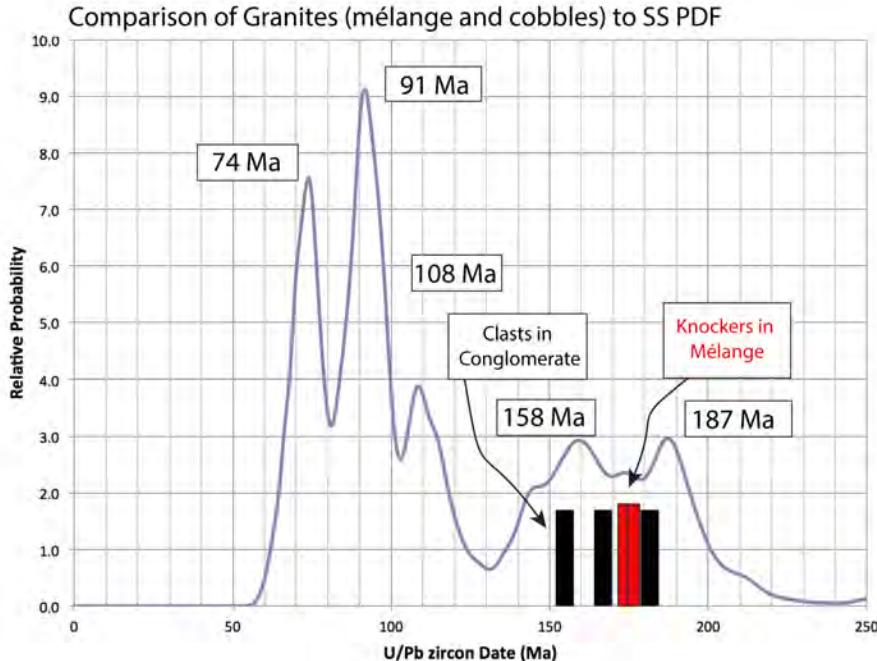
Figure 13: *Plot displaying the combined of PDF peaks from detrital zircon samples: YB16-06, RF16-23a, RF16-25a, RF16-25b.2, and RF16-21 (n Total=1193) and displaying the comparison to the age of granites in the mélange and conglomerate facies.*

Concordia Analysis of Plutonic Clasts

For a single igneous granite clast, a single age is expected in simple systems with no inheritance or mixing of lithologies. Yet, when looking at the full concordia plots for both clasts RF16-23B1 (B1) and RF16-23B2 (B2) this is not the case. Both clasts appear to have many grains corresponding to a variety of concordant grains (Figure 14). However, when looking at the primary modes of these clasts, it can be hypothesized that they are Jurassic, although there is an additional problem when comparing B1 and B2 to one another. The Jurassic cluster for B2 appears to be ~168 Ma, whereas B1 is yielding two Jurassic clusters at ~155 and 180 Ma (Figure 15).

One hypothesis for there being multiple clusters is that there are discordant grains being taken into consideration. To investigate this possibility, concordia plots were made for B1 and B2 that only take the most concordant grains. These grain percentages are determined by dividing $^{206}Pb/^{238}U$ by $^{206}Pb/^{207}Pb$ and multiplying by 100. Thus, the most concordant grains should approach 100%. For these new concordia plots, any grains yielding within 10% of 100% were considered. For B1, 8 out of 35 grains are considered most concordant. For B2, 6 out of 31 grains were considered most concordant. The lack of concordance indicates that the U/Pb system for these grains is not typical. This exercise does not help the problem: the concordia plot for B1 still

yields concordant ages at ~140 Ma, ~155 Ma and ~180 Ma, while B2 plots a cluster around ~168 Ma (Figure 16).

There are three potential hypotheses for these clasts to yield multiple concordant dates: 1) Introduction of grains in magma; 2) Introduction of grains in sedimentary system; 3) Introduction of contamination grains in lab. It is possible that there was a magmatic event at 180 Ma, and these rocks were later intruded at magma at 155 Ma. Further analysis of the zircon grains is necessary to support this hypothesis, such as the observation of younger magmatic rims with older cores. For the second hypothesis, because these U/Pb ages come from clasts within the mélange that may have reworked itself over time, these clasts were possibly contaminated by the enclosing sediments. This mixing would lead to natural contamination within these clasts, especially through cracking and fractures within the clasts. In the lab, matrix was removed, and the sandstone contains most U/Pb grain ages between 70-90 Ma, which is not seen here. The last hypothesis, however, is a laboratory error. Cross contamination between samples may have occurred during the zircon extraction procedures and this scenario cannot be ruled out. However, it would be expected that laboratory-induced contamination would yield U/Pb ages randomly above and below the Jurassic ages. The majority of the concordant ages for these clasts are older than Jurassic as opposed to younger. Both clasts contained at least two Precambrian grains as well. This observation of non-random contamination would suggest that laboratory contamination may not be the most probable hypothesis as opposed to others for explaining these multiple concordant ages in these clasts.
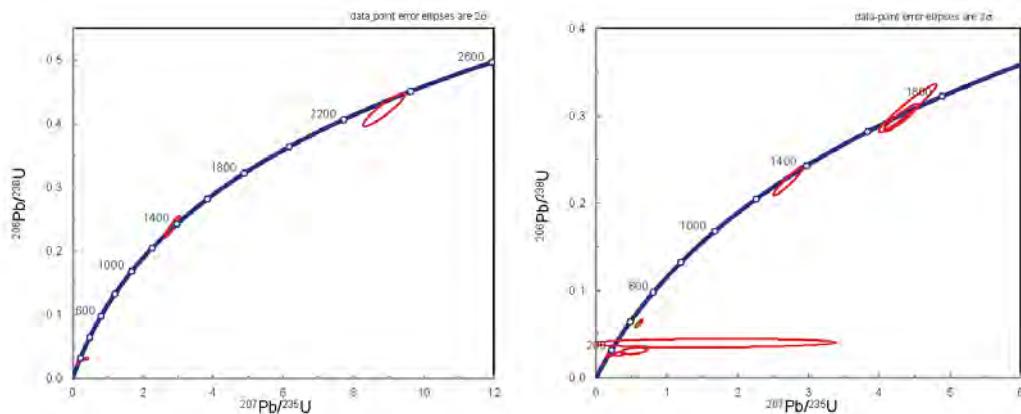
Figure 14: The full concordia plot of RF16-23B1(left) and of RF16-23B2 (right). For B1, a Jurassic mode is visible in addition to two Precambrian grains. For B2, a Jurassic mode is visible in addition to a population ~200 Ma and two Precambrian modes. Circle ellipses represent single grain error bars. Grains that plot below the concordia line have experienced Pb loss, while grains that plot above the concordia line have experienced U loss. Circle ellipses represent single grain error bars.
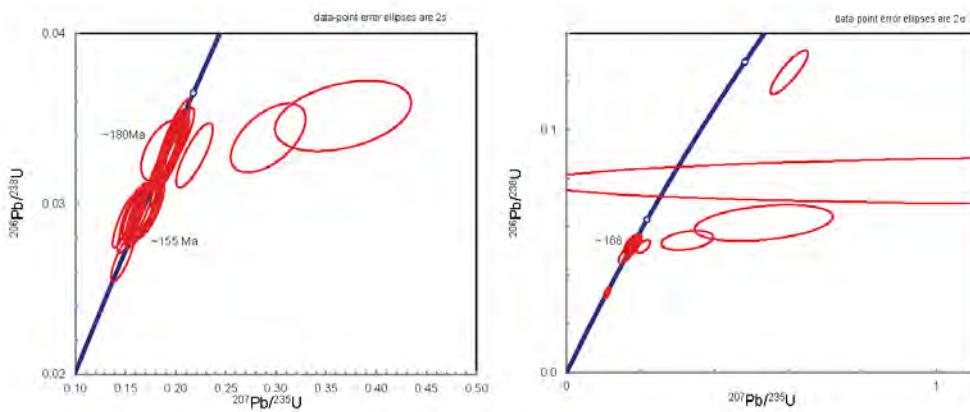
Figure 15: *A rescaled concordia plot of RF16-23B1 (left) and RF16-23B2 (right). There are two distinct Jurassic modes at ~155 and ~180 Ma for B1 and a distinct Jurassic mode at ~186 Ma for B2. There are many disconcordant ages. The grains that yield ages off to the right of the concordia line have an introduction to ^{204}Pb. This introduction may potentially be from a meteoric water source.*
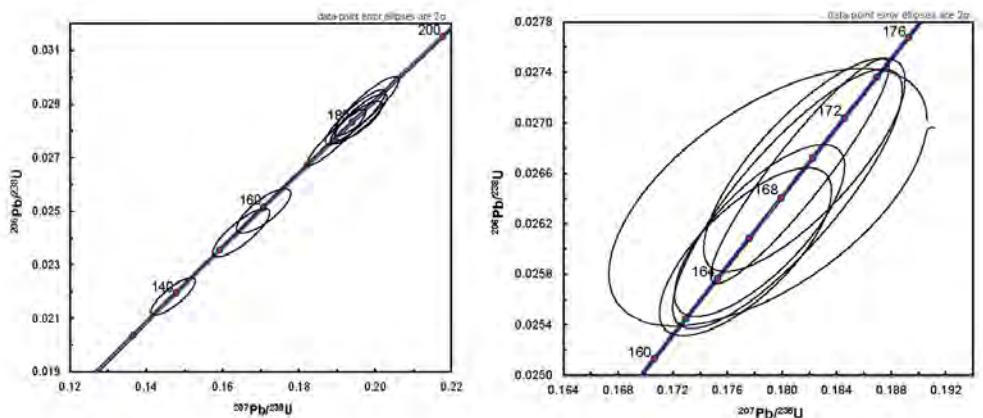
Figure 16: *A concordia plot for RF16-23B1 (left) and RF16-23B2 (right) showing only grains that have concordant 206Pb/238U and 207Pb/206Pb ratios ± 10%. It is assumed that there is a problem with lead systematics if grain is outside of 10% of this ratio. There are 8 out of 35 grains from B1 that were concordant and 6 out of 31 grains from B2. These grains yield ages at around 140 Ma, 155-160 Ma, and 180 Ma for B1 and 168 Ma for B2. Circle ellipses represent single grain error bars.*

Sandstone Clast and Source

A question is whether we have dated similar sandstones in the study to RF16-25b.2 (ss clast) so that we may infer the source. To do this I compared the grain-age population from the clast to same age sandstones from Block 1 and from Block 2. When these peaks are plotted against the normalized peaks of YB16-06 (Block One) and RF16-04 (Block Two), the SS Clast PDF is nearly identical to YB16-06 (Figure 17). Although all three peaks contain the 73 Ma peak, the 93-91 Ma Ma and 1375-1370 Ma peak and distinctive to Block 1 sandstones (in situ or the clast). Thus, it

33

can be inferred that the source of this sandstone clast is coming from Block One, and not Block Two.
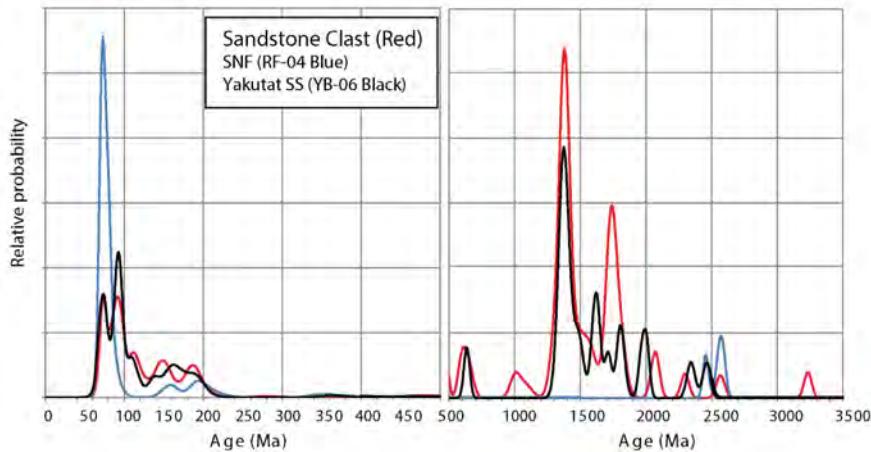
Figure 17: *The relative probability of the sandstone clast (RF16-25b.2) compared to sandstone sample in Block Two that is part of the Schist of Nunatak Fjord (RF16-04), and a sandstone sample from Block One that is part of Yakutat Bay (YB16-06). The sandstone clast is similar to the sandstone sample from block one (Yakutat mélange sample from Yakutat Bay). Both samples have peaks at 73 Ma, 93-91 Ma, and 1375-1370 Ma. Although the sandstone from Block Two has the same peak at 73 Ma, it does not correlate to the rest of the peaks. Therefore, the source of this sandstone clast is most-likely from sandstones Block 1.*

Hf in Zircon of Granites

The plutonic rock samples within the mélange have very close Jurassic ages and positive εHf(t) values and thus, it is inferred that they are homogenous to one another and derived from a juvenile crustal source. A juvenile crustal source is consistent with reported samples from the Gravina belt crustal region between the Alexander-Wrangellia terrane and the Stikine terrane (Samson et al., 1991; Rioux et al., 2007). However, this region may not be the only source of these plutonic rocks. It is also hypothesized that the volcanic arc crustal rocks on Vancouver Island may be the southerly extension of the Wrangellia arc and also appear to be juvenile (Canil et al., 2010). Thus, a potential source of these plutonic rocks may be coming off of Wrangellia to the east, or potentially from the south.

PROVENANCE

A key question to consider is where are we seeing similar plutonic ages and geochemistry to understand what could be a potential source area for these granitoid clasts and knockers within the mélange of Yakutat Bay. Based on the U/Pb grain-age distributions of the zircons within these plutonic rocks, a potential source area should have a record of plutonic events that occurred in the Early and Late Jurassic. The source must also be juvenile and related to arc volcanism according to Hf and geochemistry results.

Talkeetna Arc in Alaska

Jurassic volcanics occur on Wrangellia and adjacent to Wrangellia in the Talkeetna Arc. The Talkeetna arc extends for ~1000 km along the southern margin of the Peninsular terrane portion of the Wrangellia composite terrane and is considered late Triassic to Early Jurassic (Farris, 2009; Rioux et al., 2010). Plutonic activity in the Talkeetna arc was active from about 200 to 153 Ma (Rioux et al., 2010). However, out of the six sites that are well dated within the arc, only one site yielded an age ~153 Ma. This lone age was sampled at the Central Talkeetna Mountains and yielded an age of 152.7 ± 1.7 Ma (with inheritance) (Rioux et al., 2010). The rest of the sites are older: in the Western Talkeetna Mountains (~190 Ma with inheritance); the Eastern Talkeetna Mountains (~178-169 Ma); the Chugach Mountains (202-181 Ma), the Alaskan Peninsula (184-161 Ma), and the pluton on Kodiak Island (213 Ma).

Bonanza Arc on Vancouver Island

The Bonanza arc on Vancouver Island consists of Jurassic volcanic and plutonic rocks. The volcanic rocks are made up of flows, breccias, and tuffs consisting of basalt, andesite, dacite, and rhyolite (D'souza and others., 2016). The plutonic rocks are made up of quartz diorite, granodirotie, quartz monzonite, and tonalite (D'souza et al., 2016). Due to the fact that the Bonanza arc isotopic data does not show a positive correlation between Sr and Nd as elemental concentrations increase, D'souza and others (2016) suggest that this arc has had little to no crustal assimilation (<10%) of older crustal material of the Sicker arc (Devonian basement rocks) (D'souza et al., 2016). The plutons have age ranges between 203 and 164 Ma and the volcanic rocks have a bimodal volcanic age distribution with modes of 198 and 171 Ma (D'souza et al., 2016). However, D'souza and others (2016) hypothesize that the bimodal age distribution of the volcanic rocks is due to sampling bias

Talkeetna Arc versus Bonanza Arc

It is possible that the clasts from the Yakutat mélange came from the Talkeetna arc, but it is very unlikely considering the lack in abundance of dates around 153 Ma (only one out of the four dated) (Amato et al., 2007). Despite the low probability, this arc cannot be ruled out and can very well be the source of the knockers. The Bonanza arc, however, yields no plutonic ages of ~155 (Amato et al., 2007). Thus, it can be assumed that unless the ~155 Ma age concentration from B1 is not magmatic, the plutonic event that occurred from this arc is too old (203 and 164 Ma) to be the provenance of the plutonic clasts of the Yakutat mélange. This arc, however correlates to the range of the other clasts as well as the knockers.

The age distributions of rocks between the Bonanza arc and the Talkeetna arc are very similar as they both had magmatic production in the Jurassic. The Bonanza rocks and the Talkeetna rocks yield very similar geochemical ranges of major elements (see Figure 2 from D'souza et al., 2016). Much of the trace element geochemistry are similar between the Talkeetna and the Bonanza (see Figure 3 from D'souza et al., 2016), with a few small differences. For example, in the Bonanza arc rocks, there is a single population that has a positive correlation between Yb and SiO_2 ("normal Yb") while the other population has a low Yb concentration with respect to high SiO_2. This is slightly different to the Yb:SiO_2 of Talkeetna rocks, which show a positive correlation but then negative one when SiO_2 is >65 wt% (see Figure 5 from D'souza et al., 2016) (D'souza et al., 2016). Some major differences do occur between these two arcs: 1) the Bonanza arc does not contain garnet, whereas the Talkeetna arc does; and 2) the geochemistry of the Talkeetna arc shows more scatter in La/Dy and Dy/Yb in as opposed to the Bonanza (see Figure 7 from D'souza et al., 2016) (D'souza et al., 2016).

Western Mélange Belt in Washington

The Western Mélange Belt (WMB) lies to the south of our study area in Washington and British Columbia and consists of metavolcanic rocks (greenstones, volcanic breccia, diabase, peraluminous tuff), meta-igneous rocks (gabbro tonalite, quartz diorite), and metasandsone and chert (Dragovich et al., 2009; 2014 2015). The metamorphic mineralogy includes actinolite, prehnite, pumpellyte, along with chlorite, epidote, titanite (sphene), and calcite as secondary minerals (Dragovich et al., 2009).

The age of the plutonic rocks within the WMB, based on data from Tabor and others (1993), is suggested to be between 170-150 Ma (Dragovich et al., 2015). However, this age only comes from four metagabbro and metatonalite samples (Tabor et al., 1993). The metagabbro rocks can be considered small knockers that have been tectonically emplaced into the sedimentary rocks. These four samples contain two U/Pb dates (^{238}U/^{206}Pb) each, which are: 164 and 173 Ma (metatonalite), 148.1 and 149.8 Ma, 148.2 and 148.1 Ma, and 152 and 148 Ma (Tabor et al., 1993, Table 2). Dragovich and others (2015) infer a full range between 170-150 Ma from these four samples that Tabor and others (1993) dated, however, the majority of these samples are ~150 Ma, with only one sample yielding an age at ~170 Ma.

Within the WMB, a number of metasedimentary rocks were also dated. These rocks include argillite, graywacke, and potassium feldspar bearing sandstones (Tabor et al., 1993). The MDA for the sandstone in the argillite is ~110 Ma (Dragovich et al., 2015). The unit also contains a distinct peak at ~160 Ma, which is similar within the range of the plutonic ages by Tabor and others (1993) (Dragovich et al., 2015). Additional MDAs from three samples of the arkosic

sandstone was determined to be ~74 Ma (Dragovich et al., 2014), ~96 Ma (Dragovich et al., 2009) (Dragovich and others., 2014). These WMB metasediments contain the fossil, *Buchia* fossils from the matrix of the argillite and graywacke beds appear to be Tithonian, and radiolarian are Kimmeridgian to Valanginian (156-131 Ma) (Danner, 1957; Tabor et al., 1993).

Previous work by Tabor and others (1993) suggest that the phyllitic rocks represent the highest metamorphic grade during imbrication of the Paleozoic and Mesozoic rocks. Thus, the minimum age of the mélange formation, based on K-Ar dating, must be ~48 Ma (Tabor et al., 1993), which is consistent with the ZFT cooling ages of the Yakutat block ~50 Ma (Suarez, 2016)

Fossils have been observed within the limestones of the WMB that appear are Permian, Mississippian to Permian, and younger (Late Jurassic to Early Cretaceous) (Brown and Dragovich, 2003). These younger fossils are consistent with the ages of the plutonic and metasedimentary rocks within the WMB (Brown and Dragovich, 2003). The older marble facies within the WMB contained ichthtyolith fragments and other tetrapods that most likely correlate to the Mississippian to the Early Permian (Tabor et al., 1993).

Western Mélange Belt and Yakutat Mélange Comparison

One of the bimodal peaks of plutonic clast RF16-23B.1 is at 154.6 ± 2.3 Ma and very close to the majority of the plutonic ages of the WMB. Thus, there is the possibility that the plutonic clasts in the conglomerate within the mélange of Yakutat Bay and the plutonic rocks of the WMB are similar. It also appears that the WMB geochemistry and the Yakutat mélange geochemistry are similar.

To further correlate the two units of the western mélange belt and the Yakutat mélange, I have compared five geochemical discriminant diagrams between the two units. All discriminant diagrams for the WMB comes from the Macdonald and others (2014) using data from Vance and others (1980), Tabor (1994), & Dragovich and others (2009, 2013, 2014).

The discriminant diagram from Pearce and others (1984) can be used to determine the tectonic setting of the plutonic rocks by using Rb-Y-Nb. After this analysis and comparison, it appears that all the samples within the WMB and the Yakutat mélange are of a volcanic arc setting (Macdonald et al., 2014) (Figure 18). The majority of the samples from the WMB and the Yakutat mélange are metaluminous and magnesian-rich rocks (Figure 19; Figure 20). Samples B2 and B7 from the Yakutat mélange are peraluminous and one metatuff and one metatrondhjemite samples out of six from the WMB are peraluminous, which Macdonald and others (2014) suggest is due to assimilation of high Al sedimentary rocks.

In the alkaline discriminant diagrams for feldspathic igneous rocks designed by Frost et al., (2001) shows that there is variation present between the value of alkaline verse calcic in the samples. For example, all six of the WMB samples were at or below the threshold for calc-alkalic, indicating that they are calcic samples (which correspond to a volcanic arc setting (Macdonald et al., 2014), while the samples from the Yakutat mélange are more variable (Figure 21). Clast B1 is the only sample from the Yakutat mélange that yielded a level below the calc-alkalic threshold whereas B7 and 16 yielded values as high as alkali-calcic (Figure 21). Because these rocks have been metamorphosed, the alkalis are mobile and may be the reason for variation. In conclusion, I hypothesize that geochemistry data for the WMB and the Yakutat mélange, further supports the hypothesis that we concluded from the geochronology data that there is a chance of these plutonic samples represent the same source.
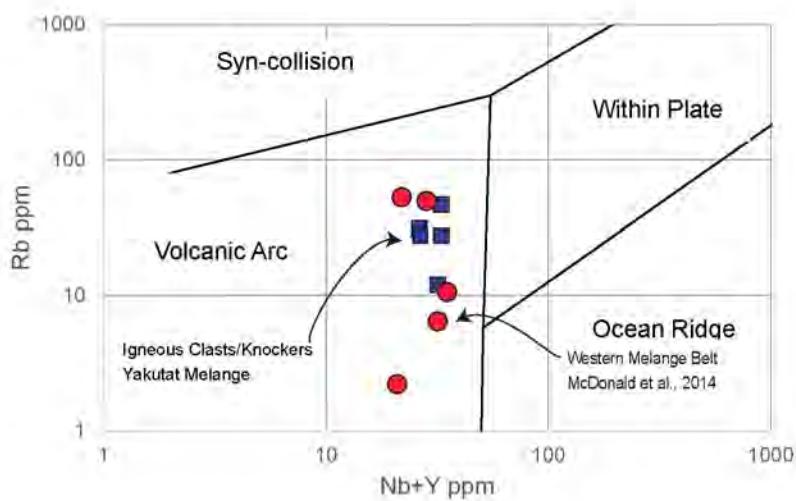
Figure 18 *Discriminate diagram comparing Rb verse Y + Nb for the WMB geochemistry of felsic samples of the Western Melange Belt from Vance and others (1980), Tabor (1994), & Dragovich and others (2009, 2013, 2014) (from Macdonald et al., 2014) (Figure 14) to plutonic samples from the Yakutat mélange. Diagram from Pearce and others (1984). All samples WMB and Yakutat samples plot within the volcanic arc section.*
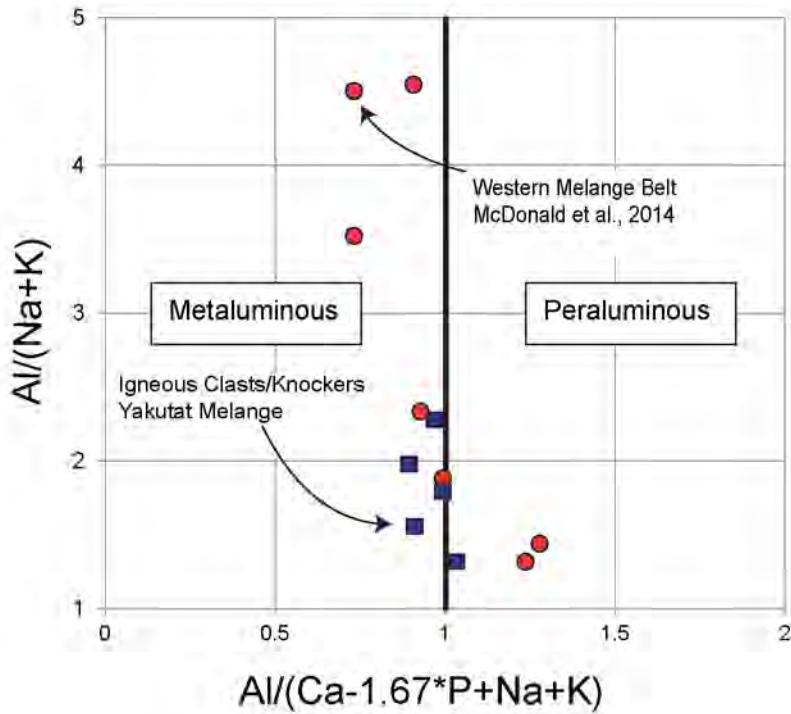
Figure 19: *Discriminate diagram from comparing plutonic samples from the Western Mélange Belt (see Macdonald and others (2014) (Figure 13)), which uses the geochemical analysis done by from Vance and others (1980), Tabor (1994), & Dragovich and others (2009, 2013, 2014) to plutonic samples from the Yakutat mélange. Diagram is from Frost and others (2001) showing the aluminum saturation index (ASI) on the x-axis. For the western mélange belt plutonic and tuff samples, 4/6 samples within the WMB appear to be metaluminous (one metatuff and one metatrondhjemite are peraluminous, which may have been because of assimilation (Macdonald et al., 2014). 4/5 samples within the Yakutat mélange appear to me metaluminous. When comparing the ASI between the WMB and Yakutat mélange, it appears that the data is very similar and this is consistent with a volcanic arc setting (Figure 5) (Macdonald et al., 2014).*
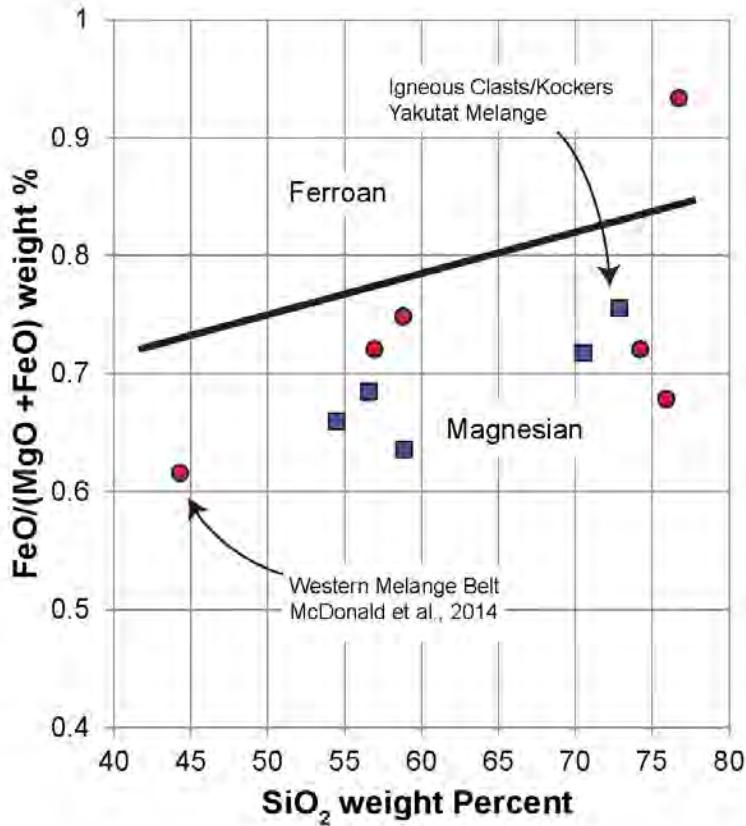
Figure 20 *A) Discriminant diagram comparing Fe-number verse SiO$_2$ for the Western Mélange Belt plutonic and tuff samples from Vance and others (1980), Tabor (1994), & Dragovich and others (2009, 2013, 2014) (from Macdonald et al., 2014 (Figure 11)) and plutonic samples of the Yakutat mélange. Diagram is from Frost and others (2001). All but one WMB sample plots as magnesian-rich. This discriminate diagram shows a strong correlation between the WMB and Yakutat mélange and this is consistent with a volcanic arc setting (Figure 5) (Macdonald et al., 2014).*
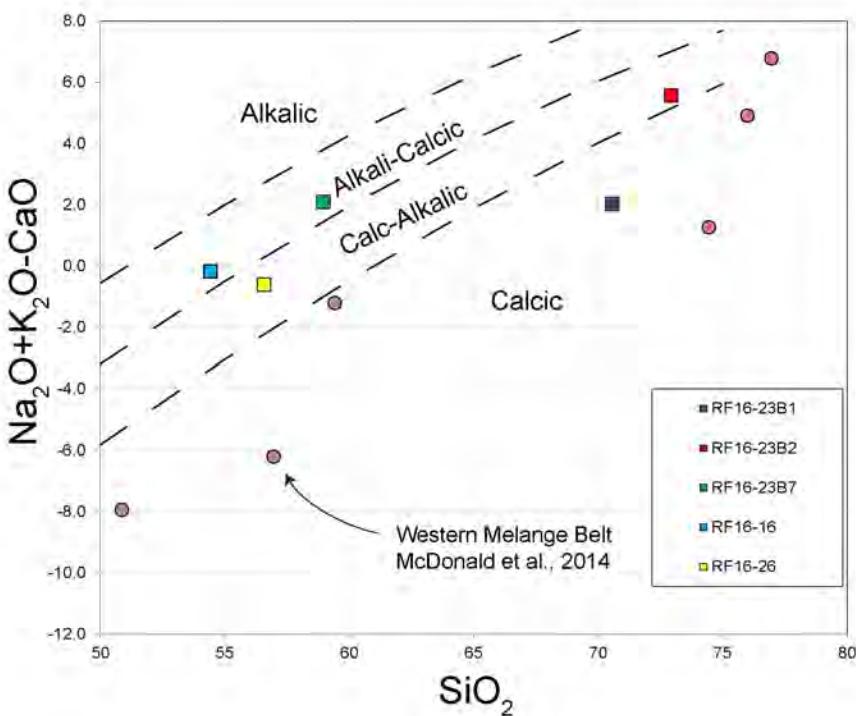
Figure 21: *Discriminant diagram comparing modified alkali lime index (MALI) verse SiO$_2$ for the Western Mélange Belt plutonic and tuff samples from Vance and others (1980), Tabor (1994), & Dragovich and others (2009, 2013, 2014) (Macdonald et al., 2014 (Figure 14)) and plutonic samples from the Yakutat mélange. Diagram is from Frost and others. (2001). The samples from the WMB are generally calcic to calc-alkalic. This result is consistent with a volcanic arc setting (Figure 5) (Macdonald et al., 2014). Plutonic rocks from the Yakutat mélange plot differently. Clasts: B1 plots as calcic, B2 as calc-alkalic, and B7 as alkali-calcic. Knockers: 16 plots as alkali-calcic and 26 as calc-alkalic.*

CONCLUSION

Plutonic clasts and knockers of the Yakutat Group mélange appear to be similar and correlated to the Western Mélange Belt in Washington, United States. This idea supports previous translation hypotheses regarding Cordilleran geology on the western margin of North America such as hypotheses by Garver and Davidson (2015) and Cowan (2003). If the Yakutat Group mélange and the Western Mélange Belt are in fact similar, a key question to consider for future research is a potential provenance of the Western Mélange Belt. The Bonanza arc on Vancouver Island may be ruled out as a potential provenance based on the U/Pb dates. No published dates from the Bonanza arc are similar to the ~155 Ma population of clast RF16-23b1 and if there was any contamination due to the sedimentary system, there would most-likely be a 70-90 Ma population.

Similarly, the Talkeetna arc is also an unlikely potential provenance of the Yakutat mélange if the correlation between the Western Mélange Belt and Yakutat Group mélange is correct. Although the Talkeetna arc contains plutonic U/Pb dates that suggest an age population around~155 Ma

similar to the clast RF16-23b1, it is situated near the current location of the Yakutat mélange and not near the Western mélange belt. Also, none of the three plutonic samples (B1, B2, and B7) appear to have garnet, which is not consistent for the Talkeetna arc.

Because the maximum depositional age of the detrital sandstones from both conglomerate units, RF16-23a and RF16-25a are similar to the ages of both the Yakutat Group mélange, and the Western Mélange Belt, I predict that the sedimentary deposition within the Yakutat mélange must have occurred during the formation of the mélange itself before it was translated. Given this hypothesis, the current separation of the Yakutat mélange from the Western Mélange Belt and timing of translation to Alaska is currently unknown and will involve additional research, but it likely postdates the 65 Ma MDA of the sandstone deposition.

Although the initial provenance of the Yakutat mélange and Western Mélange Belt is unknown, I hypothesize that it must be nearby, either adjacent to or south of, the current location of the Western Mélange Belt. This source must be a juvenile volcanic arc with Jurassic plutonic rocks that are generally metaluminous and magnesian-rich, and include a U/Pb age population at ~155 Ma. Potential sources, if locally derived, may include the Decatur terrane and the Fildalgo Complex (San Juan Islands) or perhaps the Nooksack Group, Harrison Lake, Wells Creek Volcanics (Northern Cascades). Additional U/Pb dates from plutonic rocks of the Yakutat mélange and Western Mélange Belt would be useful for this investigation. Trace element geochemistry on plutonic rocks could also play major role in locating the provenance of the Yakutat mélange and Western Mélange Belt as well as provide support or potentially contradict this correlation between the two mélange units.

The strong similarities between the plutonic rocks observed in the Yakutat Group mélange as conglomerate clasts and knockers, and the plutonic rocks of the Western Mélange Belt suggest that these two units may have once been adjacent to one another. Therefore, I hypothesize that the Yakutat Group mélange has most-likely been displaced at least ~1300 km to the north due to the system of dextral strike-slip faulting, similarly to Cowan's (2003) Baranof-Leech River hypothesis. Like Baranof Island and the Leech River rocks once being continuous and adjacent to each other, the Yakutat Group mélange and the Western Mélange Belt could have also been continuous based upon the data analyses.

REFERENCES

Amato, J. M., Rioux, M. E., Kelemen, P. B., Gehrels, G. E., Clift, P. D., Pavlis, T. L., & Draut, A. E., 2007, U-Pb geochronology of volcanic rocks from the Jurassic Talkeetna Formation and detrital zircons from prearc and postarc sequences: Implications for the age of magmatism and inheritance in the Talkeetna arc. *Geological Society of America Special Papers*, *431*, 253-271.

Barker, F., 1979, Trondhjemite: Definition, environment, and hypotheses of origin: p. 1-12, in Barker, F., ed., Trondhjemites, Dacites, and Related Rocks, Elsevier, Amsterdam, 659 p.

Bol, A. J., Coe, R. S., Gromme, C. S., and Hillhouse, J. W., 1992, Paleomagnetism of the Resurrection Peninsula, Alaska: Implications for the tectonics of southern Alaska and the Kula-Farallon ridge: Journal of Geophysical Research, v. 97, p. 17,213-17,232.

Breitsprecher, K., Thorkelson, D.J., Groome, W.G. and Dostal, J., 2003, Geochemical confirmation of the Kula-Farallon slab window beneath the Pacific Northwest in Eocene time. *Geology*, *31*(4), pp.351-354.

Brown, E. H., & Dragovich, J. D., 2003, *Tectonic elements and evolution of northwest Washington.* Washington Division of Geology and Earth Resources.

Brown, E. H., & Gehrels, G. E., 2007,. Detrital zircon constraints on terrane ages and affinities and timing of orogenic events in the San Juan Islands and North Cascades, Washington. *Canadian Journal of Earth Sciences*, *44*(10), 1375-1396.

Bruns, T. R., 1983, Model for the origin of the Yakutat block, an accreting terrane in the northern Gulf of Alaska. *Geology*, *11*(12), 718-721.

Canil, D., Styan, J., Larocque, J., Bonnet, E., & Kyba, J., 2010, Thickness and composition of the Bonanza arc crustal section, Vancouver Island, Canada. *Geological Society of America Bulletin*, B26578-1.

Collinson, C. W.,1963, Collection and preparation of conodonts through mass production techniques. *Circular no. 343.*

Cowan, D. S., 2003, Revisiting the Baranof–Leech River hypothesis for early Tertiary coastwise transport of the Chugach–Prince William terrane.*Earth and Planetary Science Letters*, *213*(3), 463-475.

Cowan, D. S., Brandon, M. T., & Garver, J. I. 1997. Geologic tests of hypotheses for large coastwise displacements-A critique illustrated by the Baja British Columbia controversy. *American Journal of Science*, *297*(2), 117-173.

Danner, W.R., 1957, A stratigraphic reconnaissance in the northwestern Cascade Mountains and San Juan Islands: Seattle, University of Washington, Ph.D. dissertation, 561 p.

D'Souza, R. J., Canil, D., & Creaser, R. A., 2016, Assimilation, differentiation, and thickening during formation of arc crust in space and time: The Jurassic Bonanza arc, Vancouver Island, Canada. *Geological Society of America Bulletin*, *128*(3-4), 543-557.

Davis, A. S., & Plafker, G., 1986, Eocene basalts from the Yakutat terrane: Evidence for the origin of an accreting terrane in southern Alaska. *Geology*, *14*(11), 963-966.

Doubrovine, P.V. and Tarduno, J.A., 2008, A revised kinematic model for the relative motion between Pacific oceanic plates and North America since the Late Cretaceous. *Journal of Geophysical Research: Solid Earth*, *113*(B12).

Dragovich, J. D., Mahan, S. A., Anderson, M. L., MacDonald Jr, J. H., Schilter, J. F., Frattali, C. L., Koger, C. J., Smith, D T., Stoker, S., DuFrane, A. S., Eddy, M. P., Cakir, Recep, & Sauer, K. B., 2015, Geologic Map of the Lake Roesiger 7.5-Minute Quadrangle, Snohomish County, Washington.

Dragovich, J. D.; Frattali, C. L.; H. A.; Anderson, M. L.; Mahan, S. A.; MacDonald, J. H., Jr.; Stoker, B. A.; Smith, D. T.; Koger, C. J.; Cakir, Recep; Dufrane, S. A.; Sauer, K. B., 2014, Geologic map of the Lake Chaplain 7.5- minute quadrangle, Snohomish County, Washington: Washington Division of Geology and Earth Resources Map Series 2014-01, 1 sheet, scale 1:24,000, with 51 p. text.

Dragovich, J. D.; Littke, H. A.; Mahan, S. A.; Anderson, M. L.; MacDonald, J. H., Jr.; Cakir, Recep; Stoker, B. A.; Koger, C. J.; Bethel, J. P.; Dufrane, S. A.; Smith, D. T.; Villeneuve, N. M., 2013, Geologic map of the Sultan 7.5- minute quadrangle, King and Snohomish Counties, Washington: Washington Division of Geology and Earth Resources Map Series 2013-01, 1 sheet, scale 1:24,000, 52 p

Dragovich, J. D.; Littke, H. A.; Anderson, M. L.; Hartog, Renate; Wessel, G. R.; DuFrane, S. A.; Walsh, T. J.; MacDonald, J. H., Jr.; Mangano, J. F.; Cakir, Recep, 2009, Geologic map of the Snoqualmie 7.5-minute quadrangle, King County, Washington: Washington Division of Geology and Earth Resources Geologic Map GM-75, 2 sheets, scale 1:24,000.

Dumoulin, J. A., 1987, Sandstone composition of the Valdez and Orca Groups, Prince William Sound, Alaska: U.S. Geological Survey Bulletin 1774, 37 p.

Enkelmann, E., Koons, P. O., Pavlis, T. L., Hallet, B., Barker, A., Elliott, J., ... & Ridgway, K. D. (2015). Cooperation among tectonic and surface processes in the St. Elias Range, Earth's highest coastal mountains. *Geophysical Research Letters*, *42*(14), 5838-5846.

Enkelmann, E., Zeitler, P. K., Garver, J. I., Pavlis, T. L., & Hooks, B. P., 2010, The thermochronological record of tectonic and surface process interaction at the Yakutat– North American collision zone in southeast Alaska. *American Journal of Science*, *310*(4), 231-260.

Farris, D. W., 2009, Construction and evolution of the Kodiak Talkeetna arc crustal section, southern Alaska. *Geological Society of America Special Papers*, *456*, 69-96.

Frost, B. R., Barnes, C. G., Collins, W. J., Arculus, R. J., Ellis, D. J., & Frost, C. D., 2001, A geochemical classification for granitic rocks. *Journal of petrology*, *42*(11), 2033-2048.

Gallen, S. F., ms, 2008, An investigation of the magnetic fabrics and the paleomagnetism of the Ghost Rocks Formation, Kodiak Islands, Alaska: Bellingham, Washington, Western Washington University, Master of Science Thesis, 119 p.

Garver, J. I., & Davidson, C. M., 2015, Southwestern Laurentian zircons in Upper Cretaceous flysch of the Chugach-Prince William terrane in Alaska. *American Journal of Science*, *315*(6), 537-556.

Garver, J. I., & Kamp, P. J., 2002, Integration of zircon color and zircon fission-track zonation patterns in orogenic belts: application to the Southern Alps, New Zealand. Tectonophysics, 349(1), 203-219.

Gasser, D., Bruand, E., Rubatto, D., & Stüwe, K., 2012, The behaviour of monazite from greenschist facies phyllites to anatectic gneisses: An example from the Chugach Metamorphic Complex, southern Alaska. *Lithos*, *134*, 108-122.

Gehrels, G., 2010, U-Th-Pb analytical Methods. Arizona Laserchron Center, University of Arizona.

Gehrels, G., Valencia, V., & Pullen, A., 2006, Detrital zircon geochronology by laser-ablation multicollector ICPMS at the Arizona LaserChron Center. *Paleontological Society Papers*, *12*, 67.

Gehrels, G., Valencia, V., & Ruiz, J., 2008, Enhanced precision, accuracy, efficiency, and spatial resolution of U-Pb ages by laser ablation-multicollector-inductively coupled plasma-mass spectrometry: Geochemistry, Geophysics, Geosystems, v. 9, Q03017.

Grimm, B., 2015, Provenance of the Chugach-Prince William terrane, Alaska, focusing on the Paleogene Orca Group using U-Pb dating of detrital zircons: Short Contributions, Keck Geology Consortium 28th Annual Symposium Volume, Union College, NY

Haeussler, P. J., Bradley, D. C., Wells, R. E., & Miller, M. L., 2003, Life and death of the Resurrection plate: Evidence for its existence and subduction in the northeastern Pacific in Paleocene–Eocene time. *Geological Society of America Bulletin*, *115*(7), 867-880.

Hilbert-Wolf, H.L., 2012, U/Pb detrital zircon provenance of the flysch of the Paleogene Orca Group, Chugach-Prince William terrane, Alaska; Proceedings from the 25th Keck Geology Consortium Undergraduate Research Symposium, Amherst MA, 23-32

Housen, B. A., & Beck, M. E., 1999, Testing terrane transport: An inclusive approach to the Baja BC controversy. *Geology*, *27*(12), 1143-1146.

Housen, B. A., Roeske, S. M., Gallen, S., & O'Connell, K., 2008, Paleomagnetism of the Paleocene Ghost Rocks, Kodiak Islands, Alaska: Implications for Paleocene Pacific-Basin/North America plate configurations. In *AGU Fall Meeting Abstracts*.

Keller, G., Huene, R., McDougall, K., & Bruns, T. R., 1984, Paleoclimatic evidence for Cenozoic migration of Alaskan terranes. *Tectonics*, *3*(4), 473-495.

LeBas, M.J., LeMaitre, R.W., Streckeisen, A., and Zanettin, B., 1986, A chemical classification of volcanic rocks based on the total alkali-silica diagram: Journal of Petrology, v. 27, p. 745-750.

Macdonald Jr, J.H., Dragovich, J.D., Frattali, C.L., Anderson, M., Stoker, B.A., Littke, H.A., … & Koger, C.J., 2014, Geochemistry of Metaigneous Rocks from the Western Melange Belt, Lake Chaplain, Snoqualmue, and Sultan 7.5 Minute Quadrangles, Western Cascades, Washington. Evidence for a Predominantly Volcanic Arc Setting. In *2014 GSA Annual Meeting in Vancouver, British Columbia.*

Mahoney, J. B., Mustard, P. S., Haggart, J. W., Friedman, R. M., Fanning, C. M., & McNicoll, V. J. 1999, Archean zircons in Cretaceous strata of the western Canadian Cordillera: The "Baja BC" hypothesis fails a "crucial test".*Geology*, *27*(3), 195-198.

Marsellos, A.E. and Garver, J.I., 2010, Radiation damage and uranium concentration in zircon as assessed by Raman spectroscopy and neutron irradiation. American Mineralogist, 95(8-9), pp.1192-1201.

Middlemost, E.A., 1994, Naming materials in the magma/igneous rock system: Earth-Science Reviews, v. 37, p. 215-224.

Münker, C., Weyer, S., Scherer, E., & Mezger, K., 2001, Separation of high field strength elements (Nb, Ta, Zr, Hf) and Lu from rock samples for MC-ICPMS measurements. *Geochemistry, Geophysics, Geosystems*, *2*(12)

Pearce, J.A., Harris, N.B.W., and Tindle, A.G., 1984, Trace element discrimination diagrams for the tectonic interpretation of granitic rocks: Journal of Petrology, v. 25, p.

Perry, S.E., Garver, J.I. and Ridgway, K.D., 2009, Transport of the Yakutat terrane, southern Alaska: Evidence from sediment petrology and detrital zircon fission-track and U/Pb double dating. The Journal of Geology, 117(2), pp.156-173.

Plafker, G., Moore, J. C., and Winkler, G. R., 1994, Geology of the southern Alaska margin, in Plafker, G., and Berg, H. C., editors, The Geology of Alaska: Boulder, Colorado, Geological Society of America, The Geology of North America, v. G-1, p. 389–449.

Plumley, P. W., Coe, R. S., Byrne, T., Reid, M. R., and Moore, J. C., 1982, Paleomagnetism of the volcanic rocks of the Kodiak Islands indicates northward latitudinal displacement: Nature, v. 300, p. 50–52.

Rioux, M., Hacker, B., Mattinson, J., Kelemen, P., Blusztajn, J., & Gehrels, G., 2007, Magmatic development of an intra-oceanic arc: High-precision U-Pb zircon and whole-rock isotopic analyses from the accreted Talkeetna arc, south-central Alaska. *Geological Society of America Bulletin*, *119*(9-10), 1168-1184.

Rioux, M., Mattinson, J., Hacker, B., Kelemen, P., Blusztajn, J., Hanghøj, K., & Gehrels, G., 2010, Intermediate to felsic middle crust in the accreted Talkeetna arc, the Alaska Peninsula and Kodiak Island, Alaska: An analogue for low-velocity middle crust in modern arcs. *Tectonics*, *29*(3).

Samson, S. D., Patchett, P. J., McClelland, W. C., & Gehrels, G. E., 1991, Nd isotopic characterization of metamorphic rocks in the Coast Mountains, Alaskan and Canadian Cordillera: ancient crust bounded by juvenile terranes. *Tectonics*, *10*(4), 770-780.

Sisson, V. B., Poole, A. R., Harris, N. R., Burner, H. C., Pavlis, T. L., Copeland, P, Donelick, R. A.,& McLelland, W. C., 2003, Geochemical and geochronologic constraints for genesis of a tonalite-trondhjemite suite and associated mafic intrusive rocks in the eastern Chugach Mountains, Alaska: A record of ridge-transform subduction. *Special Papers-Geological Society of America*, 293-326.

Söderlund, U., Patchett, P. J., Vervoort, J. D., & Isachsen, C. E., 2004, The 176 Lu decay constant determined by Lu–Hf and U–Pb isotope systematics of Precambrian mafic intrusions. *Earth and Planetary Science Letters*, *219*(3), 311-324.

Stacey, J.T. and Kramers, J., 1975, Approximation of terrestrial lead isotope evolution by a two-stage model. Earth and planetary science letters, 26(2), p.207-221.

Streckeisen, A., 1967, Classification and nomenclature of igneous rocks. Nues Jarbuch fur Mineralogie Abhandlungen, v. 107, p. 144-240.

Suarez, K. A., 2016, Thermal Evolution and Provenance Revealed Through Detrital Zircon Fission Track Dating of the Yakutat Group, Yakutat Bay, Alaska. Unpublished BSc Thesis, Union College Geology Department, 59 pp.

Tabor, R.W., 1994, Late Mesozoic and possible early Tertiary accretion in western Washington State: The Helena-Haystack mélange and the Darrington–Devils Mountain fault zone: Geological Society of America Bulletin, v. 106, p. 217–232.

Tabor, R. W., Frizzell, Jr, V.A., Booth, R.B., Whetten, J.T., and Zartman, R.E., 1993, Geologic map of the Skykomish River 30-by 60-minute quadrangle, Washington.

Tysdal, R. G., and Case, J. E., 1979, Geologic map of the Seward and Blying Sound quadrangles, Alaska: U.S. Geological Survey Miscellaneous Investigations Series Map 1-1150.

Vance, J. A., Blanchard, D. P., Rhodes, J. M., & Dungan, M. A., 1980, Tectonic setting and trace element geochemistry of Mesozoic ophiolitic rocks in western Washington. *American Journal of Science*, *280*(Part I), 359-388.

Vervoort, J. D., & Blichert-Toft, J. 1999, Evolution of the depleted mantle: Hf isotope evidence from juvenile rocks through time. *Geochimica et Cosmochimica Acta*, *63*(3), 533-556.

Vervoort, J. D., & Patchett, P. J. 1996, Behavior of hafnium and neodymium isotopes in the crust: constraints from Precambrian crustally derived granites. *Geochimica et Cosmochimica Acta*, *60*(19), 3717-3733.

Vervoort, J. D., Patchett, P. J., Blichert-Toft, J., & Albarède, F. 1999, Relationships between Lu–Hf and Sm–Nd isotopic systems in the global sedimentary system. *Earth and Planetary Science Letters*, *168*(1), 79-99.

Wilson, F.H., Labay, K. A., Shew, N.B., Preller, C.C., Mohadjer, S., Richter, D.H., 2005, Preliminary integrated geologic map databases for the United States: digital data for the geology of Wrangell-Saint Elias National Park and Preserve, Alaska: U.S. Geological Survey Open-File Report 2005-1342

Woodhead, J., Hergt, J., Shelley, M., Eggins, S., & Kemp, R. 2004, Zircon Hf-isotope analysis with an excimer laser, depth profiling, ablation of complex geometries, and concomitant age estimation. *Chemical Geology*, *209*(1), 121-135.

Worthington, L. L., Van Avendonk, H. J., Gulick, S. P., Christeson, G. L., & Pavlis, T. L., 2012, Crustal structure of the Yakutat terrane and the evolution of subduction and collision in southern Alaska. *Journal of Geophysical Research: Solid Earth*, *117*(B1).

APPENDIX A:

Sample GPS Coordinates

Sample	Unit	General Description	GSP Coordinates	U/Pb Data	Geochemistry Data	Raman Spectroscopy	Hf/Hf
YB-16-06	Yakutat Group Mélange Facies	Sandstone	59.94009°N, 139.53526°W	Y			
RF16-04	Schist of Nunatak Fjord	Sandstone	59.84210°N, 139.09860°W	Y			
RF16-16	Yakutat Group Tonalite Mass	Plutonic Knocker	59.93722°N, 139.39713°W	Y	Y		Y
RF16-26	Yakutat Group Tonalite Mass	Plutonic Knocker	59.85071°N, 139.31404°W	Y	Y		
RF16-23A*	Yakutat Group Flysch Facies	Sandstone	59.982948°N, 139.29526°W	Y		Y	
RF16-23B1	Yakutat Group Flysch Facies	Plutonic Clast	59.982948°N, 139.29526°W	Y	Y		
RF16-23B2	Yakutat Group Flysch Facies	Plutonic Clast	59.982948°N, 139.29526°W	Y	Y		Y
RF16-23B3	Yakutat Group Flysch Facies	Plutonic Clast	59.982948°N, 139.29526°W				
RF16-23B4	Yakutat Group Flysch Facies	Plutonic Clast	59.982948°N, 139.29526°W				
RF16-23B5	Yakutat Group Flysch Facies	Plutonic Clast	59.982948°N, 139.29526°W				
RF16-23B6	Yakutat Group Flysch Facies	Plutonic Clast	59.982948°N, 139.29526°W				
RF16-23B7	Yakutat Group Flysch Facies	Plutonic Clast	59.982948°N, 139.29526°W		Y		
RF16-23B8	Yakutat Group Flysch Facies	Plutonic Clast	59.982948°N, 139.29526°W				
RF16-23B9	Yakutat Group Flysch Facies	Plutonic Clast	59.982948°N, 139.29526°W				
RF16-23B10	Yakutat Group Flysch Facies	Plutonic Clast	59.982948°N, 139.29526°W				
RF16-23B12	Yakutat Group Flysch Facies	Plutonic Clast	59.982948°N, 139.29526°W				
RF16-23B13	Yakutat Group Flysch Facies	Plutonic Clast	59.982948°N, 139.29526°W				
RF16-23B14	Yakutat Group Flysch Facies	Plutonic Clast	59.982948°N, 139.29526°W				

Sample	Unit	Lithology	Coordinates	
RF16-23B15	Yakutat Group Flysch Facies	Plutonic Clast	59.982948°N, 139.29526°W	
RF16-23B16	Yakutat Group Flysch Facies	Plutonic Clast	59.982948°N, 139.29526°W	
RF16-23C1	Yakutat Group Flysch Facies	Limestone Clast	59.982948°N, 139.29526°W	
RF16-23C2	Yakutat Group Flysch Facies	Limestone Clast	59.982948°N, 139.29526°W	
RF16-23C3	Yakutat Group Flysch Facies	Limestone Clast	59.982948°N, 139.29526°W	
RF16-23C4	Yakutat Group Flysch Facies	Limestone Clast	59.982948°N, 139.29526°W	
RF16-23C5	Yakutat Group Flysch Facies	Limestone Clast	59.982948°N, 139.29526°W	
RF16-23C6	Yakutat Group Flysch Facies	Limestone Clast	59.982948°N, 139.29526°W	
RF16-23C7	Yakutat Group Flysch Facies	Limestone Clast	59.982948°N, 139.29526°W	
RF16-23C8	Yakutat Group Flysch Facies	Limestone Clast	59.982948°N, 139.29526°W	
RF16-23D	Yakutat Group Flysch Facies	Sandstone Clast	59.982948°N, 139.29526°W	
RF16-25A*	Yakutat Group Mélange Facies	Sandstone	59.83974°N, 139.32799°W	
RF16-25B1	Yakutat Group Mélange Facies	Sandstone Clast	59.83974°N, 139.32799°W	
RF16-25B2	Yakutat Group Mélange Facies	Sandstone Clast	59.83974°N, 139.32799°W	Y
RF16-25B3	Yakutat Group Mélange Facies	Sandstone Clast	59.83974°N, 139.32799°W	
RF16-25C1	Yakutat Group Mélange Facies	Limestone Clast	59.83974°N, 139.32799°W	
RF16-25C2	Yakutat Group Mélange Facies	Limestone Clast	59.83974°N, 139.32799°W	
RF16-25C3	Yakutat Group Mélange Facies	Limestone Clast	59.83974°N, 139.32799°W	

Notes

1) * Indicates handpicked Precambrian grains.
2) Not all sample listed in this appendix are included within this thesis. This thesis is a collaborative project with various researchers.

APPENDIX B:

U/Pb Data Tables

| Analysis | U | 206Pb | U/Th | Isotope ratios | | | | | | | Apparent ages (Ma) | | | | | | | |
| | | | | 206Pb* | ± | 207Pb* | ± | 206Pb* | ± | error | 206Pb* | ± | 207Pb* | ± | 206Pb* | ± | Best age | ± |
	(ppm)	204Pb		207Pb*	(%)	235U*	(%)	238U	(%)	corr.	238U*	(Ma)	235U	(Ma)	207Pb*	(Ma)	(Ma)	(Ma)
Sample, RF16-25A, Yakutat Group Melange Facies, (59.83974°, -139.32799°)																		
RF16-25A-149	243	4383	2.7	21.991	2.4	0.0636	4.3	0.0102	3.5	0.83	65.1	2.3	62.6	2.6	NA	NA	65.1	2.3
RF16-25A-171	314	5270	3.4	21.567	1.8	0.0655	3.1	0.0102	2.6	0.82	65.7	1.7	64.4	2.0	16.7	43.5	65.7	1.7
RF16-25A-224	546	7145	2.9	21.546	1.6	0.0657	3.4	0.0103	3.0	0.88	65.9	1.9	64.6	2.1	19.1	38.4	65.9	1.9
RF16-25A-131	290	3814	2.4	22.852	2.3	0.0624	3.5	0.0104	2.7	0.75	66.4	1.8	61.5	2.1	NA	NA	66.4	1.8
RF16-25A-169	641	4713	1.2	22.416	2.3	0.0642	3.1	0.0104	2.2	0.69	67.0	1.4	63.2	1.9	NA	NA	67.0	1.4
RF16-25A-213	368	6831	3.7	21.399	1.8	0.0674	3.4	0.0105	2.9	0.85	67.1	1.9	66.2	2.2	35.5	43	67.1	1.9
RF16-25A-145	228	4311	2.2	22.643	2.3	0.0642	3.4	0.0106	2.4	0.72	67.7	1.6	63.2	2.1	NA	NA	67.7	1.6
RF16-25A PC-71	388	6055	5.6	21.584	2.1	0.0686	3.7	0.0107	3.0	0.82	68.9	2.1	67.4	2.4	14.8	50.3	68.9	2.1
RF16-25A-136	163	2799	3.0	23.000	4.9	0.0647	5.5	0.0108	2.5	0.45	69.3	1.7	63.7	3.4	NA	NA	69.3	1.7
RF16-25A PC-35	203	57871	1.6	20.601	2.2	0.0725	3.7	0.0108	3.0	0.80	69.5	2.1	71.1	2.6	125.8	52.7	69.5	2.1
RF16-25A-184	761	15022	5.8	21.071	1.6	0.0709	2.9	0.0108	2.4	0.83	69.5	1.7	69.6	2.0	72.4	39	69.5	1.7
RF16-25A-143	249	28029	1.9	19.788	1.7	0.0757	3.6	0.0109	3.1	0.88	69.6	2.2	74.0	2.6	219.7	40	69.6	2.2
RF16-25A-91	168	1573	1.2	24.380	3.4	0.0620	5.5	0.0110	4.3	0.78	70.4	3.0	61.1	3.3	NA	NA	70.4	3.0
RF16-25A PC-66	179	12388	1.6	21.189	2.5	0.0718	4.0	0.0110	3.1	0.78	70.8	2.2	70.4	2.7	59.1	59.5	70.8	2.2
RF16-25A-202	387	67485	5.9	20.997	2.2	0.0727	4.1	0.0111	3.4	0.85	71.0	2.4	71.2	2.8	80.8	51.5	71.0	2.4
RF16-25A-95	165	4580	1.8	21.015	2.8	0.0729	4.1	0.0111	3.0	0.73	71.3	2.1	71.5	2.8	78.7	65.7	71.3	2.1
RF16-25A-87	252	3446	5.9	23.063	2.5	0.0668	3.7	0.0112	2.7	0.73	71.6	1.9	65.6	2.4	NA	NA	71.6	1.9
RF16-25A-301	97	2321	1.8	22.434	4.3	0.0689	5.1	0.0112	2.8	0.54	71.9	2.0	67.7	3.3	NA	NA	71.9	2.0
RF16-25A-295	242	10184	5.5	21.310	2.4	0.0727	3.7	0.0112	2.9	0.77	72.0	2.1	71.2	2.6	45.5	56.6	72.0	2.1
RF16-25A-158	340	3510	3.4	21.782	3.3	0.0711	4.0	0.0112	2.3	0.56	72.1	1.6	69.8	2.7	NA	NA	72.1	1.6
RF16-25A-244	415	3870	2.3	22.667	2.8	0.0684	3.5	0.0113	2.1	0.60	72.1	1.5	67.2	2.3	NA	NA	72.1	1.5
RF16-25A-288	541	2054047	2.3	21.245	1.6	0.0736	2.7	0.0113	2.2	0.80	72.7	1.6	72.1	1.9	52.8	39.2	72.7	1.6
RF16-25A-197	207	2607	2.2	23.799	7.1	0.0658	7.6	0.0114	2.5	0.33	72.8	1.8	64.7	4.7	NA	NA	72.8	1.8
RF16-25A-128	118	12442	1.4	21.715	2.8	0.0727	4.0	0.0115	2.9	0.73	73.5	2.1	71.3	2.8	NA	NA	73.5	2.1
RF16-25A-117	172	2116	2.1	24.118	2.4	0.0655	3.2	0.0115	2.0	0.65	73.5	1.5	64.4	2.0	NA	NA	73.5	1.5
RF16-25A-289	225	3072	1.9	22.816	2.6	0.0693	3.8	0.0115	2.8	0.72	73.5	2.0	68.0	2.5	NA	NA	73.5	2.0
RF16-25A-216	273	5494	1.6	21.261	2.1	0.0747	3.3	0.0115	2.5	0.77	73.8	1.9	73.1	2.3	51.0	50	73.8	1.9
RF16-25A-119	751	12643	2.2	21.444	1.1	0.0749	2.2	0.0117	1.9	0.87	74.7	1.5	73.3	1.6	30.5	26.1	74.7	1.5
RF16-25A PC-40	479	4587	2.1	22.577	2.5	0.0716	3.5	0.0117	2.4	0.69	75.2	1.8	70.2	2.3	NA	NA	75.2	1.8
RF16-25A-204	561	67389	2.6	20.519	1.5	0.0792	3.1	0.0118	2.7	0.88	75.5	2.1	77.4	2.3	135.1	34.6	75.5	2.1
RF16-25A-272	491	5529	2.0	21.153	2.0	0.0772	3.0	0.0118	2.2	0.75	75.9	1.7	75.5	2.2	63.1	46.6	75.9	1.7
RF16-25A-280	239	2093	1.4	23.408	3.4	0.0699	4.3	0.0119	2.5	0.59	76.1	1.9	68.6	2.8	NA	NA	76.1	1.9
RF16-25A-270	161	4653	1.2	21.939	4.2	0.0746	5.1	0.0119	2.9	0.57	76.1	2.2	73.1	3.6	NA	NA	76.1	2.2
RF16-25A-238	105	5765	1.5	21.709	4.4	0.0756	5.1	0.0119	2.6	0.51	76.3	2.0	74.0	3.6	NA	NA	76.3	2.0
RF16-25A-273	383	4278	2.4	22.465	3.3	0.0734	4.0	0.0120	2.3	0.56	76.7	1.7	72.0	2.8	NA	NA	76.7	1.7
RF16-25A-113	631	15376	1.6	21.646	1.6	0.0762	3.1	0.0120	2.7	0.85	76.7	2.0	74.6	2.3	7.9	39.7	76.7	2.0
RF16-25A-260	190	2322	2.2	19.255	6.6	0.0860	7.2	0.0120	2.7	0.38	77.0	2.1	83.8	5.8	282.6	151	77.0	2.1
RF16-25A-222	33	725	1.0	32.944	8.6	0.0506	9.6	0.0121	4.2	0.43	77.4	3.2	50.1	4.7	NA	NA	77.4	3.2
RF16-25A-250	277	10771	1.4	20.855	2.5	0.0803	3.4	0.0121	2.3	0.68	77.8	1.8	78.4	2.6	96.8	58.6	77.8	1.8
RF16-25A-195	106	4820	1.7	22.668	3.6	0.0739	4.4	0.0121	2.6	0.58	77.8	2.0	72.4	3.1	NA	NA	77.8	2.0
RF16-25A-275	244	1025434	2.2	20.549	1.9	0.0816	2.9	0.0122	2.3	0.77	77.9	1.7	79.6	2.3	131.7	44.5	77.9	1.7
RF16-25A-152	244	4099	1.1	21.041	2.1	0.0801	3.2	0.0122	2.4	0.76	78.3	1.9	78.2	2.4	75.7	49.1	78.3	1.9
RF16-25A-200	330	4240	1.7	21.876	2.9	0.0774	3.9	0.0123	2.6	0.66	78.7	2.0	75.7	2.9	NA	NA	78.7	2.0
RF16-25A PC-59	1630	18028	6.7	21.042	1.1	0.0809	2.0	0.0124	1.7	0.83	79.1	1.3	79.0	1.5	75.7	26.9	79.1	1.3
RF16-25A PC-64	1394	20603	7.6	21.361	1.0	0.0803	2.5	0.0124	2.3	0.91	79.8	1.8	78.4	1.9	39.8	24.6	79.8	1.8
RF16-25A-176	216	1796	1.6	24.260	2.4	0.0714	3.4	0.0126	2.4	0.70	80.5	1.9	70.0	2.3	NA	NA	80.5	1.9
RF16-25A PC-38	550	2879	3.7	22.753	1.3	0.0771	2.7	0.0127	2.5	0.86	81.5	1.9	75.4	1.9	NA	NA	81.5	1.9
RF16-25A-236	303	22238	1.6	20.211	2.4	0.0873	3.4	0.0128	2.5	0.73	82.0	2.0	85.0	2.8	170.5	55.1	82.0	2.0
RF16-25A PC-41	3395	962983	13.0	20.743	1.1	0.0858	2.6	0.0129	2.4	0.91	82.7	2.0	83.6	2.1	109.6	25	82.7	2.0
RF16-25A PC-69	3205	175358	364.0	20.856	0.7	0.0856	1.9	0.0130	1.8	0.92	83.0	1.5	83.4	1.6	96.7	17.6	83.0	1.5
RF16-25A-205	784	10257	8.9	20.839	1.4	0.0857	2.6	0.0130	2.2	0.85	83.0	1.8	83.5	2.1	98.6	32	83.0	1.8
RF16-25A PC-4	648	73367	3.9	20.635	1.4	0.0869	2.7	0.0130	2.3	0.85	83.3	1.9	84.6	2.2	121.9	33.1	83.3	1.9
RF16-25A-292	200	53735	2.6	21.261	2.1	0.0847	3.0	0.0131	2.2	0.74	83.7	1.9	82.5	2.3	51.0	49	83.7	1.9
RF16-25A-90	170	11577	2.3	21.554	2.6	0.0846	3.6	0.0132	2.5	0.68	84.7	2.1	82.5	2.9	18.3	63.3	84.7	2.1
RF16-25A-182	2909	77154	15.4	21.317	0.9	0.0861	2.2	0.0133	2.0	0.92	85.3	1.7	83.9	1.7	44.7	20.3	85.3	1.7
RF16-25A-214	708	22976	1.9	20.227	1.6	0.0910	2.8	0.0134	2.3	0.82	85.5	1.9	88.4	2.3	168.7	36.6	85.5	1.9
RF16-25A-207	831	17507	1.6	20.576	1.4	0.0904	2.7	0.0135	2.3	0.85	86.4	2.0	87.9	2.3	128.6	33.8	86.4	2.0
RF16-25A-268	112	16744	0.8	19.748	2.7	0.0944	3.6	0.0135	2.3	0.65	86.6	2.0	91.6	3.2	224.3	63.4	86.6	2.0
RF16-25A-253	264	9463	2.8	20.640	1.9	0.0904	3.2	0.0135	2.6	0.81	86.7	2.2	87.9	2.7	121.3	43.8	86.7	2.2
RF16-25A-168	261	20749	2.4	20.407	2.0	0.0917	3.3	0.0136	2.6	0.79	86.9	2.2	89.1	2.8	148.0	47	86.9	2.2
RF16-25A-134	867	20829	2.5	20.749	1.2	0.0904	2.5	0.0136	2.2	0.88	87.1	1.9	87.9	2.1	108.8	28.6	87.1	1.9
RF16-25A-208	105	6719	3.4	19.905	2.6	0.0943	3.6	0.0136	2.6	0.71	87.2	2.2	91.5	3.2	206.1	59.8	87.2	2.2
RF16-25A-139	390	15122	1.3	20.519	1.8	0.0917	2.6	0.0137	1.9	0.72	87.4	1.6	89.1	2.2	135.1	41.8	87.4	1.6
RF16-25A-173	408	7918	3.3	22.107	2.4	0.0858	3.7	0.0138	2.8	0.76	88.1	2.4	83.6	3.0	NA	NA	88.1	2.4
RF16-25A-228	132	2002	2.3	23.023	2.7	0.0830	4.1	0.0139	3.1	0.75	88.8	2.7	80.9	3.2	NA	NA	88.8	2.7
RF16-25A-120	123	1491	2.5	24.937	4.0	0.0770	4.8	0.0139	2.6	0.54	89.2	2.3	75.3	3.5	NA	NA	89.2	2.3
RF16-25A-206	52	1399	4.2	27.255	7.1	0.0708	7.9	0.0140	3.5	0.45	89.7	3.1	69.5	5.3	NA	NA	89.7	3.1
RF16-25A-88	353	4497	2.6	22.322	1.9	0.0866	2.8	0.0140	2.1	0.73	89.8	1.8	84.3	2.3	NA	NA	89.8	1.8
RF16-25A-283	803	8587	5.3	21.547	1.3	0.0901	2.9	0.0141	2.6	0.90	90.2	2.3	87.6	2.4	19.0	30.5	90.2	2.3
RF16-25A-109	933	210081	1.5	20.753	1.1	0.0937	2.3	0.0141	2.1	0.89	90.3	1.9	90.9	2.0	108.4	25.4	90.3	1.9
RF16-25A-303	562	20917	2.2	20.271	1.7	0.0963	3.3	0.0142	2.8	0.86	90.7	2.5	93.4	2.9	163.6	39.1	90.7	2.5
RF16-25A-305	138	20395	2.5	18.701	2.3	0.1049	3.8	0.0142	3.0	0.79	91.1	2.7	101.3	3.6	349.0	52.7	91.1	2.7
RF16-25A-137	1082	68306	2.5	20.204	1.1	0.0976	2.5	0.0143	2.3	0.91	91.6	2.1	94.6	2.3	171.3	25.1	91.6	2.1
RF16-25A-218	122	2782	1.5	25.077	7.0	0.0787	7.3	0.0143	2.4	0.32	91.6	2.1	76.9	5.4	NA	NA	91.6	2.1
RF16-25A-80	141	4996	5.0	22.103	1.8	0.0893	3.1	0.0143	2.4	0.80	91.6	2.2	86.8	2.5	NA	NA	91.6	2.2
RF16-25A-175	777	11729	3.8	21.135	1.3	0.0935	2.7	0.0143	2.4	0.87	91.8	2.2	90.8	2.4	65.2	31.5	91.8	2.2
RF16-25A-154	1536	314186	174.3	20.496	1.1	0.0968	2.5	0.0144	2.2	0.88	92.1	2.1	93.8	2.2	137.7	24.8	92.1	2.1
RF16-25A-229	1616	26840	3.4	20.639	1.1	0.0962	2.1	0.0144	1.8	0.85	92.2	1.7	93.3	1.9	121.4	26	92.2	1.7
RF16-25A-226	281	7832	1.8	21.724	2.1	0.0916	3.4	0.0144	2.6	0.78	92.4	2.4	89.0	2.9	NA	NA	92.4	2.4
RF16-25A PC-12	1449	69290	9.1	20.716	1.3	0.0962	2.5	0.0145	2.2	0.84	92.5	1.9	93.2	2.2	112.6	31	92.5	1.9
RF16-25A-231	1114	48709	4.6	20.527	1.2	0.0972	2.3	0.0145	1.9	0.84	92.6	1.8	94.2	2.0	134.2	29.2	92.6	1.8
RF16-25A-111	572	22769	2.5	20.836	1.0	0.0964	2.5	0.0146	2.3	0.91	93.3	2.1	93.5	2.3	99.0	24.3	93.3	2.1
RF16-25A-286	1326	64006	5.3	20.557	1.0	0.0981	2.5	0.0146	2.3	0.91	93.6	2.1	95.0	2.2	130.8	24.5	93.6	2.1
RF16-25A-166	254	25877	2.0	21.079	1.8	0.0958	3.6	0.0147	3.1	0.86	93.8	2.8	92.9	3.2	71.5	43.8	93.8	2.8
RF16-25A-274	119	4427	1.4	21.632	3.4	0.0936	4.6	0.0147	3.1	0.67	94.0	2.8	90.8	4.0	9.6	81.6	94.0	2.8
RF16-25A-256	109	5423	1.9	21.480	2.7	0.0948	3.6	0.0148	2.3	0.64	94.5	2.2	92.0	3.1	26.4	65.7	94.5	2.2
RF16-25A PC-49	2485	514332	31.3	20.722	1.1	0.0983	2.6	0.0148	2.4	0.91	94.6	2.2	95.2	2.4	111.9	25.6	94.6	2.2
RF16-25A-258	160	2375	16.6	23.102	2.5	0.0882	3.6	0.0148	2.5	0.70	94.6	2.4	85.8	2.9	NA	NA	94.6	2.4
RF16-25A-199	487	959491	1.7	21.036	1.5	0.0971	2.9	0.0148	2.5	0.86	94.8	2.4	94.1	2.6	76.3	36.2	94.8	2.4
RF16-25A-194	500	8950	2.4	21.282	2.3	0.0961	3.2	0.0148	2.3	0.71	94.9	2.1	93.2	2.9	48.6	54	94.9	2.1
RF16-25A PC-11	2724	500858	10.4	20.585	0.8	0.1004	2.0	0.0150	1.9	0.92	95.9	1.8	97.1	1.9	127.6	19.1	95.9	1.8
RF16-25A-203	622	11819	1.7	20.833	1.2	0.0996	2.9	0.0151	2.6	0.90	96.3	2.5	96.4	2.6	99.3	29.4	96.3	2.5
RF16-25A-102	848	13557	2.1	21.031	1.5	0.0991	2.5	0.0151	2.0	0.81	96.7	1.9	95.9	2.3	76.9	34.6	96.7	1.9
RF16-25A-142	553	117694	3.9	20.693	1.3	0.1010	2.5	0.0152	2.1	0.86	97.1	2.0	97.7	2.3	115.2	30.3	97.1	2.0
RF16-25A PC-79	4266	96969	2.9	21.041	0.9	0.0995	2.5	0.0152	2.3	0.92	97.2	2.2	96.3	2.3	75.8	22.5	97.2	2.2
RF16-25A-164	2490	54749	1.2	20.684	1.0	0.1018	1.8	0.0153	1.5	0.84	97.7	1.4	98.4	1.6	116.3	22.6	97.7	1.4
RF16-25A-284	1487	82621	101.6	21.150	2.3	0.0997	2.5	0.0153	2.3	0.92	97.9	2.3	96.5	2.3	63.5	23.3	97.9	2.3
RF16-25A-239	242	6729	2.2	21.780	2.1	0.0969	3.8	0.0153	3.1	0.83	98.0	3.0	93.9	3.4	NA	NA	98.0	3.0
RF16-25A-308	191	11629	1.5	20.745	2.4	0.1019	3.6	0.0153	2.7	0.75	98.1	2.6	98.5	3.4	109.3	56.7	98.1	2.6
RF16-25A-248	205	5059	3.5	21.572	2.2	0.0982	3.5	0.0154	2.7	0.77	98.3	2.6	95.1	3.1	16.2	53.1	98.3	2.6

Analysis	U	206Pb	U/Th	206Pb*	±	Isotope ratios 207Pb*	±	206Pb*	±	error	Apparent ages (Ma) 206Pb*	±	207Pb*	±	206Pb*	±	Best age	±
	(ppm)	204Pb		207Pb*	(%)	235U*	(%)	238U	(%)	corr.	238U*	(Ma)	235U	(Ma)	207Pb*	(Ma)	(Ma)	(Ma)
RF16-25A-144	343	7992	2.1	20.993	1.6	0.1011	2.6	0.0154	2.0	0.78	98.5	1.9	97.8	2.4	81.1	38	98.5	1.9
RF16-25A-123	222	7492	2.3	21.985	2.2	0.0968	3.5	0.0154	2.7	0.77	98.8	2.6	93.8	3.1	NA	NA	98.8	2.6
RF16-25A PC-44	3499	1377793	5.3	19.827	1.0	0.1076	2.4	0.0155	2.2	0.92	99.0	2.1	103.8	2.3	215.2	22.2	99.0	2.1
RF16-25A-130	209	17819	1.4	21.129	1.9	0.1010	2.9	0.0155	2.1	0.74	99.0	2.1	97.7	2.7	65.8	45.6	99.0	2.1
RF16-25A-309	569	46987	1.4	18.005	1.5	0.1188	2.9	0.0155	2.5	0.85	99.2	2.4	113.9	3.1	434.0	33.9	99.2	2.4
RF16-25A PC-21	1989	440241	13.9	20.375	1.0	0.1062	2.9	0.0157	2.8	0.94	100.4	2.8	102.5	2.9	151.6	23.4	100.4	2.8
RF16-25A-84	527	16361	2.5	21.379	1.4	0.1021	2.8	0.0158	2.4	0.86	101.3	2.5	98.7	2.7	37.7	34	101.3	2.5
RF16-25A PC-30	5516	77133	4.6	20.519	0.9	0.1070	1.8	0.0159	1.5	0.86	101.9	1.5	103.2	1.7	135.2	21.2	101.9	1.5
RF16-25A-307	475	14328	4.7	20.453	2.6	0.1082	4.5	0.0161	3.7	0.81	102.7	3.7	104.3	4.5	142.7	61.3	102.7	3.7
RF16-25A-138	103	8508	2.0	20.225	2.5	0.1107	3.4	0.0162	2.3	0.69	103.8	2.4	106.6	3.4	168.9	57.4	103.8	2.4
RF16-25A-190	382	7911	2.4	21.335	1.7	0.1050	2.7	0.0163	2.2	0.79	104.0	2.2	101.4	2.7	42.7	40.1	104.0	2.2
RF16-25A-291	85	3173	1.8	21.860	3.9	0.1026	5.0	0.0163	3.2	0.63	104.1	3.3	99.2	4.7	NA	NA	104.1	3.3
RF16-25A PC-2	4156	33443	1.0	20.548	1.1	0.1100	2.8	0.0164	2.6	0.92	104.9	2.7	106.0	2.8	131.7	25.1	104.9	2.7
RF16-25A-181	202	19959	2.0	19.987	2.4	0.1143	3.2	0.0166	2.1	0.66	105.9	2.2	109.8	3.3	196.5	55.9	105.9	2.2
RF16-25A-106	96	4722	1.4	21.964	2.4	0.1043	3.8	0.0166	2.9	0.77	106.3	3.1	100.8	3.7	NA	NA	106.3	3.1
RF16-25A PC-67	811	71130	1.3	20.640	1.3	0.1111	2.9	0.0166	2.6	0.90	106.4	2.7	107.0	2.9	121.3	29.7	106.4	2.7
RF16-25A-165	65	1601	1.9	24.928	5.2	0.0921	6.0	0.0167	3.0	0.49	106.5	3.1	89.4	5.2	NA	NA	106.5	3.1
RF16-25A-185	470	9729	2.2	20.612	1.5	0.1116	3.0	0.0167	2.6	0.87	106.7	2.8	107.4	3.1	124.5	34.2	106.7	2.8
RF16-25A PC-52	199	5061	2.1	21.637	1.8	0.1063	3.5	0.0167	3.0	0.86	106.7	3.2	102.6	3.4	9.0	42.3	106.7	3.2
RF16-25A PC-8	137	9746	1.9	19.864	2.4	0.1160	4.2	0.0167	3.4	0.81	106.9	3.6	111.5	4.4	210.9	55.9	106.9	3.6
RF16-25A-124	200	4957	2.3	21.575	2.4	0.1076	3.8	0.0168	3.0	0.79	107.6	3.2	103.7	3.8	15.9	56.6	107.6	3.2
RF16-25A-312	341	3946	3.0	21.816	2.5	0.1065	3.4	0.0169	2.4	0.69	107.7	2.5	102.7	3.4	NA	NA	107.7	2.5
RF16-25A-151	156	2011	3.3	21.886	8.3	0.1064	8.5	0.0169	2.0	0.24	108.0	2.2	102.7	8.3	NA	NA	108.0	2.2
RF16-25A-235	7284	714921	2.5	21.036	0.8	0.1111	1.9	0.0170	1.8	0.91	108.4	1.9	106.9	1.9	76.3	18.6	108.4	1.9
RF16-25A-290	248	6280	1.6	21.276	2.6	0.1109	3.7	0.0171	2.6	0.70	109.5	2.8	106.8	3.7	49.3	63.1	109.5	2.8
RF16-25A-225	454	19046	1.1	21.005	1.4	0.1134	3.4	0.0173	3.1	0.91	110.5	3.4	109.1	3.6	79.8	33.1	110.5	3.4
RF16-25A-98	122	3743	2.0	22.768	3.1	0.1047	4.0	0.0173	2.6	0.64	110.6	2.8	101.1	3.9	NA	NA	110.6	2.8
RF16-25A-121	1009	50878	2.8	20.519	1.4	0.1168	2.5	0.0174	2.2	0.91	111.1	2.5	112.2	2.6	135.1	23.6	111.1	2.5
RF16-25A-150	257	7583	4.2	21.040	2.6	0.1150	4.0	0.0176	3.0	0.76	112.2	3.4	110.6	4.2	75.9	61.5	112.2	3.4
RF16-25A PC-42	279	10026	1.5	20.997	1.9	0.1156	3.2	0.0176	2.5	0.80	112.5	2.8	111.1	3.3	80.7	45.5	112.5	2.8
RF16-25A-89	176	6974	1.5	21.809	2.8	0.1121	4.0	0.0177	2.9	0.72	113.4	3.3	107.9	4.1	NA	NA	113.4	3.3
RF16-25A-241	420	120500	3.5	20.116	1.6	0.1216	2.8	0.0177	2.3	0.82	113.4	2.6	116.5	3.1	181.5	37.3	113.4	2.6
RF16-25A PC-27	3401	23267	2.2	18.495	1.3	0.1323	2.5	0.0178	2.1	0.84	113.4	2.4	126.1	3.0	373.9	30.2	113.4	2.4
RF16-25A-259	178	3606	2.4	21.188	3.0	0.1156	4.2	0.0178	3.0	0.71	113.6	3.4	111.1	4.4	59.2	71	113.6	3.4
RF16-25A-198	593	8862	3.6	21.029	3.2	0.1171	3.2	0.0179	2.8	0.87	114.2	3.2	112.4	3.4	77.1	36.8	114.2	3.2
RF16-25A-178	255	8928	1.3	21.230	1.5	0.1164	3.3	0.0179	2.9	0.89	114.6	3.3	111.8	3.5	54.5	36.2	114.6	3.3
RF16-25A PC-16	2644	37795	53.7	17.481	2.8	0.1418	5.8	0.0180	5.1	0.87	114.9	5.8	134.6	7.3	499.4	62.2	114.9	5.8
RF16-25A-107	442	59194	1.8	20.458	1.2	0.1214	3.1	0.0180	2.8	0.91	115.1	3.2	116.3	3.4	142.1	29.9	115.1	3.2
RF16-25A-170	129	3823	1.8	22.354	3.4	0.1116	4.3	0.0181	2.5	0.59	115.7	2.9	107.5	4.3	NA	NA	115.7	2.9
RF16-25A-247	143	1928	2.7	23.296	3.2	0.1114	4.6	0.0188	3.3	0.72	120.2	4.0	107.2	4.7	NA	NA	120.2	4.0
RF16-25A-193	60	1034	2.1	21.158	5.8	0.1235	6.3	0.0190	2.5	0.40	121.1	3.0	118.2	7.0	62.5	138	121.1	3.0
RF16-25A-122	54	16290	3.3	20.200	3.3	0.1299	4.5	0.0190	3.0	0.67	121.6	3.7	124.0	5.3	171.8	78	121.6	3.7
RF16-25A-252	400	7138	2.2	21.280	1.6	0.1253	3.2	0.0193	2.2	0.87	123.5	3.5	119.9	3.7	48.8	38.1	123.5	3.5
RF16-25A-232	463	16489	1.2	19.673	1.4	0.1513	2.9	0.0216	2.5	0.88	137.7	3.4	143.0	3.8	233.2	31.9	137.7	3.4
RF16-25A-85	127	10720	2.3	21.005	1.4	0.1451	2.8	0.0221	2.0	0.72	141.0	2.8	137.5	3.6	79.8	46.3	141.0	2.8
RF16-25A-254	143	29257	2.2	19.739	2.2	0.1581	3.1	0.0226	2.2	0.71	144.4	3.2	149.1	4.3	225.4	50.4	144.4	3.2
RF16-25A PC-55	106	4032	2.9	21.233	2.0	0.1514	3.9	0.0233	3.3	0.85	148.7	4.8	143.2	5.2	54.1	48.2	148.7	4.8
RF16-25A-146	164	19065	1.3	19.875	2.0	0.1628	3.2	0.0235	2.5	0.79	149.6	3.7	153.2	4.5	209.6	45.2	149.6	3.7
RF16-25A-264	210	18943	2.0	19.804	2.0	0.1638	3.0	0.0235	2.2	0.74	150.0	3.3	154.0	4.2	217.8	45.8	150.0	3.3
RF16-25A-125	227	6423	1.5	21.110	3.0	0.1551	3.6	0.0238	2.0	0.54	151.3	2.9	146.4	4.9	68.0	72.2	151.3	2.9
RF16-25A-192	561	33556	1.1	19.972	1.1	0.1642	3.0	0.0238	2.8	0.93	151.6	4.2	154.3	4.3	198.2	25.6	151.6	4.2
RF16-25A-140	617	61750	1.3	20.071	1.0	0.1638	2.6	0.0238	2.3	0.91	151.9	3.5	154.0	3.6	186.7	24.1	151.9	3.5
RF16-25A PC-29	475	17489	1.9	20.235	1.3	0.1627	2.6	0.0239	2.3	0.87	152.2	3.4	153.0	3.7	167.8	29.2	152.2	3.4
RF16-25A-311	451	127208	1.7	20.038	1.4	0.1647	2.4	0.0240	2.0	0.85	152.6	2.9	154.8	3.5	190.6	33.4	152.6	2.9
RF16-25A PC-15	530	20455	1.5	20.313	1.2	0.1632	2.0	0.0241	1.6	0.79	153.2	2.4	153.5	2.8	158.8	27.8	153.2	2.4
RF16-25A-129	299	4912	1.3	21.708	1.3	0.1528	2.7	0.0241	2.3	0.87	153.3	3.5	144.4	3.6	1.0	31.3	153.3	3.5
RF16-25A-237	910	16172	1.5	20.400	1.0	0.1638	2.5	0.0242	2.3	0.91	154.4	3.5	154.0	3.5	148.7	24	154.4	3.5
RF16-25A-211	73	68391	1.9	19.492	2.1	0.1715	3.9	0.0243	3.2	0.84	154.5	4.9	160.7	5.7	254.5	48.6	154.5	4.9
RF16-25A-223	933	24330	1.5	20.802	1.5	0.1609	3.8	0.0243	3.5	0.92	154.7	5.4	151.5	5.4	102.9	35	154.7	5.4
RF16-25A-116	473	44269	2.1	19.647	1.4	0.1722	3.1	0.0245	2.7	0.89	156.3	4.2	161.3	4.6	236.3	32.9	156.3	4.2
RF16-25A-189	57	5214	4.2	20.173	3.0	0.1684	4.1	0.0247	2.7	0.67	157.0	4.3	158.1	6.0	175.0	70.3	157.0	4.3
RF16-25A-186	91	9081	1.8	19.996	3.1	0.1707	4.4	0.0248	3.0	0.70	157.7	4.7	160.0	6.5	195.5	72.9	157.7	4.7
RF16-25A-97	131	3081	4.0	22.051	2.3	0.1551	3.6	0.0248	2.8	0.77	158.0	4.4	146.4	5.0	NA	NA	158.0	4.4
RF16-25A-314	312	18436	1.0	20.507	1.5	0.1669	2.7	0.0248	2.3	0.85	158.2	3.6	156.7	4.0	136.5	34.2	158.2	3.6
RF16-25A-196	123	47616	1.9	20.787	1.6	0.1661	3.1	0.0251	2.6	0.85	159.5	4.1	156.0	4.4	104.5	38.3	159.5	4.1
RF16-25A-100	275	14619	2.0	20.728	1.3	0.1669	2.9	0.0251	2.7	0.90	159.8	4.2	156.7	4.3	111.3	30.1	159.8	4.2
RF16-25A-103	143	5668	2.6	21.527	2.0	0.1619	3.2	0.0253	2.5	0.78	161.0	3.9	152.3	4.5	21.2	47.5	161.0	3.9
RF16-25A-155	158	2928	2.0	21.840	1.7	0.1609	3.0	0.0255	2.4	0.81	162.3	3.9	151.5	4.2	NA	NA	162.3	3.9
RF16-25A-300	107	1867	2.7	23.096	1.9	0.1525	2.9	0.0256	2.2	0.76	162.7	3.5	144.1	3.8	NA	NA	162.7	3.5
RF16-25A-126	273	11174	1.8	20.503	1.4	0.1729	2.5	0.0257	2.0	0.81	163.7	3.2	161.9	3.7	136.9	33.7	163.7	3.2
RF16-25A-161	152	15549	1.5	19.765	2.3	0.1795	3.3	0.0257	2.4	0.72	163.9	3.9	167.7	5.2	222.4	53.3	163.9	3.9
RF16-25A-249	177	44415	3.7	19.788	2.0	0.1801	3.2	0.0259	2.5	0.79	164.6	4.1	168.1	4.9	219.7	45.2	164.6	4.1
RF16-25A-302	115	5030	1.8	20.862	2.0	0.1710	3.7	0.0259	3.2	0.85	164.7	5.2	160.3	5.5	96.0	46.6	164.7	5.2
RF16-25A-296	188	4110	3.3	20.960	4.1	0.1706	4.7	0.0259	2.4	0.51	165.1	4.0	159.9	7.0	85.0	96.4	165.1	4.0
RF16-25A-255	315	6228	1.1	16.602	3.9	0.2192	4.6	0.0264	2.6	0.53	168.0	4.0	201.2	8.3	611.9	83.4	168.0	4.0
RF16-25A-210	186	4238	2.3	21.222	4.6	0.1721	3.2	0.0265	2.8	0.87	168.6	4.6	161.2	4.7	55.3	37.9	168.6	4.6
RF16-25A-180	1350	349610	2.0	19.938	1.0	0.1837	2.5	0.0266	2.3	0.92	169.1	3.9	171.2	4.0	202.2	23.2	169.1	3.9
RF16-25A PC-17	2637	1606004	2.1	20.330	0.9	0.1806	2.4	0.0266	2.2	0.93	169.5	3.7	168.6	3.7	156.8	19.9	169.5	3.7
RF16-25A PC-18	89	2428	1.8	22.697	3.1	0.1628	4.3	0.0268	3.0	0.69	170.6	5.1	153.2	6.2	NA	NA	170.6	5.1
RF16-25A-94	398	9972	1.6	17.927	3.6	0.2064	5.4	0.0268	4.0	0.74	170.8	6.8	190.5	9.4	443.7	80.3	170.8	6.8
RF16-25A-157	241	4615	1.6	20.494	1.8	0.1815	3.2	0.0270	2.9	0.90	171.7	4.9	169.4	5.0	138.0	32.5	171.7	4.9
RF16-25A PC-19	391	36028	1.7	19.970	1.2	0.1865	2.6	0.0270	2.3	0.89	171.9	3.9	173.7	4.2	198.5	28	171.9	3.9
RF16-25A PC-7	571	39336	1.7	19.800	1.0	0.1920	2.7	0.0276	2.5	0.92	175.4	4.3	178.3	4.4	218.3	23.6	175.4	4.3
RF16-25A-127	360	11966	1.6	20.718	1.2	0.1835	2.5	0.0276	2.2	0.87	175.4	3.7	171.1	3.9	112.4	28.2	175.4	3.7
RF16-25A-299	440	7211	1.2	20.886	1.5	0.1823	2.9	0.0276	2.4	0.85	175.7	4.2	170.0	4.5	93.3	35.4	175.7	4.2
RF16-25A-86	392	11540	2.0	20.712	1.4	0.1848	3.0	0.0278	2.6	0.88	176.5	4.6	172.1	4.7	113.1	33.1	176.5	4.6
RF16-25A-174	232	7885	2.0	20.002	1.5	0.1927	3.0	0.0280	2.6	0.86	177.8	4.5	179.0	4.9	194.8	34.6	177.8	4.5
RF16-25A-306	157	35533	2.5	19.194	1.5	0.2022	2.8	0.0282	2.4	0.85	179.0	4.2	187.0	4.8	289.7	33.4	179.0	4.2
RF16-25A-240	1215	84645	3.3	20.148	0.9	0.1954	2.3	0.0286	2.1	0.92	181.6	3.8	181.3	3.8	177.8	21.4	181.6	3.8
RF16-25A PC-74	2354	76167	1.3	20.558	1.0	0.1939	2.3	0.0289	2.1	0.90	183.8	3.8	180.0	3.8	130.7	24.2	183.8	3.8
RF16-25A PC-31	341	27966	2.2	19.961	1.4	0.2007	3.0	0.0291	2.6	0.88	184.7	4.8	185.7	5.1	199.5	33.3	184.7	4.8
RF16-25A-177	206	4172	1.5	20.601	1.2	0.1957	2.2	0.0293	1.8	0.83	185.9	3.4	181.5	3.7	125.7	28.9	185.9	3.4
RF16-25A-188	134	6761	3.1	20.326	2.1	0.1993	3.1	0.0294	2.4	0.75	186.7	4.3	184.5	5.3	157.3	48.6	186.7	4.3
RF16-25A PC-75	357	40728	1.5	19.902	1.2	0.2039	2.2	0.0294	1.9	0.84	187.1	3.4	188.4	3.8	206.4	27.6	187.1	3.4
RF16-25A PC-10	1092	27171	7.9	20.082	1.2	0.2021	2.6	0.0295	2.4	0.93	187.1	4.5	186.9	4.5	185.5	22.9	187.1	4.5
RF16-25A-227	1604	31995	25.3	19.968	0.9	0.2045	2.2	0.0296	2.0	0.91	188.3	3.7	189.0	3.8	198.7	21.4	188.3	3.7
RF16-25A-132	175	58258	2.8	19.867	1.8	0.2107	2.8	0.0304	2.2	0.78	192.9	4.2	194.2	5.0	210.5	41.1	192.9	4.2
RF16-25A PC-33	388	33713	1.6	19.882	1.3	0.2124	2.7	0.0306	2.4	0.88	194.6	4.5	195.6	4.8	208.7	30.4	194.6	4.5
RF16-25A-215	142	61644	4.1	19.717	2.1	0.2148	3.6	0.0307	2.9	0.81	195.1	5.6	197.6	6.4	228.0	48.4	195.1	5.6
RF16-25A-183	1388	62086	18.1	20.112	1.1	0.2116	3.0	0.0309	2.8	0.93	196.1	5.4	194.9	5.3	181.9	25.5	196.1	5.4
RF16-25A-81	220	17484	2.3	20.741	1.7	0.2073	3.2	0.0312	2.7	0.85	198.0	5.2	191.3	5.5	109.8	39.7	198.0	5.2

					Isotope ratios						Apparent ages (Ma)							
Analysis	U	206Pb	U/Th	206Pb*	±	207Pb*	±	206Pb*	±	error	206Pb*	±	207Pb*	±	206Pb*	±	Best age	±
	(ppm)	204Pb		207Pb*	(%)	235U*	(%)	238U	(%)	corr.	238U*	(Ma)	235U	(Ma)	207Pb*	(Ma)	(Ma)	(Ma)
RF16-25A PC-68	363	66060	2.9	19.866	1.4	0.2172	2.8	0.0313	2.4	0.87	198.7	4.7	199.6	5.0	210.5	32	198.7	4.7
RF16-25A-257	165	29688	2.0	19.750	1.5	0.2206	2.9	0.0316	2.5	0.87	200.6	5.0	202.4	5.4	224.1	34.1	200.6	5.0
RF16-25A-92	66	4585	2.5	20.531	3.1	0.2190	4.0	0.0326	2.5	0.62	207.0	5.1	201.1	7.3	133.7	73.9	207.0	5.1
RF16-25A-112	89	8371	1.6	17.227	2.7	0.2628	3.9	0.0329	2.8	0.72	208.4	5.7	236.9	8.2	531.6	58.4	208.4	5.7
RF16-25A-163	494	13558	2.1	19.971	1.3	0.2301	2.9	0.0333	2.6	0.90	211.5	5.4	210.3	5.5	198.3	29.7	211.5	5.4
RF16-25A PC-5	234	39889	2.7	19.515	1.1	0.2363	2.2	0.0335	1.9	0.86	212.2	4.0	215.4	4.3	251.8	26.1	212.2	4.0
RF16-25A-201	139	6062	5.6	19.842	2.1	0.2397	3.5	0.0345	2.8	0.80	218.7	6.0	218.2	6.8	213.4	48.4	218.7	6.0
RF16-25A-265	1133	120696	2.3	15.798	3.1	0.3252	4.9	0.0373	3.8	0.77	235.9	8.7	285.9	12.2	718.3	65.8	235.9	8.7
RF16-25A PC-72	356	114338	1.6	19.023	1.3	0.3510	2.8	0.0484	2.5	0.89	305.0	7.4	305.5	7.3	310.2	28.5	305.0	7.4
RF16-25A PC-60	261	14855	2.6	18.953	1.4	0.3885	3.3	0.0534	3.0	0.91	335.5	9.9	333.2	9.5	318.5	32.1	335.5	9.9
RF16-25A-96	2125	291352	2.7	17.408	1.0	0.5491	2.4	0.0694	2.1	0.90	432.3	8.9	444.4	8.5	508.6	22.8	432.3	8.9
RF16-25A-187	389	86955	1.0	16.196	1.2	0.8739	2.7	0.1027	2.4	0.89	630.2	14.5	637.7	12.8	665.3	26.5	630.2	14.5
RF16-25A PC-54	431	54120	6.8	13.779	0.9	1.5303	3.3	0.1530	3.1	0.96	917.7	26.9	942.6	20.1	1002.1	18.8	1002.1	18.8
RF16-25A PC-32	297	67856	2.4	13.138	0.8	1.8998	2.8	0.1811	2.7	0.96	1073.0	26.9	1081.0	18.8	1098.1	15.7	1098.1	15.7
RF16-25A PC-73	422	689908	2.0	13.094	0.9	1.9411	2.5	0.1844	2.3	0.92	1091.0	22.7	1095.4	16.4	1104.9	18.9	1104.9	18.9
RF16-25A-230	89	12961	1.7	12.581	1.2	2.1238	2.5	0.1939	2.3	0.92	1142.3	24.2	1156.6	17.4	1184.3	19.8	1184.3	19.8
RF16-25A-279	76	30065	1.3	12.549	1.4	2.2029	3.4	0.2006	3.1	0.92	1178.4	33.8	1182.0	23.9	1189.3	27	1189.3	27.0
RF16-25A-262	1550	528910	1.6	11.666	0.8	2.6309	2.1	0.2227	1.9	0.91	1296.1	22.3	1309.3	15.3	1331.9	16.3	1331.9	16.3
RF16-25A-110	836	129010	4.5	11.570	0.8	2.8506	2.5	0.2393	2.3	0.95	1383.2	29.2	1369.0	18.6	1347.7	14.7	1347.7	14.7
RF16-25A-243	289	79335	1.9	11.569	0.8	2.7525	2.5	0.2310	2.3	0.94	1340.0	27.9	1342.8	18.3	1348.0	16	1348.0	16.0
RF16-25A PC-53	181	25509	1.8	11.562	1.1	2.7035	2.6	0.2268	2.4	0.91	1317.7	28.1	1329.4	19.3	1349.2	21.3	1349.2	21.3
RF16-25A-298	161	95877	2.9	11.557	0.8	2.9053	2.2	0.2436	2.1	0.94	1405.5	26.6	1383.5	16.9	1350.0	14.6	1350.0	14.6
RF16-25A-310	325	468700	2.8	11.523	0.7	2.7770	2.3	0.2322	2.2	0.92	1345.9	26.2	1349.4	17.0	1355.7	14.2	1355.7	14.2
RF16-25A-93	500	272741	6.5	11.493	0.7	2.7885	2.5	0.2325	2.4	0.96	1347.7	29.1	1352.5	18.6	1360.8	13.5	1360.8	13.5
RF16-25A-99	453	197645	7.7	11.492	0.8	2.8163	2.9	0.2348	2.8	0.96	1359.8	34.4	1359.9	21.9	1360.8	15.8	1360.8	15.8
RF16-25A-297	94	55267	1.0	11.487	0.8	2.8852	2.4	0.2405	2.2	0.93	1389.2	27.9	1378.1	18.1	1361.7	16.7	1361.7	16.7
RF16-25A-118	957	178946	3.8	11.469	0.9	2.7974	2.5	0.2328	2.3	0.94	1349.1	28.5	1354.8	18.7	1364.7	16.6	1364.7	16.6
RF16-25A-141	344	63468	1.8	11.469	0.9	2.3579	2.7	0.1962	2.6	0.97	1155.0	27.1	1229.9	18.9	1364.7	13.1	1364.7	13.1
RF16-25A-133	1600	734930	6.3	11.458	1.0	2.8536	2.2	0.2372	1.9	0.90	1372.3	23.9	1369.8	16.2	1366.6	18.4	1366.6	18.4
RF16-25A PC-57	969	311731	2.7	11.437	0.9	2.6471	2.3	0.2197	2.1	0.92	1280.1	24.9	1313.8	17.2	1370.1	17.6	1370.1	17.6
RF16-25A-245	751	215867	4.6	11.430	1.1	2.7722	2.9	0.2299	2.7	0.93	1334.0	32.4	1348.1	21.6	1371.3	20.5	1371.3	20.5
RF16-25A-233	427	277928	3.6	11.420	0.8	2.7886	3.1	0.2311	3.0	0.97	1340.0	36.8	1352.5	23.4	1373.0	14.6	1373.0	14.6
RF16-25A-105	760	141377	8.3	11.413	0.9	2.8379	2.4	0.2350	2.3	0.91	1360.7	26.3	1365.6	17.7	1374.2	18.7	1374.2	18.7
RF16-25A-159	244	74130	1.8	11.404	0.9	2.5546	2.8	0.2114	2.7	0.95	1236.2	30.2	1287.6	20.6	1375.7	16.8	1375.7	16.8
RF16-25A PC-23	65	41831	1.3	11.325	1.2	2.9048	2.7	0.2387	2.4	0.90	1379.9	29.9	1383.2	20.2	1389.0	22.4	1389.0	22.4
RF16-25A-278	856	227377	5.9	11.309	0.7	2.8733	2.3	0.2358	2.2	0.95	1364.7	26.4	1374.9	17.0	1391.7	13.5	1391.7	13.5
RF16-25A-156	1595	1221235	15.5	11.303	1.2	2.6600	3.2	0.2182	3.0	0.93	1272.1	34.3	1317.4	23.6	1392.7	23	1392.7	23.0
RF16-25A-269	1009	1839951	1.4	11.299	0.8	2.8615	1.8	0.2346	1.7	0.94	1358.6	20.4	1371.8	13.3	1393.4	11.1	1393.4	11.1
RF16-25A-294	585	277858	2.4	11.292	0.9	2.8006	2.4	0.2295	2.2	0.92	1331.7	26.8	1355.7	18.1	1394.5	18.2	1394.5	18.2
RF16-25A-162	447	445999	2.1	11.276	1.1	2.8686	3.2	0.2347	3.0	0.94	1359.1	36.5	1373.7	23.8	1397.3	20.4	1397.3	20.4
RF16-25A-315	316	477666	6.6	11.269	0.7	2.8416	3.0	0.2323	2.9	0.97	1346.7	34.9	1366.6	22.3	1398.6	14.2	1398.6	14.2
RF16-25A-242	1209	14658210	12.2	11.269	1.2	2.7517	3.0	0.2250	2.4	0.82	1308.2	32.7	1342.6	22.3	1398.6	22.3	1398.6	22.3
RF16-25A PC-34	1220	426625	12.1	11.266	1.0	2.7926	2.3	0.2283	2.1	0.91	1325.5	25.1	1353.6	17.3	1399.0	18.9	1399.0	18.9
RF16-25A PC-36	651	290750	1.6	11.266	0.9	2.9183	2.3	0.2386	2.2	0.93	1379.2	26.8	1386.7	17.6	1399.0	16.8	1399.0	16.8
RF16-25A-251	910	1287697	2.2	11.228	0.8	2.8573	2.8	0.2328	2.7	0.96	1349.1	32.9	1370.7	21.2	1405.5	15.5	1405.5	15.5
RF16-25A PC-65	671	189091	7.4	11.216	1.0	2.9136	2.5	0.2371	2.3	0.92	1371.7	28.4	1385.4	18.9	1407.5	19.1	1407.5	19.1
RF16-25A-313	886	729712	1.8	10.968	2.0	3.0909	2.0	0.2460	1.8	0.89	1417.7	23.0	1430.4	15.7	1450.2	18.3	1450.2	18.3
RF16-25A-179	311	78873	2.2	10.937	0.8	3.0979	2.6	0.2459	2.4	0.95	1417.0	31.0	1432.2	19.6	1455.5	15	1455.5	15.0
RF16-25A-83	77	17793	0.8	10.529	1.1	3.6065	2.4	0.2755	2.2	0.90	1568.8	30.1	1551.0	19.2	1527.6	20.2	1527.6	20.2
RF16-25A-147	288	364678	1.9	10.501	0.8	3.4436	2.5	0.2624	2.4	0.94	1502.0	31.6	1514.4	19.7	1532.5	15.9	1532.5	15.9
RF16-25A-281	2088	271801	1.8	10.444	0.6	3.0325	2.2	0.2298	2.1	0.96	1333.4	25.0	1415.8	16.5	1542.9	11.3	1542.9	11.3
RF16-25A-271	407	2337321	1.2	10.433	0.9	3.2762	2.9	0.2480	2.8	0.95	1428.1	35.5	1475.4	22.7	1544.9	17.1	1544.9	17.1
RF16-25A-167	70	55712	1.6	10.349	1.0	3.6109	3.2	0.2712	3.0	0.95	1546.7	41.8	1551.9	25.4	1559.9	18.4	1559.9	18.4
RF16-25A-220	265	2736221	1.2	10.043	0.8	3.8338	2.4	0.2794	2.3	0.95	1588.2	31.8	1599.9	19.2	1612.2	14.1	1612.2	14.1
RF16-25A-287	1569	1464573	2.8	9.933	0.8	4.2167	2.1	0.3039	1.9	0.92	1710.7	28.8	1677.3	17.1	1636.5	15.1	1636.5	15.1
RF16-25A-221	637	163445	25.5	9.905	0.9	3.7641	2.4	0.2705	2.3	0.93	1543.5	31.2	1585.1	19.6	1641.7	16.6	1641.7	16.6
RF16-25A-153	1401	341655	9.1	9.901	0.8	3.5617	2.2	0.2559	2.1	0.94	1468.7	27.6	1541.0	17.7	1642.6	14.3	1642.6	14.3
RF16-25A-108	1373	229382	2.1	9.867	0.9	4.1711	2.4	0.2986	2.3	0.93	1684.5	33.7	1668.4	19.9	1648.9	16	1648.9	16.0
RF16-25A PC-46	615	96963	2.8	9.828	0.9	3.8067	2.4	0.2715	2.2	0.93	1548.2	30.8	1594.2	19.1	1656.3	14.6	1656.3	14.6
RF16-25A-285	836	460210	5.8	9.774	0.9	4.0865	2.4	0.2898	2.2	0.93	1640.6	32.4	1651.6	19.6	1666.5	16.4	1666.5	16.4
RF16-25A-148	289	527242	3.7	9.667	0.8	4.2740	2.5	0.2998	2.3	0.94	1690.3	34.4	1688.6	20.2	1686.8	15.3	1686.8	15.3
RF16-25A PC-1	313	138676	4.1	9.655	0.9	4.2952	2.5	0.3009	2.4	0.94	1695.7	35.7	1692.4	21.0	1689.1	16.1	1689.1	16.1
RF16-25A-293	792	816341	2.2	9.643	0.9	3.9902	2.3	0.2792	2.1	0.93	1587.2	29.6	1632.0	18.4	1691.5	15.7	1691.5	15.7
RF16-25A PC-13	266	650212	2.2	9.631	0.7	4.2412	2.6	0.2964	2.4	0.96	1673.4	36.0	1682.0	21.0	1693.6	13.6	1693.6	13.6
RF16-25A PC-51	276	206557	1.1	9.620	1.0	4.2888	2.6	0.2994	2.4	0.92	1688.2	35.0	1691.2	21.1	1695.8	18.6	1695.8	18.6
RF16-25A-104	204	5439510	1.8	9.603	0.9	4.3724	2.2	0.3047	2.0	0.91	1714.4	29.9	1707.1	18.0	1699.1	16.4	1699.1	16.4
RF16-25A-246	340	2140737	4.9	9.592	0.6	4.3381	2.4	0.3019	2.3	0.97	1700.9	34.6	1700.6	19.8	1701.1	11.4	1701.1	11.4
RF16-25A PC-48	436	618446	12.6	9.557	1.0	4.3591	3.3	0.3023	3.2	0.95	1702.6	47.7	1704.6	27.7	1707.9	18.6	1707.9	18.6
RF16-25A PC-43	261	62536	2.2	9.545	0.8	4.4277	1.8	0.3066	1.6	0.89	1724.2	23.8	1717.5	14.7	1710.2	15	1710.2	15.0
RF16-25A-217	576	576403	1.1	9.524	0.9	4.3024	2.5	0.2973	2.4	0.94	1678.0	35.2	1693.8	20.9	1714.3	16.1	1714.3	16.1
RF16-25A PC-61	1679	639883	8.6	9.503	0.8	4.1314	2.5	0.2849	2.3	0.94	1615.8	33.3	1660.5	20.2	1718.4	14.9	1718.4	14.9
RF16-25A PC-70	1008	184825	9.0	9.501	0.9	4.2039	2.5	0.2898	2.3	0.93	1640.6	33.7	1674.8	20.4	1718.7	16.5	1718.7	16.5
RF16-25A-212	491	177342	2.0	9.488	0.8	4.1328	1.8	0.2845	1.6	0.91	1614.1	23.3	1660.8	14.7	1721.2	13.9	1721.2	13.9
RF16-25A-209	506	305086	32.7	9.483	1.0	3.8950	2.8	0.2680	2.5	0.92	1530.7	34.6	1612.7	22.2	1722.2	19.3	1722.2	19.3
RF16-25A-219	251	77187	2.1	9.449	0.9	4.3903	2.0	0.3010	1.7	0.89	1696.2	26.1	1710.5	16.2	1728.8	16.2	1728.8	16.2
RF16-25A-276	223	19272	1.8	9.427	1.5	3.9659	3.1	0.2713	2.7	0.88	1547.3	37.6	1627.2	25.3	1733.0	27.7	1733.0	27.7
RF16-25A PC-26	323	1324608	2.6	9.411	1.0	4.2474	2.8	0.2900	2.6	0.93	1641.7	37.8	1683.2	23.0	1736.1	18.4	1736.1	18.4
RF16-25A-304	465	231984	1.7	9.408	0.8	4.4576	2.7	0.3043	2.6	0.97	1712.5	38.7	1723.1	22.1	1736.7	12.1	1736.7	12.1
RF16-25A PC-14	514	104146	5.6	9.377	0.8	4.4443	2.6	0.3024	2.5	0.95	1703.2	36.8	1720.6	21.6	1742.7	15.6	1742.7	15.6
RF16-25A-266	203	126337	2.9	9.374	0.8	4.3346	2.6	0.2948	2.4	0.95	1665.6	35.6	1700.0	21.2	1743.4	15.3	1743.4	15.3
RF16-25A PC-9	346	162646	1.8	9.334	0.9	4.2467	3.4	0.2876	3.2	0.96	1629.5	46.7	1683.1	27.6	1751.3	16.2	1751.3	16.2
RF16-25A PC-20	371	86820	2.1	9.333	0.7	4.3514	2.2	0.2947	2.1	0.95	1664.9	31.0	1703.2	18.4	1751.4	12.9	1751.4	12.9
RF16-25A PC-76	426	64261	4.1	9.322	0.8	4.2644	3.5	0.2885	3.4	0.96	1633.8	49.0	1686.5	28.7	1753.5	14.8	1753.5	14.8
RF16-25A PC-50	387	10383963	3.7	9.301	1.0	4.7858	2.3	0.3230	2.0	0.91	1804.3	32.1	1782.4	18.9	1757.7	17.5	1757.7	17.5
RF16-25A-135	120	40066	4.2	9.250	0.9	4.8138	2.6	0.3231	2.5	0.93	1804.9	38.6	1787.3	22.1	1767.7	17.3	1767.7	17.3
RF16-25A-267	289	100427	1.1	9.195	0.9	4.4793	2.6	0.2989	2.4	0.93	1685.6	36.0	1727.1	21.5	1778.6	16.3	1778.6	16.3
RF16-25A PC-6	191	94177	1.2	9.158	0.7	4.7554	2.2	0.3160	2.1	0.95	1770.2	33.1	1777.1	18.9	1786.0	12.7	1786.0	12.7
RF16-25A PC-56	134	5640749	3.0	9.081	0.6	4.8894	2.2	0.3222	2.1	0.96	1800.3	33.6	1800.4	18.8	1801.4	11.2	1801.4	11.2
RF16-25A PC-63	130	40611	4.7	8.392	1.2	5.7872	2.5	0.3524	2.4	0.94	1946.1	39.6	1944.5	21.7	1943.6	15.4	1943.6	15.4
RF16-25A PC-77	1448	179603	12.4	6.762	0.9	8.5456	2.7	0.4193	2.5	0.94	2257.1	48.3	2290.8	24.5	2321.7	15.8	2321.7	15.8
RF16-25A PC-39	289	421087	1.6	6.467	0.7	9.3268	2.6	0.4377	2.5	0.96	2340.2	49.2	2370.7	23.9	2397.7	11.7	2397.7	11.7
RF16-25A PC-22	258	78201	0.9	6.396	0.9	9.0187	2.7	0.4186	2.5	0.94	2254.0	48.2	2339.9	24.6	2416.4	15.2	2416.4	15.2
RF16-25A PC-45	144	701866	2.2	6.288	1.2	10.1753	2.9	0.4643	2.7	0.92	2458.4	54.7	2450.8	27.0	2445.3	19.7	2445.3	19.7
Analysis	U	206Pb	U/Th	206Pb*	±	207Pb*	±	206Pb*	±	error	206Pb*	±	207Pb*	±	206Pb*	±	Best age	±
	(ppm)	204Pb		207Pb*	(%)	235U*	(%)	238U	(%)	corr.	238U*	(Ma)	235U	(Ma)	207Pb*	(Ma)	(Ma)	(Ma)

Sample, RF16-25B2, Yakutat Group Melange Facies, (59.83974°, -139.32799°)

Analysis	U	206Pb	U/Th	206Pb*	±	207Pb*	±	206Pb*	±	error	206Pb*	±	207Pb*	±	206Pb*	±	Best age	±
RF16-25b2-114	132	5435	2.5	20.505	2.3	0.0749	3.5	0.0111	2.6	0.75	71.4	1.8	73.3	2.4	136.7	53.8	71.4	1.8

Analysis	U	206Pb	U/Th	206Pb*	±	Isotope ratios 207Pb*	±	206Pb*	±	error	Apparent ages (Ma) 206Pb*	±	207Pb*	±	206Pb*	±	Best age	±
	(ppm)	204Pb		207Pb*	(%)	235U*	(%)	238U	(%)	corr.	238U*	(Ma)	235U	(Ma)	207Pb*	(Ma)	(Ma)	(Ma)
RF16-25b2-127	65	1170	3.7	26.530	3.8	0.0580	5.2	0.0112	3.5	0.67	71.6	2.5	57.3	2.9	NA	NA	71.6	2.5
RF16-25b2-102	62	1485	3.7	24.692	7.0	0.0629	7.6	0.0113	3.0	0.39	72.2	2.1	61.9	4.6	NA	NA	72.2	2.1
RF16-25b2-140	311	5819	1.4	21.658	2.1	0.0719	4.7	0.0113	4.1	0.89	72.4	3.0	70.5	3.2	6.6	51.7	72.4	3.0
RF16-25b2-139	210	5668	2.2	22.221	1.8	0.0701	3.1	0.0113	2.5	0.82	72.4	1.8	68.8	2.1	NA	NA	72.4	1.8
RF16-25b2 PC-3	61	4577	3.4	22.391	2.8	0.0697	4.5	0.0113	3.4	0.77	72.6	2.5	68.4	2.9	NA	NA	72.6	2.5
RF16-25b2 PC-25	2606	31006	23.8	20.875	0.8	0.0747	2.8	0.0113	2.7	0.95	72.6	1.9	73.2	2.0	94.6	19.8	72.6	1.9
RF16-25b2-189	154	12642	2.5	20.432	2.1	0.0766	3.8	0.0114	3.2	0.83	72.8	2.3	74.9	2.8	145.0	49.5	72.8	2.3
RF16-25b2-145	47	809	3.2	31.269	4.6	0.0501	5.8	0.0114	3.6	0.62	72.8	2.6	49.6	2.8	NA	NA	72.8	2.6
RF16-25b2-147	132	4509	2.3	22.414	3.8	0.0700	4.9	0.0114	3.1	0.64	73.0	2.3	68.7	3.3	NA	NA	73.0	2.3
RF16-25b2-115	1224	49962	1.7	19.634	1.3	0.0802	3.0	0.0114	2.7	0.91	73.2	2.0	78.3	2.3	237.7	29.2	73.2	2.0
RF16-25b2-87	263	4091	1.8	22.915	1.8	0.0687	3.3	0.0114	2.7	0.83	73.2	2.0	67.5	2.2	NA	NA	73.2	2.0
RF16-25b2-111	53	2526	4.1	22.275	3.6	0.0708	4.8	0.0114	3.2	0.65	73.3	2.3	69.4	3.2	NA	NA	73.3	2.3
RF16-25b2-194	41	1381	2.9	26.482	3.9	0.0595	5.7	0.0114	4.1	0.72	73.3	3.0	58.7	3.2	NA	NA	73.3	3.0
RF16-25b2-197	258	2443	1.5	23.560	2.8	0.0669	4.0	0.0114	2.9	0.72	73.3	2.1	65.8	2.5	NA	NA	73.3	2.1
RF16-25b2-161	81	7603	4.5	20.972	2.4	0.0753	3.2	0.0115	2.1	0.65	73.4	1.5	73.7	2.3	83.5	57.8	73.4	1.5
RF16-25b2-183	56	76100	3.4	19.221	2.9	0.0829	4.5	0.0116	3.4	0.76	74.1	2.5	80.9	3.5	286.6	66.8	74.1	2.5
RF16-25b2-172	46	4024	1.7	20.309	3.1	0.0786	4.7	0.0116	3.6	0.76	74.2	2.6	76.8	3.5	159.3	71.5	74.2	2.6
RF16-25b2-135	324	17934	2.3	20.802	1.7	0.0767	3.6	0.0116	3.2	0.88	74.2	2.4	75.1	2.6	102.9	40.9	74.2	2.4
RF16-25b2-128	314	6534	4.0	22.392	1.9	0.0720	3.6	0.0117	3.0	0.85	75.0	2.3	70.6	2.4	NA	NA	75.0	2.3
RF16-25b2-110	135	53815	2.8	21.200	2.4	0.0764	3.5	0.0117	2.5	0.71	75.3	1.8	74.7	2.5	57.9	57.9	75.3	1.8
RF16-25b2-96	137	1910	2.6	25.579	2.9	0.0636	4.1	0.0118	2.8	0.69	75.6	2.1	62.6	2.5	NA	NA	75.6	2.1
RF16-25b2-106	176	44166	2.6	20.850	2.4	0.0807	3.5	0.0122	2.6	0.74	78.2	2.0	78.8	2.7	97.4	56.5	78.2	2.0
RF16-25b2-163	55	948	2.8	28.286	17.0	0.0618	17.3	0.0127	3.1	0.18	81.2	2.5	60.9	10.2	NA	NA	81.2	2.5
RF16-25b2-137	542	14640	1.5	20.899	1.4	0.0842	2.5	0.0128	2.1	0.82	81.8	1.7	82.1	2.0	91.8	33.9	81.8	1.7
RF16-25b2 PC-62	2591	69901	13.6	20.819	1.1	0.0859	3.0	0.0130	2.8	0.94	83.1	2.4	83.7	2.4	101.0	25.6	83.1	2.4
RF16-25b2-155	1718	59406	9.8	20.693	1.0	0.0872	2.5	0.0131	2.3	0.92	83.8	1.9	84.9	2.1	115.3	23.4	83.8	1.9
RF16-25b2-107	223	3292	1.8	21.909	3.3	0.0824	3.8	0.0131	1.8	0.48	83.9	1.5	80.4	2.9	NA	NA	83.9	1.5
RF16-25b2-173	123	3123	4.3	22.379	5.8	0.0819	6.3	0.0133	2.5	0.40	85.1	2.1	79.9	4.8	NA	NA	85.1	2.1
RF16-25b2-187	111	2573	2.9	21.050	2.8	0.0871	3.5	0.0133	2.1	0.61	85.2	1.8	84.8	2.9	74.8	66.4	85.2	1.8
RF16-25b2-157	785	5344	3.6	21.880	1.4	0.0846	2.8	0.0134	2.4	0.86	86.0	2.1	82.5	2.2	NA	NA	86.0	2.1
RF16-25b2-177	485	31339	5.3	20.567	1.3	0.0908	3.0	0.0135	2.7	0.90	86.7	2.3	88.2	2.5	129.6	30.2	86.7	2.3
RF16-25b2 PC-28	538	4624	73.6	21.648	1.6	0.0870	3.3	0.0137	2.9	0.87	87.5	2.5	84.7	2.7	7.8	38.6	87.5	2.5
RF16-25b2-158	58	1321	3.0	27.414	13.2	0.0705	13.5	0.0140	2.9	0.21	89.8	2.5	69.2	9.0	NA	NA	89.8	2.5
RF16-25b2 PC-19	751	30459	2.2	21.000	1.5	0.0922	3.6	0.0140	3.3	0.91	89.9	3.0	89.5	3.1	80.4	35.1	89.9	3.0
RF16-25b2-174	1941	25367	8.1	21.141	1.1	0.0918	2.4	0.0141	2.1	0.90	90.1	1.9	89.1	2.0	64.4	25.2	90.1	1.9
RF16-25b2 PC-66	1672	18441	1.6	20.667	1.2	0.0940	2.2	0.0141	1.9	0.84	90.2	1.7	91.2	1.9	118.1	28.3	90.2	1.7
RF16-25b2-119	330	10830	2.0	20.762	1.4	0.0938	3.2	0.0141	2.8	0.90	90.4	2.5	91.0	2.8	107.3	33.2	90.4	2.5
RF16-25b2 PC-41	90	3734	3.0	22.079	2.7	0.0883	3.8	0.0141	2.7	0.71	90.6	2.4	85.9	3.1	NA	NA	90.6	2.4
RF16-25b2-92	66	3510	4.9	21.960	4.0	0.0894	4.8	0.0142	2.7	0.55	91.2	2.4	86.9	4.0	NA	NA	91.2	2.4
RF16-25b2-91	86	1156	2.9	26.952	17.5	0.0729	17.9	0.0143	3.5	0.20	91.3	3.2	71.5	12.4	NA	NA	91.3	3.2
RF16-25b2 PC-48	127	3170	2.5	22.110	5.2	0.0890	5.5	0.0143	1.9	0.35	91.4	1.8	86.6	4.6	NA	NA	91.4	1.8
RF16-25b2-104	148	1892	3.1	24.484	2.1	0.0805	3.6	0.0143	2.7	0.79	91.5	2.4	78.6	2.5	NA	NA	91.5	2.4
RF16-25b2 PC-59	39	623	2.5	38.880	11.4	0.0509	11.9	0.0144	3.2	0.27	91.9	2.9	50.4	5.8	NA	NA	91.9	2.9
RF16-25b2-124	452	28118	1.9	20.537	1.3	0.0964	3.1	0.0144	2.8	0.91	91.9	2.6	93.4	2.8	133.1	30.2	91.9	2.6
RF16-25b2-90	546	28271	4.8	20.593	1.4	0.0961	2.8	0.0144	2.4	0.87	91.9	2.2	93.2	2.5	126.7	32.5	91.9	2.2
RF16-25b2 PC-70	154	5380	3.6	21.187	2.5	0.0938	3.7	0.0144	2.7	0.74	92.3	2.5	91.0	3.2	59.4	58.6	92.3	2.5
RF16-25b2-190	339	2859	1.8	22.382	4.9	0.0894	5.6	0.0145	2.7	0.48	93.0	2.5	87.0	4.6	NA	NA	93.0	2.5
RF16-25b2 PC-58	1333	40080	4.3	20.707	0.9	0.0971	2.5	0.0146	2.3	0.93	93.3	2.2	94.1	2.3	113.6	21.6	93.3	2.2
RF16-25b2-122	705	24832	3.9	20.800	1.0	0.0973	2.9	0.0147	2.7	0.93	94.0	2.6	94.3	2.6	103.0	24.7	94.0	2.6
RF16-25b2-166	180	12367	3.1	20.129	1.5	0.1020	3.0	0.0149	2.6	0.87	95.3	2.4	98.8	2.8	180.0	34.6	95.3	2.4
RF16-25b2 PC-26	180	4345	2.4	21.575	1.9	0.0959	3.0	0.0150	2.3	0.78	96.0	2.2	93.0	2.7	15.9	45.1	96.0	2.2
RF16-25b2-159	549	38763	9.2	20.500	1.2	0.1009	2.6	0.0150	2.3	0.89	96.0	2.2	97.6	2.4	137.3	28.3	96.0	2.2
RF16-25b2-133	479	33029	1.2	20.217	1.3	0.1028	2.5	0.0151	2.1	0.84	96.5	2.0	99.4	2.4	169.9	31.3	96.5	2.0
RF16-25b2 PC-71	91	4120	3.0	22.435	2.0	0.0937	3.3	0.0153	2.6	0.80	97.6	2.5	91.0	2.9	NA	NA	97.6	2.5
RF16-25b2-180	102	1698	2.6	24.512	3.7	0.0860	4.6	0.0153	2.7	0.60	97.8	2.6	83.8	3.7	NA	NA	97.8	2.6
RF16-25b2 PC-49	1272	37884	3.1	21.037	1.0	0.1002	1.8	0.0153	1.5	0.83	97.9	1.4	97.0	1.7	76.2	23.6	97.9	1.4
RF16-25b2-142	64	2847	2.3	21.671	3.6	0.0984	4.6	0.0155	2.9	0.62	99.0	2.8	95.3	4.2	5.2	87.4	99.0	2.8
RF16-25b2 PC-73	428	7311	12.3	21.181	2.4	0.1017	3.7	0.0156	2.8	0.76	99.9	2.8	98.3	3.5	60.0	57.3	99.9	2.8
RF16-25b2-175	306	36547	1.7	20.203	1.4	0.1078	2.8	0.0158	2.4	0.87	101.0	2.4	103.9	2.7	171.5	31.8	101.0	2.4
RF16-25b2 PC-1	16	388	11.9	80.338	56.6	0.0280	56.7	0.0163	3.1	0.06	104.3	3.2	28.0	15.7	NA	NA	104.3	3.2
RF16-25b2 PC-60	71	2127	2.8	21.700	2.5	0.1075	3.8	0.0169	2.9	0.76	108.2	3.1	103.7	3.8	2.0	60.1	108.2	3.1
RF16-25b2 PC-69	102	1619	2.5	24.718	5.4	0.0947	5.8	0.0170	2.2	0.38	108.6	2.4	91.9	5.1	NA	NA	108.6	2.4
RF16-25b2-105	62	5083	2.4	20.249	2.2	0.1156	3.5	0.0170	2.8	0.79	108.6	3.0	111.1	3.7	166.2	50.6	108.6	3.0
RF16-25b2-149	201	9102	4.0	21.163	1.9	0.1115	3.9	0.0171	3.4	0.87	109.5	3.7	107.4	4.0	62.1	45	109.5	3.7
RF16-25b2-170	57	7934	2.6	20.232	3.0	0.1175	4.2	0.0172	3.1	0.72	110.2	3.3	112.8	4.5	168.1	69	110.2	3.3
RF16-25b2 PC-83	117	9235	2.7	20.632	2.4	0.1152	3.8	0.0173	2.9	0.78	110.3	3.2	110.8	4.0	122.2	55.9	110.3	3.2
RF16-25b2-95	212	27137	6.3	20.171	1.9	0.1199	3.2	0.0176	2.5	0.80	112.2	2.8	115.0	3.4	175.1	44.3	112.2	2.8
RF16-25b2-162	125	7685	2.2	20.134	1.9	0.1216	3.4	0.0178	2.9	0.84	113.5	3.2	116.5	3.8	179.5	43.6	113.5	3.2
RF16-25b2-99	843	27494	34.4	17.596	1.4	0.1395	3.2	0.0178	2.8	0.90	113.8	3.2	132.6	3.9	485.1	30.9	113.8	3.2
RF16-25b2-182	82	1867	10.9	23.691	3.1	0.1046	4.2	0.0180	2.8	0.66	114.8	3.1	101.0	4.0	NA	NA	114.8	3.1
RF16-25b2-150	890	17936	1.8	20.976	1.2	0.1185	2.7	0.0180	2.4	0.90	115.3	2.7	113.8	2.9	83.1	28	115.3	2.7
RF16-25b2-156	135	8347	2.2	20.434	1.7	0.1221	3.8	0.0181	3.4	0.89	115.7	3.9	117.0	4.2	144.8	40.4	115.7	3.9
RF16-25b2-169	90	1798	2.4	23.582	6.6	0.1064	7.1	0.0182	2.7	0.37	116.3	3.1	102.7	7.0	NA	NA	116.3	3.1
RF16-25b2 PC-39	178	5603	3.3	20.803	2.1	0.1221	3.4	0.0184	2.7	0.79	117.7	3.2	117.0	3.8	102.6	49.2	117.7	3.2
RF16-25b2-120	70	1996	2.0	23.328	7.4	0.1133	8.1	0.0192	3.3	0.41	122.4	4.0	108.9	8.4	NA	NA	122.4	4.0
RF16-25b2-181	74	583	2.1	7.012	11.4	0.3856	12.0	0.0196	3.8	0.32	125.2	4.7	331.1	34.0	2259.2	197	125.2	4.7
RF16-25b2 PC-65	106	2623	3.2	22.249	4.0	0.1219	4.8	0.0197	2.6	0.55	125.6	3.3	116.8	5.3	NA	NA	125.6	3.3
RF16-25b2-153	82	2315	3.3	23.596	7.8	0.1167	8.2	0.0200	2.4	0.29	127.6	3.0	112.1	8.7	NA	NA	127.6	3.0
RF16-25b2 PC-81	758	217444	13.7	20.750	1.3	0.1399	3.4	0.0211	3.2	0.93	134.4	4.2	133.0	4.3	108.7	30.3	134.4	4.2
RF16-25b2-103	20	281	3.4	1442.250	488.1	0.0020	488.1	0.0211	2.9	0.01	134.5	3.8	2.0	10.0	NA	NA	134.5	3.8
RF16-25b2-164	347	6781	1.1	20.727	2.1	0.1477	3.5	0.0222	2.8	0.80	141.6	3.9	139.9	4.6	111.4	50.1	141.6	3.9
RF16-25b2 PC-63	424	20763	1.9	20.730	1.2	0.1485	2.2	0.0223	1.8	0.83	142.4	2.5	140.6	2.9	111.0	29	142.4	2.5
RF16-25b2 PC-17	223	4376	3.0	21.098	1.8	0.1484	3.7	0.0227	3.2	0.87	144.8	4.6	140.5	4.8	69.3	42.6	144.8	4.6
RF16-25b2-123	21	596	3.4	38.073	48.6	0.0829	48.7	0.0229	2.9	0.06	145.9	4.1	80.8	37.9	NA	NA	145.9	4.1
RF16-25b2-89	50	32472	2.9	20.952	2.9	0.1506	4.0	0.0229	2.6	0.67	145.9	3.8	142.5	5.3	85.8	70	145.9	3.8
RF16-25b2 PC-82	62	2355	2.7	21.450	3.9	0.1483	4.6	0.0231	2.5	0.54	147.1	3.7	140.4	6.1	29.8	93.6	147.1	3.7
RF16-25b2 PC-27	114	2441	2.3	21.699	3.1	0.1471	4.1	0.0232	2.7	0.66	147.6	4.0	139.3	5.4	2.1	75.4	147.6	4.0
RF16-25b2-108	168	28695	2.7	19.713	1.6	0.1644	3.2	0.0235	2.7	0.83	149.9	4.0	154.6	4.5	228.5	36.5	149.9	4.0
RF16-25b2-154	920	1575	2.2	9.183	10.5	0.3534	11.8	0.0235	5.4	0.46	150.0	8.0	307.3	31.4	1781.0	192	150.0	8.0
RF16-25b2-196	86	2720	3.5	22.223	3.6	0.1479	4.1	0.0238	2.0	0.49	151.9	3.0	140.0	5.4	NA	NA	151.9	3.0
RF16-25b2-130	56	1456	5.1	23.595	4.4	0.1394	5.5	0.0239	3.4	0.61	152.1	5.1	132.5	6.9	NA	NA	152.1	5.1
RF16-25b2 PC-2	168	7806	3.9	20.863	2.1	0.1578	3.4	0.0239	2.7	0.78	152.1	4.0	148.7	4.7	95.8	49.8	152.1	4.0
RF16-25b2-136	28	2135	3.5	22.894	7.3	0.1452	7.9	0.0241	3.0	0.38	153.6	4.6	137.7	10.2	NA	NA	153.6	4.6
RF16-25b2-88	157	8246	7.8	20.152	1.8	0.1664	3.6	0.0243	3.1	0.86	155.0	4.8	156.3	5.2	177.4	42.2	155.0	4.8
RF16-25b2 PC-22	26	1026	3.4	25.945	11.5	0.1296	12.0	0.0244	3.4	0.29	155.4	5.3	123.7	14.0	NA	NA	155.4	5.3
RF16-25b2 PC-84	372	45554	1.7	19.931	1.4	0.1690	3.1	0.0244	2.8	0.89	155.6	4.3	158.5	4.6	203.1	32.8	155.6	4.3
RF16-25b2 PC-75	390	74916	1.3	20.168	1.3	0.1686	3.3	0.0247	3.1	0.92	157.2	4.7	158.2	4.9	175.5	30.2	157.2	4.7
RF16-25b2-160	110	2090	2.8	22.700	1.5	0.1503	3.0	0.0248	2.7	0.88	157.6	4.2	142.2	4.0	NA	NA	157.6	4.2
RF16-25b2-195	696	360966	2.2	20.059	1.2	0.1840	2.7	0.0268	2.4	0.90	170.3	4.1	171.5	4.3	188.2	27.8	170.3	4.1
RF16-25b2-132	12	247	0.7	4.597	2.1	0.8489	3.8	0.0283	3.2	0.84	180.0	5.6	624.1	17.8	2962.7	33.8	180.0	5.6
RF16-25b2 PC-52	95	2300	3.9	22.506	2.0	0.1758	3.6	0.0287	3.0	0.83	182.5	5.4	164.4	5.5	NA	NA	182.5	5.4

| Analysis | U | 206Pb | U/Th | 206Pb* | ± | 207Pb* | ± | 206Pb* | ± | error | 206Pb* | ± | 207Pb* | ± | 206Pb* | ± | Best age | ± |
	(ppm)	204Pb		207Pb*	(%)	235U*	(%)	238U	(%)	corr.	238U* (Ma)	(Ma)	235U (Ma)	(Ma)	207Pb* (Ma)	(Ma)	(Ma)	(Ma)
RF16-25b2-138	83	2060	3.0	23.292	8.0	0.1701	8.4	0.0287	2.6	0.31	182.7	4.7	159.5	12.4	NA	NA	182.7	4.7
RF16-25b2 PC-18	46	6318	3.3	19.789	2.4	0.2010	3.5	0.0289	2.6	0.72	183.4	4.6	186.0	6.0	219.6	56.4	183.4	4.6
RF16-25b2-117	277	9542	2.0	20.356	1.4	0.1955	2.7	0.0289	2.3	0.85	183.5	4.1	181.3	4.4	153.8	33.1	183.5	4.1
RF16-25b2 PC-21	207	15790	4.1	20.106	1.2	0.1983	3.1	0.0289	2.8	0.92	183.8	5.1	183.7	5.2	182.7	28.6	183.8	5.1
RF16-25b2-112	78	2702	2.2	21.693	2.6	0.1860	3.6	0.0293	2.6	0.70	186.0	4.7	173.2	5.8	2.8	62.2	186.0	4.7
RF16-25b2 PC-79	105	14267	2.9	19.660	1.5	0.2053	2.9	0.0293	2.4	0.85	186.0	4.5	189.6	4.9	234.8	34.3	186.0	4.5
RF16-25b2 PC-77	432	12115	2.4	19.947	1.1	0.2033	2.8	0.0294	2.5	0.91	187.0	4.6	187.9	4.7	201.2	26.5	187.0	4.6
RF16-25b2 PC-76	229	276958	1.9	19.340	1.2	0.2106	3.4	0.0296	3.1	0.93	187.7	5.8	194.1	5.9	272.4	28.2	187.7	5.8
RF16-25b2-116	543	75274	2.4	20.098	1.1	0.2032	2.1	0.0296	1.8	0.85	188.2	3.3	187.8	3.5	183.6	25.3	188.2	3.3
RF16-25b2-185	213	21755	1.9	20.104	1.4	0.2032	3.2	0.0296	2.9	0.90	188.3	5.3	187.8	5.5	182.9	32	188.3	5.3
RF16-25b2 PC-68	63	1655	3.5	23.857	2.5	0.1730	3.7	0.0300	2.7	0.73	190.3	5.1	162.1	5.6	NA	NA	190.3	5.1
RF16-25b2 PC-148	78	2203	3.0	22.880	4.8	0.1816	5.4	0.0301	2.6	0.48	191.5	4.9	169.4	8.5	NA	NA	191.5	4.9
RF16-25b2 PC-40	200	6913	4.5	20.758	1.3	0.2027	2.7	0.0305	2.4	0.88	193.9	4.6	187.4	4.7	107.9	30.8	193.9	4.6
RF16-25b2 PC-47	56	1586	3.3	23.202	3.2	0.1819	4.0	0.0306	2.8	0.71	194.5	5.4	169.7	6.2	NA	NA	194.5	5.4
RF16-25b2-134	49	3971	5.0	20.433	4.3	0.2142	5.0	0.0318	2.7	0.53	201.5	5.3	197.0	9.0	145.0	100	201.5	5.3
RF16-25b2-144	121	7263	2.9	20.669	1.8	0.2206	2.9	0.0331	2.3	0.79	209.8	4.7	202.4	5.2	118.0	41.3	209.8	4.7
RF16-25b2 PC-4	28	1353	3.0	22.912	7.8	0.2680	8.3	0.0445	3.0	0.36	281.0	8.2	241.1	17.9	NA	NA	281.0	8.2
RF16-25b2-193	98	25837	1.6	17.312	1.5	0.6153	2.5	0.0773	2.0	0.81	479.9	9.2	486.9	9.5	520.8	31.9	479.9	9.2
RF16-25b2-131	314	65176	4.0	15.976	1.2	0.8339	2.7	0.0967	2.5	0.90	594.8	14.1	615.8	12.7	694.5	25	594.8	14.1
RF16-25b2 PC-55	185	35071	1.5	16.236	1.1	0.8600	3.3	0.1013	3.1	0.94	622.1	18.2	630.1	15.3	659.9	24	622.1	18.2
RF16-25b2-188	117	14303	1.8	16.123	1.1	0.9155	2.9	0.1071	2.7	0.93	655.9	16.9	660.0	14.1	674.8	23	655.9	16.9
RF16-25b2 PC-56	202	105137	4.5	13.787	0.9	1.7336	2.3	0.1734	2.1	0.92	1031.0	20.4	1021.1	15.0	1000.9	18.7	1000.9	18.7
RF16-25b2 PC-57	893	284141	2.5	13.281	1.3	1.8293	3.1	0.1763	2.7	0.90	1046.6	26.5	1056.0	20.0	1076.4	26.7	1076.4	26.7
RF16-25b2-167	325	104524	19.5	11.931	0.9	2.0555	3.1	0.1779	3.0	0.96	1055.7	29.3	1134.1	21.4	1288.5	16.8	1288.5	16.8
RF16-25b2-126	1006	229688	17.7	11.626	1.4	2.6143	3.4	0.2205	3.1	0.91	1284.6	36.3	1304.7	25.2	1338.5	27.9	1338.5	27.9
RF16-25b2 PC-85	918	298156	3.5	11.565	1.1	2.3581	3.2	0.1979	3.0	0.94	1163.9	31.7	1230.0	22.7	1348.7	21.8	1348.7	21.8
RF16-25b2-98	282	184222	5.3	11.564	1.0	2.7827	2.8	0.2335	2.6	0.94	1352.7	31.8	1350.9	20.8	1348.9	19	1348.9	19.0
RF16-25b2 PC-86	164	67369	2.0	11.526	1.1	2.9073	3.4	0.2431	3.2	0.94	1403.0	40.1	1383.8	25.5	1355.1	21.7	1355.1	21.7
RF16-25b2-186	219	102663	4.1	11.504	0.8	2.8640	2.8	0.2391	2.7	0.96	1381.8	33.9	1372.5	21.4	1358.9	15.5	1358.9	15.5
RF16-25b2-143	291	399349	3.0	11.495	0.9	2.7227	2.3	0.2271	2.2	0.93	1319.2	25.9	1334.7	17.4	1360.4	16.8	1360.4	16.8
RF16-25b2-118	118	67529	1.9	11.487	1.2	2.7822	2.6	0.2319	2.3	0.89	1344.4	28.1	1350.8	19.4	1361.7	22.7	1361.7	22.7
RF16-25b2 PC-51	113	38266	3.4	11.462	1.1	2.7221	3.0	0.2264	2.8	0.93	1315.5	33.2	1334.5	22.2	1366.0	21	1366.0	21.0
RF16-25b2-179	327	164941	7.8	11.430	1.1	2.8712	3.1	0.2381	3.0	0.95	1376.9	36.7	1374.4	23.6	1371.3	19.5	1371.3	19.5
RF16-25b2-129	135	83687	2.4	11.412	1.2	2.8710	2.9	0.2377	2.6	0.90	1374.9	32.0	1374.3	21.5	1374.3	23.4	1374.3	23.4
RF16-25b2-141	211	59524	2.7	11.400	0.8	2.7626	2.6	0.2285	2.5	0.96	1326.8	30.4	1345.5	19.7	1376.3	14.4	1376.3	14.4
RF16-25b2-101	371	36155	1.7	11.393	0.7	2.7397	2.1	0.2265	1.9	0.93	1316.1	22.8	1339.3	15.3	1377.5	14.2	1377.5	14.2
RF16-25b2-171	211	35243	3.5	11.366	1.0	2.8532	2.6	0.2353	2.4	0.92	1362.2	29.7	1369.7	19.7	1382.1	19.2	1382.1	19.2
RF16-25b2 PC-29	272	48267	3.9	11.320	1.0	2.8766	2.8	0.2363	2.6	0.93	1367.3	32.6	1375.8	21.3	1389.8	19.4	1389.8	19.4
RF16-25b2-121	555	50692	1.1	11.300	0.8	2.7097	2.0	0.2222	1.8	0.93	1293.3	21.5	1331.1	14.7	1393.3	14.4	1393.3	14.4
RF16-25b2 PC-20	308	63219	6.3	11.273	0.9	2.7554	3.1	0.2254	2.9	0.95	1310.2	34.8	1343.5	23.0	1397.9	18.2	1397.9	18.2
RF16-25b2-178	301	42644	8.1	11.266	1.2	2.8344	2.8	0.2317	2.5	0.90	1343.4	30.1	1364.7	20.7	1399.0	22.9	1399.0	22.9
RF16-25b2-176	66	168920	1.5	11.216	0.9	2.8174	2.5	0.2293	2.4	0.90	1330.8	28.4	1360.2	19.0	1407.5	17.5	1407.5	17.5
RF16-25b2-192	288	222092	4.8	11.206	0.9	2.7957	2.2	0.2273	2.0	0.91	1320.4	24.0	1354.4	16.5	1409.3	17.7	1409.3	17.7
RF16-25b2-168	255	67295	9.4	11.175	1.0	2.8585	2.8	0.2318	2.6	0.94	1343.8	32.1	1371.4	21.2	1414.5	18.3	1414.5	18.3
RF16-25b2 PC-38	87	580527	1.8	10.873	1.2	3.1335	2.5	0.2472	2.3	0.89	1424.1	28.8	1441.0	19.5	1466.8	21.9	1466.8	21.9
RF16-25b2-184	658	197422	4.1	10.688	1.0	3.3455	2.6	0.2594	2.4	0.92	1487.0	32.2	1491.7	20.6	1499.4	19.6	1499.4	19.6
RF16-25b2 PC-42	516	87049	1.7	10.666	1.1	3.1844	2.8	0.2464	2.5	0.92	1420.0	32.2	1453.4	21.3	1503.3	20.8	1503.3	20.8
RF16-25b2-152	434	112725	6.3	10.396	1.3	3.2374	3.2	0.2442	3.0	0.91	1408.5	37.4	1466.2	25.2	1551.5	24.9	1551.5	24.9
RF16-25b2 PC-54	1863	388516	38.3	10.321	0.9	3.7776	2.2	0.2829	2.0	0.90	1605.9	28.6	1588.0	17.8	1565.1	17.3	1565.1	17.3
RF16-25b2 PC-72	1319	958119	2.5	10.089	1.0	4.0778	2.0	0.2985	1.8	0.87	1683.9	26.2	1649.9	16.5	1607.6	18.4	1607.6	18.4
RF16-25b2 PC-45	84	624194	1.3	9.553	1.0	4.3795	2.6	0.3035	2.3	0.92	1708.9	35.1	1708.5	21.1	1708.8	18.8	1708.8	18.8
RF16-25b2 PC-6	140	40956	2.0	9.511	1.0	4.3084	2.8	0.2973	2.6	0.93	1678.0	39.0	1695.0	23.2	1716.8	18.5	1716.8	18.5
RF16-25b2-97	188	117992	2.0	9.496	1.0	4.4066	2.8	0.3036	2.6	0.94	1709.2	39.1	1713.6	23.0	1719.8	17.6	1719.8	17.6
RF16-25b2 PC-64	195	124025	1.4	9.484	1.1	4.4810	2.9	0.3084	2.6	0.90	1732.6	39.7	1727.5	24.0	1722.0	22.9	1722.0	22.9
RF16-25b2 PC-67	79	13853	5.2	9.438	1.4	4.4359	3.5	0.3038	3.2	0.92	1709.9	47.9	1719.1	28.8	1731.0	25.3	1731.0	25.3
RF16-25b2 PC-53	124	72010	3.2	9.437	1.0	4.2625	2.3	0.2919	2.0	0.90	1650.9	29.7	1686.2	18.7	1731.0	18.3	1731.0	18.3
RF16-25b2-146	65	32297	3.3	9.433	0.9	4.3525	3.6	0.2979	3.4	0.97	1680.9	50.9	1703.4	29.4	1731.9	16.7	1731.9	16.7
RF16-25b2-94	165	41759	1.9	9.360	0.9	4.5757	2.5	0.3108	2.3	0.93	1744.4	35.2	1744.9	20.5	1746.2	16.2	1746.2	16.2
RF16-25b2 PC-33	189	90703	3.4	9.329	0.9	4.4032	2.2	0.2981	2.0	0.93	1681.6	29.9	1712.9	17.9	1752.2	14.5	1752.2	14.5
RF16-25b2 PC-46	60	13133	2.5	9.217	1.0	4.5753	3.1	0.3060	2.9	0.95	1720.9	44.3	1744.8	25.8	1774.3	17.9	1774.3	17.9
RF16-25b2-165	216	151261	3.3	9.167	0.9	4.7698	2.7	0.3173	2.5	0.94	1776.3	39.0	1779.6	22.3	1784.2	16	1784.2	16.0
RF16-25b2 PC-50	63	35755	1.0	8.978	1.4	5.0914	3.4	0.3317	3.2	0.92	1846.5	50.8	1834.7	29.3	1822.0	24.9	1822.0	24.9
RF16-25b2 PC-12	336	70113	26.5	8.978	0.9	4.1864	2.7	0.2727	2.6	0.95	1554.6	35.3	1671.4	22.1	1822.1	15.6	1822.1	15.6
RF16-25b2 PC-61	74	32814	3.0	7.854	0.9	6.8156	2.9	0.3884	2.7	0.95	2115.4	49.4	2087.7	25.6	2061.3	16.4	2061.3	16.4
RF16-25b2 PC-44	108	57967	1.8	7.782	0.8	6.4961	2.8	0.3668	2.7	0.95	2014.3	46.6	2045.4	24.8	2077.6	14.8	2077.6	14.8
RF16-25b2 PC-8	354	84139	7.7	6.858	0.9	7.5513	2.2	0.3757	2.0	0.91	2056.3	35.3	2179.1	19.7	2297.5	15.4	2297.5	15.4
RF16-25b2 PC-34	552	327940	1.0	5.847	1.0	9.3403	2.6	0.3962	2.4	0.93	2151.7	43.6	2372.0	23.6	2567.8	16.4	2567.8	16.4
RF16-25b2 PC-43	70	50863	3.1	3.879	0.9	22.9640	2.7	0.6463	2.5	0.94	3213.7	64.5	3225.4	26.4	3233.4	14.6	3233.4	14.6

| Analysis | U | 206Pb | U/Th | 206Pb* | ± | 207Pb* | ± | 206Pb* | ± | error | 206Pb* | ± | 207Pb* | ± | 206Pb* | ± | Best age | ± |
	(ppm)	204Pb		207Pb*	(%)	235U*	(%)	238U	(%)	corr.	238U* (Ma)	(Ma)	235U (Ma)	(Ma)	207Pb* (Ma)	(Ma)	(Ma)	(Ma)

Sample, RF16-23A, Yakutat Group Flysch Facies, (59.80011°,-139.295269°)

Analysis	U	206Pb	U/Th	206Pb*	±	207Pb*	±	206Pb*	±	error	206Pb*	±	207Pb*	±	206Pb*	±	Best age	±
RF16-23A-128	212	650	2.5	48.931	2.5	0.0283	3.4	0.0101	2.3	0.67	64.5	1.5	28.4	1.0	NA	NA	64.5	1.5
RF16-23A-204	101	1413	2.7	26.621	4.3	0.0538	4.8	0.0104	2.0	0.43	66.6	1.4	53.2	2.5	NA	NA	66.6	1.4
RF16-23A-122	219	4277	2.6	21.895	2.7	0.0656	4.1	0.0104	3.1	0.76	66.9	2.1	64.5	2.6	NA	NA	66.9	2.1
RF16-23A PC-74	178	3725	2.5	22.616	2.8	0.0636	3.8	0.0104	2.6	0.68	67.0	1.7	62.7	2.3	NA	NA	67.0	1.7
RF16-23A PC-84	1844	21856	3.2	21.020	1.2	0.0686	2.1	0.0105	1.7	0.81	67.1	1.1	67.3	1.4	78.2	29	67.1	1.1
RF16-23A PC-69	237	2188	1.9	23.153	8.4	0.0632	8.9	0.0106	2.9	0.33	68.1	2.0	62.2	5.4	NA	NA	68.1	2.0
RF16-23A PC-72	117	2327	3.0	23.493	8.3	0.0630	8.7	0.0107	2.6	0.31	68.9	1.9	62.0	5.2	NA	NA	68.9	1.9
RF16-23A-164	426	29139	1.6	20.857	1.9	0.0713	3.1	0.0108	2.4	0.79	69.2	1.7	70.0	2.1	96.6	44.4	69.2	1.7
RF16-23A-188	1746	18171	2.9	20.664	1.4	0.0724	2.0	0.0109	1.5	0.75	69.6	1.1	71.0	1.4	118.6	31.9	69.6	1.1
RF16-23A-190	287	4574	2.5	21.837	3.0	0.0696	3.7	0.0110	2.1	0.57	70.7	1.5	68.3	2.4	NA	NA	70.7	1.5
RF16-23A-200	343	5295	2.1	20.877	1.9	0.0733	3.1	0.0111	2.4	0.79	71.2	1.7	71.8	2.1	94.3	44.9	71.2	1.7
RF16-23A-219	260	18876	1.9	20.894	2.1	0.0761	2.8	0.0115	1.9	0.67	73.9	1.4	74.5	2.0	92.4	49.5	73.9	1.4
RF16-23A-148	318	9006	2.3	20.980	2.0	0.0784	3.1	0.0119	2.4	0.77	76.5	1.9	76.6	2.3	82.7	43.6	76.5	1.9
RF16-23A PC-60	1328	21897	2.2	20.882	1.3	0.0788	2.6	0.0119	2.2	0.86	76.5	1.7	77.0	1.9	93.8	30.9	76.5	1.7
RF16-23A-147	189	3237	2.4	23.202	3.9	0.0711	4.6	0.0120	2.4	0.52	76.7	1.8	69.8	3.1	NA	NA	76.7	1.8
RF16-23A-155	193	2264	3.6	24.884	6.0	0.0669	6.5	0.0121	2.5	0.39	77.4	2.0	65.8	4.2	NA	NA	77.4	2.0
RF16-23A-102	182	1352	3.5	28.515	2.8	0.0591	4.1	0.0122	3.0	0.73	78.3	2.3	58.3	2.3	NA	NA	78.3	2.3
RF16-23A PC-97	226	2884	12.2	24.590	2.7	0.0699	3.7	0.0125	2.5	0.69	79.9	2.0	68.6	2.4	NA	NA	79.9	2.0
RF16-23A-154	228	3442	5.5	23.265	3.7	0.0760	4.4	0.0128	2.3	0.54	82.2	1.9	74.4	3.1	NA	NA	82.2	1.9
RF16-23A-101	1305	18043	28.3	21.267	1.6	0.0847	2.6	0.0131	2.1	0.79	83.7	1.7	82.6	2.1	50.3	38	83.7	1.7
RF16-23A-135	197	6506	2.3	21.561	2.7	0.0852	3.5	0.0133	2.3	0.64	85.3	1.9	83.0	2.8	17.4	64	85.3	1.9
RF16-23A-166	131	2127	2.3	24.336	5.8	0.0759	6.2	0.0134	2.3	0.36	85.8	1.9	74.3	4.5	NA	NA	85.8	1.9
RF16-23A-111	298	5889	4.3	21.532	2.2	0.0859	3.4	0.0134	2.6	0.76	85.9	2.2	83.7	2.7	20.7	53.4	85.9	2.2
RF16-23A PC-40	253	89049	1.9	20.562	2.2	0.0902	3.1	0.0135	2.2	0.72	86.2	1.9	87.7	2.6	130.2	51.1	86.2	1.9
RF16-23A PC-100	139	1461	2.8	23.989	9.2	0.0783	9.5	0.0136	2.4	0.25	87.3	2.1	76.5	7.0	NA	NA	87.3	2.1
RF16-23A-159	487	3809	1.7	22.897	3.0	0.0828	3.8	0.0138	2.2	0.59	88.1	1.9	80.8	2.9	NA	NA	88.1	1.9

| Analysis | U | 206Pb | U/Th | 206Pb* | ± | 207Pb* | ± | 206Pb* | ± | error | Isotope ratios | | Apparent ages (Ma) | | | | | |
| | | | | | | | | | | | 206Pb* | ± | 207Pb* | ± | 206Pb* | ± | Best age | ± |
	(ppm)	204Pb		207Pb*	(%)	235U*	(%)	238U	(%)	corr.	238U* (Ma)	(Ma)	235U (Ma)	(Ma)	207Pb* (Ma)	(Ma)	(Ma)	(Ma)
RF16-23A-195	132	15569	3.6	20.816	2.8	0.0919	3.8	0.0139	2.6	0.68	88.8	2.3	89.2	3.2	101.2	65.3	88.8	2.3
RF16-23A-206	254	7271	5.4	21.768	2.2	0.0893	3.2	0.0141	2.4	0.73	90.3	2.1	86.9	2.7	NA	NA	90.3	2.1
RF16-23A-165	191	4633	1.9	22.528	2.5	0.0866	3.5	0.0142	2.5	0.71	90.6	2.2	84.3	2.8	NA	NA	90.6	2.2
RF16-23A PC-83	1970	31611	57.7	20.860	1.0	0.0936	2.3	0.0142	2.1	0.90	90.7	1.9	90.9	2.0	96.2	23.7	90.7	1.9
RF16-23A-208	179	153752	2.4	20.347	2.5	0.0960	3.2	0.0142	1.9	0.61	90.7	1.7	93.1	2.8	154.9	58.5	90.7	1.7
RF16-23A-123	90	4857	3.4	21.191	3.4	0.0926	4.7	0.0142	3.2	0.69	91.1	2.9	89.9	4.0	58.9	80.2	91.1	2.9
RF16-23A PC-3	166	5580	2.1	21.077	2.7	0.0933	3.8	0.0143	2.7	0.70	91.4	2.4	90.6	3.3	71.8	65.3	91.4	2.4
RF16-23A-106	565	33711	5.8	20.883	1.4	0.0955	2.8	0.0145	2.5	0.88	92.6	2.3	92.6	2.5	93.7	32	92.6	2.3
RF16-23A-202	718	7369	1.3	21.162	1.1	0.0943	2.6	0.0145	2.4	0.91	92.7	2.2	91.5	2.3	62.1	25.6	92.7	2.2
RF16-23A PC-51	180	3007	3.9	18.684	3.6	0.1071	4.1	0.0145	1.9	0.47	93.0	1.8	103.4	4.1	351.0	82.4	93.0	1.8
RF16-23A PC-63	1200	33070	4.0	20.420	1.0	0.0988	2.3	0.0146	2.1	0.90	93.7	1.9	95.7	2.1	146.5	23.3	93.7	1.9
RF16-23A-116	800	6811	1.9	21.605	1.2	0.0944	2.6	0.0148	2.3	0.89	94.7	2.2	91.6	2.3	12.5	29.1	94.7	2.2
RF16-23A PC-67	2804	88137	61.3	20.606	0.8	0.0994	2.2	0.0149	2.1	0.93	95.1	2.0	96.2	2.1	125.1	20	95.1	2.0
RF16-23A-113	583	5966	2.0	21.937	1.4	0.0936	2.6	0.0149	2.1	0.83	95.4	2.0	90.9	2.2	NA	NA	95.4	2.0
RF16-23A-182	60	5829	3.8	19.923	4.4	0.1032	5.0	0.0149	2.4	0.47	95.4	2.2	99.7	4.8	203.9	103	95.4	2.2
RF16-23A-181	423	6714	3.0	21.498	2.8	0.0957	3.7	0.0149	2.4	0.65	95.5	2.3	92.8	3.3	24.4	67.2	95.5	2.3
RF16-23A-168	203	18584	1.7	21.899	2.1	0.0943	3.0	0.0150	2.1	0.71	95.8	2.0	91.5	2.6	NA	NA	95.8	2.0
RF16-23A-152	1779	30156	7.8	19.533	1.3	0.1062	2.4	0.0151	2.0	0.84	96.3	1.9	102.5	2.3	249.6	29.9	96.3	1.9
RF16-23A-130	2959	97751	0.3	20.192	1.0	0.1028	2.4	0.0151	2.2	0.91	96.4	2.1	99.3	2.3	172.7	23.4	96.4	2.1
RF16-23A-211	293	8862	3.7	21.209	1.8	0.0988	2.7	0.0152	2.0	0.75	97.3	1.9	95.7	2.4	56.9	41.8	97.3	1.9
RF16-23A-131	195	18467	2.6	19.925	2.6	0.1058	3.7	0.0153	2.7	0.72	97.9	2.6	102.2	3.6	203.7	59.9	97.9	2.6
RF16-23A-109	341	3925	2.4	22.355	2.2	0.0945	3.2	0.0153	2.3	0.72	98.0	2.3	91.7	2.8	NA	NA	98.0	2.3
RF16-23A PC-8	129	2125	2.7	23.359	7.3	0.0906	7.7	0.0154	2.5	0.32	98.2	2.4	88.0	6.5	NA	NA	98.2	2.4
RF16-23A PC-48	4174	43761	23.7	20.632	1.0	0.1027	2.3	0.0154	2.1	0.91	98.4	2.0	99.3	2.2	122.2	22.6	98.4	2.0
RF16-23A PC-57	2729	1463650	8.5	20.913	1.0	0.1024	2.0	0.0155	1.7	0.87	99.4	1.7	99.0	1.9	90.2	22.9	99.4	1.7
RF16-23A PC-71	149	34478	3.5	19.321	2.6	0.1112	3.0	0.0156	1.6	0.52	99.7	1.6	107.0	3.1	274.7	59.5	99.7	1.6
RF16-23A PC-38	155	6837	2.1	20.145	2.8	0.1103	3.8	0.0161	2.5	0.67	103.1	2.6	106.3	3.8	178.2	65.6	103.1	2.6
RF16-23A PC-12	561	14499	1.8	20.878	1.2	0.1088	2.9	0.0165	2.6	0.91	105.4	2.7	104.9	2.8	94.2	27.7	105.4	2.7
RF16-23A-133	170	3397	1.5	23.299	2.6	0.0976	3.7	0.0165	2.6	0.71	105.4	2.7	94.5	3.3	NA	NA	105.4	2.7
RF16-23A-151	113	2443	2.1	22.222	3.1	0.1036	3.9	0.0167	2.4	0.62	106.7	2.6	100.1	3.7	NA	NA	106.7	2.6
RF16-23A-185	160	7738	1.8	20.553	2.6	0.1126	3.3	0.0168	2.1	0.63	107.4	2.2	108.4	3.4	131.2	60.2	107.4	2.2
RF16-23A-156	135	18349	2.8	21.221	2.5	0.1095	4.3	0.0169	3.5	0.81	107.8	3.8	105.5	4.3	55.5	59.9	107.8	3.8
RF16-23A-170	106	5597	2.3	20.585	2.7	0.1134	3.5	0.0169	2.2	0.63	108.3	2.4	109.1	3.7	127.6	64.5	108.3	2.4
RF16-23A-146	241	17489	1.8	20.571	1.9	0.1141	3.0	0.0170	2.2	0.76	108.8	2.4	109.7	3.1	129.2	45.4	108.8	2.4
RF16-23A PC-13	150	4614	2.3	21.357	1.8	0.1114	3.1	0.0173	2.6	0.82	110.3	2.8	107.2	3.2	40.3	43.4	110.3	2.8
RF16-23A-173	627	26871	1.3	20.188	1.6	0.1179	2.8	0.0173	2.3	0.82	110.4	2.5	113.2	3.0	173.1	37.1	110.4	2.5
RF16-23A-141	167	27511	2.6	20.195	2.4	0.1184	3.4	0.0173	2.4	0.70	110.9	2.6	113.6	3.6	172.4	56	110.9	2.6
RF16-23A-145	140	6243	2.1	13.842	7.9	0.1738	8.3	0.0175	2.8	0.33	111.6	3.1	162.7	12.5	992.8	160	111.6	3.1
RF16-23A-207	180	17254	3.4	20.507	2.1	0.1183	3.4	0.0176	2.7	0.79	112.4	3.0	113.5	3.6	136.5	49	112.4	3.0
RF16-23A PC-99	92	1341	3.2	26.029	2.6	0.0933	3.8	0.0176	2.8	0.73	112.6	3.1	90.6	3.3	NA	NA	112.6	3.1
RF16-23A PC-46	2201	43712	1.2	20.473	1.2	0.1200	2.1	0.0178	1.8	0.83	113.9	2.0	115.0	2.3	140.4	27.8	113.9	2.0
RF16-23A-132	157	19046	2.8	21.373	2.2	0.1160	2.9	0.0180	2.0	0.67	114.9	2.2	111.4	3.1	38.4	51.9	114.9	2.2
RF16-23A-110	172	15532	2.9	20.949	2.7	0.1230	3.3	0.0187	2.0	0.59	119.4	2.3	117.8	3.7	86.2	63.9	119.4	2.3
RF16-23A-161	80	828	2.3	32.385	11.7	0.0798	11.9	0.0187	2.3	0.20	119.7	2.8	77.9	8.9	NA	NA	119.7	2.8
RF16-23A PC-28	188	11872	1.8	20.778	2.1	0.1266	3.3	0.0191	2.6	0.78	121.9	3.1	121.1	3.8	105.6	49.7	121.9	3.1
RF16-23A-186	101	2532	3.0	23.575	3.9	0.1173	4.5	0.0201	2.3	0.51	128.0	2.9	112.6	4.8	NA	NA	128.0	2.9
RF16-23A-183	79	5473	3.7	22.304	2.4	0.1253	3.4	0.0203	2.4	0.71	129.4	3.1	119.8	3.9	NA	NA	129.4	3.1
RF16-23A PC-56	140	23031	2.9	20.402	2.4	0.1430	3.1	0.0212	1.9	0.64	135.0	2.6	135.7	3.9	148.6	55.3	135.0	2.6
RF16-23A-210	102	4840	4.1	21.838	2.8	0.1364	3.5	0.0216	2.1	0.61	137.8	2.9	129.8	4.2	NA	NA	137.8	2.9
RF16-23A-149	267	9071	1.7	21.091	1.7	0.1464	2.6	0.0224	2.1	0.78	142.9	2.9	138.8	3.4	70.1	39.3	142.9	2.9
RF16-23A-142	128	5002	3.6	22.168	2.9	0.1395	3.5	0.0224	1.8	0.54	143.1	2.6	132.6	4.3	NA	NA	143.1	2.6
RF16-23A-193	110	2917	2.9	21.644	2.7	0.1430	3.5	0.0225	2.3	0.66	143.2	3.3	135.7	4.5	8.1	64.1	143.2	3.3
RF16-23A-134	1037	50339	3.0	20.510	1.1	0.1526	2.7	0.0227	2.4	0.91	144.7	3.5	144.2	3.6	136.2	26.3	144.7	3.5
RF16-23A PC-90	157	5867	2.8	21.427	3.4	0.1466	4.2	0.0228	2.6	0.61	145.3	3.7	138.9	5.5	32.4	80.9	145.3	3.7
RF16-23A-212	80	9929	1.7	20.980	2.4	0.1500	3.8	0.0228	3.0	0.79	145.5	4.3	141.9	5.1	82.6	55.9	145.5	4.3
RF16-23A PC-81	349	20543	2.4	20.286	1.5	0.1553	2.7	0.0229	2.3	0.84	145.7	3.3	146.6	3.7	161.9	35.2	145.7	3.3
RF16-23A-178	263	3190	1.5	22.489	1.8	0.1401	3.0	0.0229	2.5	0.81	145.7	3.5	133.1	3.8	NA	NA	145.7	3.5
RF16-23A-187	118	15672	4.2	20.166	2.5	0.1568	3.5	0.0229	2.5	0.70	146.2	3.5	147.9	4.8	175.8	58.4	146.2	3.5
RF16-23A-175	753	181172	2.5	20.107	1.2	0.1625	2.4	0.0237	2.1	0.88	151.1	3.1	152.9	3.4	182.6	27.2	151.1	3.1
RF16-23A-167	126	4194	2.2	21.394	2.3	0.1528	3.5	0.0237	2.7	0.77	151.1	4.1	144.4	4.8	36.1	54.1	151.1	4.1
RF16-23A PC-23	467	1187990	4.2	20.621	1.7	0.1594	2.9	0.0238	2.4	0.81	151.9	3.5	150.1	4.1	123.5	40.3	151.9	3.5
RF16-23A PC-25	1860	40320	2.7	20.034	1.1	0.1690	2.1	0.0246	1.9	0.88	156.4	2.9	158.5	3.1	191.0	23.2	156.4	2.9
RF16-23A-169	343	134799	3.2	20.021	1.4	0.1693	2.5	0.0246	2.1	0.82	156.6	3.2	158.8	3.7	192.6	33.2	156.6	3.2
RF16-23A-174	281	47581	2.7	20.080	1.5	0.1689	2.6	0.0246	2.0	0.80	156.7	3.1	158.5	3.7	185.7	35.9	156.7	3.1
RF16-23A-126	205	5919	3.1	20.629	1.7	0.1647	2.6	0.0246	2.0	0.77	157.0	3.1	154.8	3.7	122.6	39.2	157.0	3.1
RF16-23A PC-16	842	198816	2.3	19.799	1.0	0.1738	2.3	0.0250	2.1	0.90	159.0	3.2	162.7	3.4	218.5	22.7	159.0	3.2
RF16-23A-177	588	17874	2.2	18.127	3.0	0.1904	3.7	0.0250	2.1	0.58	159.4	3.4	177.0	6.0	418.9	67.4	159.4	3.4
RF16-23A-201	1160	11710	2.3	20.195	1.2	0.1711	2.3	0.0251	1.9	0.84	159.7	3.0	160.4	3.3	172.4	28.2	159.7	3.0
RF16-23A PC-79	579	9489	2.9	20.749	1.2	0.1681	2.6	0.0253	2.2	0.88	161.1	3.6	157.8	3.7	108.8	28.8	161.1	3.6
RF16-23A-172	271	124206	4.7	19.892	1.4	0.1756	2.5	0.0253	2.1	0.84	161.3	3.3	164.3	3.8	207.6	32	161.3	3.3
RF16-23A-150	249	241392	2.6	19.963	1.6	0.1767	2.6	0.0256	2.1	0.80	162.9	3.4	165.2	4.0	199.3	36.1	162.9	3.4
RF16-23A-205	98	3262	2.6	21.325	2.3	0.1657	3.3	0.0256	2.3	0.72	163.2	3.8	155.7	4.7	43.8	54.5	163.2	3.8
RF16-23A-119	192	3748	1.9	22.265	2.4	0.1590	3.2	0.0257	2.1	0.65	163.5	3.3	149.8	4.4	NA	NA	163.5	3.3
RF16-23A-140	114	5424	2.8	22.574	2.2	0.1588	3.2	0.0260	2.3	0.73	165.5	3.8	149.6	4.4	NA	NA	165.5	3.8
RF16-23A PC-62	2492	201369	2.5	19.801	1.0	0.1844	2.6	0.0265	2.4	0.92	168.5	4.0	171.8	4.1	218.2	22.7	168.5	4.0
RF16-23A-129	182	2337	3.2	22.667	3.3	0.1624	3.3	0.0267	3.0	0.89	170.0	5.0	152.8	4.7	NA	NA	170.0	5.0
RF16-23A PC-68	297	8786	1.6	21.088	2.3	0.1761	3.0	0.0270	2.2	0.65	171.4	3.4	164.7	4.6	70.4	55	171.4	3.4
RF16-23A-137	534	37852	1.4	20.329	1.4	0.1848	2.9	0.0273	2.6	0.89	173.3	4.4	172.1	4.5	156.9	30.8	173.3	4.4
RF16-23A PC-78	899	28512	1.4	19.579	1.1	0.1922	2.2	0.0273	1.9	0.86	173.6	3.3	178.5	3.6	244.2	25.6	173.6	3.3
RF16-23A-209	303	31739	2.4	19.920	1.1	0.1898	2.5	0.0274	2.2	0.89	174.4	3.9	176.4	4.1	204.3	25.9	174.4	3.9
RF16-23A-215	607	24817	3.3	19.945	1.2	0.1906	2.4	0.0276	2.0	0.85	175.4	3.5	177.2	3.8	201.3	28.4	175.4	3.5
RF16-23A-157	166	3636	1.8	21.574	2.7	0.1764	3.7	0.0276	2.5	0.68	175.6	4.3	164.9	5.6	15.9	65.2	175.6	4.3
RF16-23A PC-7	1480	63329	2.4	20.135	1.1	0.1913	2.4	0.0280	2.2	0.89	177.7	3.8	177.8	3.9	179.3	25.5	177.7	3.8
RF16-23A PC-58	581	28558	1.8	20.140	1.1	0.1925	3.0	0.0281	2.8	0.93	178.9	5.0	178.8	5.0	178.7	25.9	178.9	5.0
RF16-23A PC-35	688	34595	2.4	20.129	0.9	0.1980	2.8	0.0289	2.7	0.95	183.8	4.8	183.5	4.7	180.0	20.1	183.8	4.8
RF16-23A-216	242	14200	4.7	19.574	1.7	0.2039	2.6	0.0290	1.9	0.74	184.0	3.4	188.4	4.4	244.8	39.5	184.0	3.4
RF16-23A-192	263	5866	3.2	20.194	1.7	0.1984	3.0	0.0291	2.5	0.83	184.7	4.6	183.8	5.1	172.5	39.2	184.7	4.6
RF16-23A PC-88	905	19559	2.4	20.195	1.8	0.1993	3.0	0.0292	2.7	0.82	185.6	5.0	184.5	5.0	172.3	29.1	185.6	5.0
RF16-23A-160	328	63107	2.0	19.876	1.4	0.2037	2.8	0.0294	2.4	0.86	186.7	4.5	188.3	4.9	209.4	33.5	186.7	4.5
RF16-23A PC-55	3258	65701	0.8	19.926	0.8	0.2033	2.1	0.0294	1.9	0.92	186.7	3.5	187.9	3.5	203.6	19.1	186.7	3.5
RF16-23A PC-19	225	13997	1.6	20.261	2.0	0.2008	3.0	0.0295	2.2	0.74	187.5	4.1	185.8	5.1	164.7	47	187.5	4.1
RF16-23A-194	202	22847	2.4	19.706	1.3	0.2065	2.6	0.0295	2.2	0.86	187.6	4.2	190.6	4.5	229.3	30.8	187.6	4.2
RF16-23A PC-34	116	20526	2.6	19.282	2.3	0.2116	3.2	0.0296	2.2	0.70	188.1	4.1	194.9	5.6	279.4	51.5	188.1	4.1
RF16-23A PC-44	228	7244	2.9	20.409	1.9	0.2000	2.8	0.0296	2.1	0.74	188.2	3.9	185.2	4.8	147.8	44.9	188.2	3.9
RF16-23A PC-45	335	10157	2.5	20.488	1.2	0.2002	2.3	0.0298	2.0	0.85	189.0	3.7	185.3	3.9	138.7	28.6	189.0	3.7
RF16-23A PC-15	215	12534	2.7	20.068	1.9	0.2044	3.5	0.0298	2.9	0.83	189.1	5.4	188.9	6.0	187.1	44.5	189.1	5.4
RF16-23A-117	426	59842	1.9	20.172	1.4	0.2084	3.0	0.0305	2.6	0.88	193.6	5.0	192.5	5.2	175.1	32.8	193.6	5.0
RF16-23A PC-73	153	3443	2.7	20.509	2.1	0.2054	3.1	0.0306	2.3	0.74	194.1	4.4	189.7	5.3	136.3	49.4	194.1	4.4
RF16-23A-103	481	30148	3.9	19.632	1.2	0.2146	3.0	0.0306	2.8	0.92	194.2	5.3	197.4	5.4	237.9	27.4	194.2	5.3
RF16-23A-158	332	6498	2.0	21.469	2.9	0.1967	4.2	0.0306	3.0	0.73	194.5	5.8	182.3	7.0	27.7	68.7	194.5	5.8
RF16-23A-162	269	5301	2.2	20.639	1.6	0.2053	3.3	0.0307	2.9	0.87	195.2	5.6	189.6	5.8	121.3	38.9	195.2	5.6

Analysis	U	206Pb	U/Th	206Pb*	±	207Pb*	±	206Pb*	±	error	206Pb*	±	207Pb*	±	206Pb*	±	Best age	±
	(ppm)	204Pb		207Pb*	(%)	235U*	(%)	238U	(%)	corr.	238U* (Ma)	(Ma)	235U (Ma)	(Ma)	207Pb* (Ma)	(Ma)	(Ma)	(Ma)
RF16-23A PC-22	741	115011	1.8	19.803	1.1	0.2344	2.3	0.0337	2.0	0.88	213.6	4.2	213.9	4.4	217.9	24.8	213.6	4.2
RF16-23A PC-75	5125	146738	1.1	20.171	0.9	0.2723	2.0	0.0398	1.8	0.90	251.9	4.4	244.5	4.3	175.1	20.4	251.9	4.4
RF16-23A PC-14	3323	78084	82.7	13.382	2.2	0.4541	3.7	0.0441	3.0	0.80	278.1	8.2	380.1	11.9	1061.2	45	278.1	8.2
RF16-23A PC-26	978	54413	2.3	17.417	0.8	0.5790	2.6	0.0732	2.5	0.95	455.2	10.9	463.8	9.6	507.5	17.2	455.2	10.9
RF16-23A-203	711	248527	1.5	17.163	1.0	0.6230	2.1	0.0776	1.9	0.88	481.7	8.7	491.7	8.3	539.8	22.3	481.7	8.7
RF16-23A-125	141	89999	3.2	17.552	1.0	0.6182	2.3	0.0787	2.1	0.91	488.5	9.8	488.7	8.9	490.5	21.2	488.5	9.8
RF16-23A PC-1	290	29380	1.8	17.548	1.2	0.6283	3.0	0.0800	2.8	0.92	496.1	13.2	495.0	11.9	491.1	26.8	496.1	13.2
RF16-23A PC-85	3106	383853	7.0	17.468	1.1	0.6465	2.3	0.0819	2.1	0.89	507.7	10.2	506.3	9.3	501.2	23.2	507.7	10.2
RF16-23A PC-29	352	128652	2.2	13.401	0.9	1.7688	2.1	0.1720	1.9	0.91	1023.1	18.2	1034.1	13.7	1058.3	18	1058.3	18.0
RF16-23A-107	723	8475433	17.2	12.671	1.3	2.0142	3.6	0.1852	3.4	0.93	1095.2	34.2	1120.3	24.6	1170.2	25.6	1170.2	25.6
RF16-23A PC-4	521	74517	2.2	12.058	0.9	2.4981	2.1	0.2186	1.9	0.91	1274.3	22.5	1271.5	15.5	1267.7	17.1	1267.7	17.1
RF16-23A PC-98	1125	5733557	2.9	11.852	1.0	2.6990	2.1	0.2321	1.9	0.89	1345.6	23.0	1328.2	15.7	1301.1	18.6	1301.1	18.6
RF16-23A-180	1330	1038123	8.0	11.805	0.8	2.6764	2.2	0.2292	2.0	0.92	1330.5	24.3	1322.0	16.2	1308.9	16.4	1308.9	16.4
RF16-23A-24	1156	12429355	2.0	11.672	0.9	2.7889	2.5	0.2362	2.4	0.94	1366.9	29.1	1352.6	18.9	1330.8	17.2	1330.8	17.2
RF16-23A-163	893	4531668	15.0	11.659	0.9	2.7150	2.8	0.2297	2.6	0.94	1332.8	31.8	1332.6	20.8	1333.0	18.2	1333.0	18.2
RF16-23A-108	978	102754	10.9	11.647	0.9	2.5606	2.5	0.2164	2.4	0.93	1262.7	27.0	1289.5	18.4	1335.1	17.6	1335.1	17.6
RF16-23A-118	784	70210	1.2	11.643	1.0	2.3420	2.2	0.1978	2.0	0.90	1163.7	21.1	1225.1	15.7	1335.7	18.9	1335.7	18.9
RF16-23A-112	569	198486	3.4	11.605	1.0	2.6967	3.0	0.2271	2.9	0.94	1319.1	34.2	1327.5	22.4	1342.0	19.2	1342.0	19.2
RF16-23A-213	436	162884	4.3	11.533	0.9	2.9039	2.4	0.2430	2.2	0.93	1402.3	27.7	1382.9	18.0	1354.0	17.4	1354.0	17.4
RF16-23A-121	938	123311	7.4	11.502	0.8	2.7157	2.4	0.2266	2.2	0.94	1316.9	26.7	1332.8	17.8	1359.1	15.9	1359.1	15.9
RF16-23A-214	609	128807	7.0	11.472	0.6	2.7877	2.7	0.2321	2.6	0.97	1345.3	31.4	1352.3	19.9	1364.1	12.4	1364.1	12.4
RF16-23A PC-5	118	10866	1.6	11.472	1.1	2.2357	2.7	0.1861	2.5	0.91	1100.2	25.0	1192.3	19.0	1364.2	21.3	1364.2	21.3
RF16-23A-189	382	54937	4.5	11.459	0.9	2.8099	2.4	0.2336	2.2	0.90	1353.5	26.7	1358.2	17.8	1366.3	17.7	1366.3	17.7
RF16-23A-217	389	174348	1.2	11.444	0.7	2.8329	1.8	0.2352	1.6	0.92	1361.8	20.1	1364.3	13.3	1369.0	13.2	1369.0	13.2
RF16-23A PC-17	412	74921	2.9	11.441	0.8	2.7893	2.3	0.2316	2.1	0.93	1342.6	25.9	1352.7	17.2	1369.4	16.1	1369.4	16.1
RF16-23A-176	430	137948	4.1	11.413	0.7	2.7393	2.4	0.2268	2.3	0.96	1317.9	27.2	1339.2	17.8	1374.2	13.3	1374.2	13.3
RF16-23A PC-89	709	94422	1.8	11.359	0.7	2.6961	2.4	0.2222	2.2	0.95	1293.5	26.3	1327.4	17.5	1383.3	13.9	1383.3	13.9
RF16-23A-104	529	60914	7.2	11.337	0.6	2.8321	2.1	0.2330	2.1	0.96	1350.1	24.7	1364.1	15.9	1387.0	11.9	1387.0	11.9
RF16-23A-144	336	65309	4.3	11.328	1.0	2.9057	2.3	0.2388	2.1	0.90	1380.5	25.8	1383.4	17.4	1388.6	19.3	1388.6	19.3
RF16-23A PC-31	648	1560043	8.1	11.308	0.9	2.7984	2.3	0.2296	2.1	0.91	1332.4	24.9	1355.1	16.9	1392.0	17.8	1392.0	17.8
RF16-23A-198	257	68564	3.5	11.241	0.8	2.8563	2.4	0.2330	2.2	0.94	1350.0	27.4	1370.5	17.9	1403.3	15.2	1403.3	15.2
RF16-23A-197	337	420772	2.8	11.227	0.9	2.8655	2.2	0.2334	2.0	0.91	1352.5	24.6	1372.9	16.6	1405.6	17.2	1405.6	17.2
RF16-23A-184	760	536154	2.4	11.127	1.5	2.5570	3.2	0.2064	3.0	0.94	1209.8	33.0	1288.4	23.4	1422.8	21.4	1422.8	21.4
RF16-23A-196	725	657603	1.5	11.054	0.8	2.9624	2.4	0.2376	2.3	0.95	1374.2	28.4	1398.0	18.5	1435.3	15.1	1435.3	15.1
RF16-23A PC-20	511	160076	1.4	11.035	0.7	3.1737	2.7	0.2541	2.6	0.96	1459.6	33.5	1450.8	20.7	1438.7	14.3	1438.7	14.3
RF16-23A PC-6	784	119986	0.7	10.995	0.8	3.1381	2.3	0.2503	2.1	0.94	1440.3	27.5	1442.1	17.4	1445.6	14.4	1445.6	14.4
RF16-23A PC-94	283	120840	2.5	10.863	0.7	3.2297	1.5	0.2546	1.4	0.89	1462.0	17.7	1464.3	11.8	1468.5	13.1	1468.5	13.1
RF16-23A-114	181	189904	1.5	10.787	0.8	3.3181	2.6	0.2597	2.4	0.95	1488.3	32.2	1485.3	19.9	1481.9	15.4	1481.9	15.4
RF16-23A PC-10	220	192184	2.3	10.752	0.7	3.4101	2.1	0.2660	2.0	0.95	1520.6	26.9	1506.7	16.5	1488.1	12.7	1488.1	12.7
RF16-23A-127	676	106733723	5.0	10.681	1.2	3.2695	2.2	0.2534	2.0	0.90	1455.9	26.2	1473.8	17.4	1500.6	18.4	1500.6	18.4
RF16-23A PC-53	703	200159	4.5	10.219	0.6	3.7822	2.3	0.2804	2.2	0.97	1593.5	31.1	1589.0	18.3	1583.7	11.1	1583.7	11.1
RF16-23A PC-32	275	58121	0.8	10.111	0.9	3.8669	2.2	0.2837	2.1	0.94	1609.9	29.5	1606.8	18.1	1603.5	16.5	1603.5	16.5
RF16-23A PC-9	629	450091	3.4	9.835	0.8	3.9809	2.5	0.2841	2.3	0.95	1611.8	33.4	1630.3	20.0	1655.0	14.4	1655.0	14.4
RF16-23A PC-41	968	168939	5.5	9.832	0.8	3.8742	1.8	0.2764	1.6	0.91	1573.2	22.8	1608.3	14.6	1655.4	14.1	1655.4	14.1
RF16-23A-143	270	157201	3.7	9.771	1.2	4.0843	2.4	0.2896	2.1	0.88	1639.3	30.8	1651.2	19.3	1667.0	21.3	1667.0	21.3
RF16-23A-179	474	64031	5.1	9.743	0.6	3.7281	2.5	0.2635	2.4	0.97	1507.9	32.5	1577.4	19.9	1672.4	10.6	1672.4	10.6
RF16-23A-120	146	77822	1.2	9.728	0.9	4.2828	2.9	0.3023	2.7	0.95	1702.7	40.6	1690.1	23.6	1675.2	17.3	1675.2	17.3
RF16-23A PC-64	440	425971	2.1	9.702	1.2	4.2605	3.1	0.2999	2.8	0.92	1690.9	42.4	1685.8	25.4	1680.2	21.9	1680.2	21.9
RF16-23A PC-96	173	88475	1.5	9.690	1.0	4.2868	2.5	0.3014	2.3	0.92	1698.2	34.4	1690.8	20.6	1682.5	17.7	1682.5	17.7
RF16-23A PC-86	537	216421	1.6	9.670	0.8	4.2541	2.4	0.2985	2.2	0.95	1683.7	33.2	1684.5	19.4	1686.3	14.1	1686.3	14.1
RF16-23A-139	293	347762	2.1	9.627	0.9	4.2933	2.0	0.2999	1.8	0.90	1690.8	27.0	1692.1	16.6	1694.4	16	1694.4	16.0
RF16-23A-136	157	75870	3.0	9.615	1.0	3.6266	2.4	0.2530	2.1	0.90	1454.0	27.7	1555.4	18.9	1696.8	19.1	1696.8	19.1
RF16-23A PC-39	329	209036	3.0	9.560	0.8	4.1913	2.0	0.2907	1.9	0.92	1645.2	27.1	1672.5	16.6	1707.3	14.2	1707.3	14.2
RF16-23A PC-65	448	140807	2.3	9.534	0.7	4.3701	2.4	0.3023	2.3	0.94	1702.8	34.8	1706.7	20.0	1712.3	12.4	1712.3	12.4
RF16-23A PC-18	162	76889	2.8	9.534	0.7	4.3733	2.3	0.3025	2.2	0.95	1703.8	33.4	1707.3	19.4	1712.4	13.6	1712.4	13.6
RF16-23A PC-21	568	143478	1.8	9.533	0.8	4.2913	2.3	0.2968	2.2	0.94	1675.6	31.9	1691.7	19.0	1712.5	14.8	1712.5	14.8
RF16-23A PC-93	249	70880	2.7	9.532	0.9	4.2973	2.5	0.2972	2.3	0.93	1677.4	34.1	1692.8	20.4	1712.8	16.7	1712.8	16.7
RF16-23A PC-37	300	76915	1.9	9.523	0.9	4.4100	2.3	0.3047	2.2	0.92	1714.7	32.4	1714.2	19.4	1714.5	16.7	1714.5	16.7
RF16-23A PC-50	989	4338929	2.2	9.425	1.1	4.7537	2.4	0.3251	2.1	0.89	1814.5	34.0	1776.8	20.4	1733.5	20.7	1733.5	20.7
RF16-23A PC-76	321	1356239	1.1	9.425	0.7	4.3619	2.3	0.2983	2.2	0.95	1682.8	32.2	1705.2	18.8	1733.5	12.7	1733.5	12.7
RF16-23A PC-87	81	183283	4.8	9.376	0.8	4.5000	2.5	0.3061	2.4	0.95	1721.7	36.4	1731.0	21.1	1743.0	14.7	1743.0	14.7
RF16-23A PC-70	98	56771	1.2	9.365	1.0	4.6374	4.0	0.3151	3.8	0.97	1765.8	59.5	1756.0	33.1	1745.2	17.5	1745.2	17.5
RF16-23A-153	162	55104	2.1	9.351	0.9	4.8101	2.5	0.3263	2.4	0.95	1820.6	37.5	1786.7	21.0	1748.0	14.7	1748.0	14.7
RF16-23A PC-11	332	143138	3.4	9.350	0.8	4.5281	2.3	0.3072	2.1	0.94	1726.9	32.5	1736.1	19.0	1748.1	14.6	1748.1	14.6
RF16-23A PC-43	335	144977	3.6	9.300	0.9	4.5403	2.4	0.3064	1.7	0.90	1722.9	26.4	1738.4	16.2	1757.9	15.9	1757.9	15.9
RF16-23A PC-30	203	47041	3.6	9.263	0.8	4.7036	2.5	0.3161	2.4	0.95	1770.9	37.1	1767.9	21.2	1765.1	14.6	1765.1	14.6
RF16-23A-138	274	255893	1.4	9.242	0.6	4.5724	1.7	0.3066	1.6	0.94	1724.0	24.6	1744.2	14.4	1769.4	10.8	1769.4	10.8
RF16-23A PC-91	201	75952	1.3	9.186	0.8	4.6006	2.4	0.3066	2.2	0.94	1724.2	33.9	1749.4	19.8	1780.4	14.3	1780.4	14.3
RF16-23A PC-95	187	110476	1.5	9.126	0.8	4.6595	2.3	0.3085	2.2	0.94	1733.5	33.4	1760.0	19.5	1792.3	14.1	1792.3	14.1
RF16-23A-218	340	182032	5.3	9.043	0.7	4.8417	2.0	0.3177	1.9	0.93	1778.4	29.5	1792.2	17.2	1809.0	13.6	1809.0	13.6
RF16-23A PC-27	259	70332	1.9	8.544	0.7	5.0847	2.7	0.3152	2.6	0.97	1766.3	40.3	1833.6	22.9	1911.5	12.7	1911.5	12.7
RF16-23A PC-49	99	156014	0.9	8.441	1.1	5.5939	2.4	0.3426	2.1	0.88	1899.1	34.5	1915.2	20.5	1933.3	20.1	1933.3	20.1
RF16-23A PC-59	290	71173	3.1	7.713	0.9	6.5162	2.4	0.3647	2.3	0.93	2004.3	39.0	2048.1	21.3	2093.2	15.3	2093.2	15.3
RF16-23A PC-33	357	189760	1.8	6.545	0.9	9.4708	2.4	0.4498	2.2	0.92	2394.2	43.4	2384.7	21.7	2377.4	16.1	2377.4	16.1
RF16-23A PC-54	322	197157	1.9	6.071	0.8	10.7970	2.0	0.4756	1.9	0.93	2507.9	38.7	2505.8	18.7	2504.8	12.9	2504.8	12.9

Analysis	U	206Pb	U/Th	206Pb*	±	207Pb*	±	206Pb*	±	error	206Pb*	±	207Pb*	±	206Pb*	±	Best age	±
	(ppm)	204Pb		207Pb*	(%)	235U*	(%)	238U	(%)	corr.	238U* (Ma)	(Ma)	235U (Ma)	(Ma)	207Pb* (Ma)	(Ma)	(Ma)	(Ma)

Sample, RF16-23B1, Yakutat Group Flysch Facies, (59.80011°,-139.295269°)

Analysis	U	206Pb	U/Th	206Pb*	±	207Pb*	±	206Pb*	±	error	206Pb*	±	207Pb*	±	206Pb*	±	Best age	±
RF16-23b1-32	268.67	11856.25049	1.6	20.449	1.8	0.1471	3.2	0.0218	2.6	0.82	139.2	3.6	139.3	4.1	143.2	43.09	139.2	3.6
RF16-23b1-35	109.69	2129.934067	2.5	22.277	1.6	0.1481	3.0	0.0239	2.6	0.85	152.5	3.9	140.2	4.0	NA	NA	152.5	3.9
RF16-23b1-19	135.9	4367.871803	1.9	21.150	2.0	0.1567	3.8	0.0241	3.3	0.86	153.2	5.0	147.8	5.3	63.5	47.25	153.2	5.0
RF16-23b1-33	98.642	19641.73075	2.7	20.219	2.1	0.1650	3.7	0.0242	3.1	0.84	154.2	4.7	155.1	5.3	169.5	48.69	154.2	4.7
RF16-23b1-31	125.95	6049.077786	2.7	20.016	2.0	0.1670	3.3	0.0242	2.7	0.79	154.5	4.1	156.8	4.9	193.2	47.32	154.5	4.1
RF16-23b1-26	108.85	3116.920401	3.0	21.647	1.6	0.1555	3.1	0.0244	2.6	0.84	155.6	4.0	146.8	4.2	7.8	39.4	155.6	4.0
RF16-23b1-34	131.7	17209.18432	2.0	20.664	1.9	0.1637	3.5	0.0245	2.9	0.83	156.3	4.4	154.0	4.9	118.6	45.1	156.3	4.4
RF16-23b1-21	143.96	4408.909297	2.8	21.234	1.7	0.1594	3.2	0.0246	2.8	0.85	156.4	4.3	150.2	4.5	54.0	40.75	156.4	4.3
RF16-23b1-20	149.17	29389.84509	2.3	19.562	2.3	0.1734	3.6	0.0246	2.8	0.78	156.7	4.3	162.4	5.4	246.2	52.01	156.7	4.3
RF16-23b1-7	214.5	31738.36373	2.5	19.860	1.3	0.1709	2.9	0.0246	2.6	0.89	156.8	4.0	160.2	4.3	211.3	30.27	156.8	4.0
RF16-23b1-23	192.02	26280.17958	2.7	20.024	2.0	0.1696	3.6	0.0246	3.0	0.83	157.0	4.7	159.1	5.4	192.2	46.65	157.0	4.7
RF16-23b1-14	119.51	8507.053343	1.8	20.041	2.8	0.1697	3.9	0.0247	2.6	0.68	157.1	4.1	159.2	5.7	190.3	66.12	157.1	4.1
RF16-23b1-29	101.69	10464.13247	2.7	20.183	2.1	0.1708	3.5	0.0250	2.7	0.79	159.3	4.3	160.1	5.1	173.8	49.91	159.3	4.3
RF16-23b1-24	99.355	50036.35315	2.6	19.898	1.9	0.1738	3.1	0.0251	2.5	0.79	159.8	3.9	162.7	4.7	206.9	44.52	159.8	3.9
RF16-23b1-27	516.97	60903.87956	1.4	20.019	1.7	0.1839	3.6	0.0267	3.2	0.89	169.9	5.4	171.4	5.7	192.8	39.23	169.9	5.4
RF16-23b1-5	371.46	67378.49066	1.3	19.855	1.0	0.1906	2.8	0.0275	2.6	0.92	174.6	4.5	177.1	4.6	211.9	25.3	174.6	4.5
RF16-23b1-15	170.83	429378.4111	2.1	19.640	1.3	0.1941	3.0	0.0277	2.7	0.91	175.9	4.7	180.1	5.0	237.0	29.4	175.9	4.7
RF16-23b1-16	579.98	168815.4083	1.6	20.139	1.2	0.1901	3.3	0.0278	3.1	0.93	176.6	5.3	176.7	5.4	178.9	28.63	176.6	5.3
RF16-23b1-11	333.39	8870.062692	1.5	17.541	2.0	0.2188	3.4	0.0278	2.8	0.81	177.0	4.9	200.9	6.2	491.9	43.82	177.0	4.9

						Isotope ratios						Apparent ages (Ma)							
Analysis	U	206Pb	U/Th	206Pb*	±	207Pb*	±	206Pb*	±	error	206Pb*	±	207Pb*	±	206Pb*	±	Best age	±
	(ppm)	204Pb		207Pb*	(%)	235U*	(%)	238U	(%)	corr.	238U*	(Ma)	235U	(Ma)	207Pb*	(Ma)	(Ma)	(Ma)
RF16-23b1-3	297.23	3692879.676	1.6	19.445	1.2	0.1982	3.2	0.0280	2.9	0.92	177.8	5.1	183.6	5.3	260.1	27.89	177.8	5.1
RF16-23b1-2	179.37	13933.92314	2.1	19.951	1.3	0.1934	2.8	0.0280	2.5	0.88	178.0	4.3	179.5	4.6	200.7	30.69	178.0	4.3
RF16-23b1-4	375.79	1229370.912	1.4	19.560	1.2	0.1972	3.2	0.0280	3.0	0.92	178.0	5.2	182.8	5.4	246.5	28.6	178.0	5.2
RF16-23b1-1	222.71	25029.1451	1.9	19.578	1.4	0.1977	2.7	0.0281	2.4	0.87	178.5	4.2	183.2	4.6	244.3	31.32	178.5	4.2
RF16-23b1-13	107.02	3831.717548	2.6	20.761	3.8	0.1867	4.6	0.0281	2.6	0.55	178.8	4.5	173.8	7.4	107.6	90.96	178.8	4.5
RF16-23b1-30	131.36	16924.98435	2.8	19.723	1.5	0.1980	2.7	0.0283	2.3	0.83	180.1	4.0	183.4	4.6	227.4	35.17	180.1	4.0
RF16-23b1-12	122.04	27037.97503	2.1	19.984	1.6	0.1958	2.6	0.0284	2.1	0.80	180.5	3.7	181.6	4.3	196.9	36.15	180.5	3.7
RF16-23b1-18	266.02	14596.90472	1.7	20.021	1.5	0.1959	3.1	0.0285	2.7	0.87	180.9	4.7	181.7	5.1	192.5	35.38	180.9	4.7
RF16-23b1-10	178.21	31031.55155	2.6	19.798	1.5	0.1983	3.1	0.0285	2.7	0.88	181.0	4.9	183.7	5.2	218.5	33.9	181.0	4.9
RF16-23b1-25	347.9	39847.27767	2.1	20.158	1.5	0.1950	3.3	0.0285	2.9	0.89	181.3	5.2	180.9	5.4	176.7	35.29	181.3	5.2
RF16-23b1-22	208.18	4151.396863	2.0	13.607	4.4	0.2923	5.2	0.0289	2.9	0.55	183.4	5.2	260.4	12.0	1027.5	88.23	183.4	5.2
RF16-23b1-9	191.64	37386.50021	2.3	19.474	1.4	0.2044	2.8	0.0289	2.4	0.86	183.5	4.4	188.8	4.9	256.6	33.05	183.5	4.4
RF16-23b1-8	149.68	10076.22511	2.0	20.149	1.6	0.1979	3.5	0.0289	3.1	0.89	183.9	5.6	183.3	5.9	177.7	37.8	183.9	5.6
RF16-23b1-6	126.27	3686.739058	2.7	11.326	7.0	0.3670	7.6	0.0302	3.1	0.37	191.6	5.3	317.4	20.7	1388.8	135.3	191.6	5.3
RF16-23b1-28	359.28	92871.75943	7.0	11.589	1.0	2.8337	3.2	0.2383	3.0	0.95	1377.7	37.5	1364.5	24.0	1344.7	20.2	1344.7	20.2
RF16-23b1-17	1496.8	1108720.569	32.3	6.557	1.1	8.8705	2.8	0.4221	2.5	0.92	2269.8	48.7	2324.8	25.2	2374.1	18.31	2374.1	18.3

						Isotope ratios						Apparent ages (Ma)							
Analysis	U	206Pb	U/Th	206Pb*	±	207Pb*	±	206Pb*	±	error	206Pb*	±	207Pb*	±	206Pb*	±	Best age	±
	(ppm)	204Pb		207Pb*	(%)	235U*	(%)	238U	(%)	corr.	238U*	(Ma)	235U	(Ma)	207Pb*	(Ma)	(Ma)	(Ma)

Sample, RF16-23B2, Yakutat Group Flysch Facies, (59.80011°,-139.295269°)

Analysis	U (ppm)	206Pb/204Pb	U/Th	206Pb*/207Pb*	± (%)	207Pb*/235U*	± (%)	206Pb*/238U	± (%)	error corr.	206Pb*/238U* (Ma)	± (Ma)	207Pb*/235U (Ma)	± (Ma)	206Pb*/207Pb* (Ma)	± (Ma)	Best age (Ma)	± (Ma)
RF16-23b2-56	286.39	19630.71536	3.9	20.113	1.5	0.1118	2.8	0.0163	2.3	0.85	104.4	2.4	107.6	2.8	181.9	34.33	104.4	2.4
RF16-23b2-37	280.8	6700.819216	1.8	21.278	1.5	0.1085	2.6	0.0167	2.2	0.83	107.1	2.3	104.6	2.6	49.0	34.9	107.1	2.3
RF16-23b2-66	168.79	4910.265271	1.8	20.964	3.4	0.1575	4.3	0.0240	2.6	0.60	152.6	3.9	148.5	6.0	84.4	81.51	152.6	3.9
RF16-23b2-57	210.63	37254.7497	2.0	20.003	1.8	0.1669	2.7	0.0242	2.0	0.74	154.3	3.0	156.7	3.9	194.7	42.04	154.3	3.0
RF16-23b2-45	516.72	138942.7211	1.4	19.729	1.3	0.1781	3.0	0.0255	2.7	0.90	162.3	4.4	166.4	4.7	226.6	31.16	162.3	4.4
RF16-23b2-40	137.51	397439.2965	2.9	19.237	1.6	0.1856	2.7	0.0259	2.2	0.81	164.9	3.6	172.9	4.3	284.7	36.01	164.9	3.6
RF16-23b2-48	152.92	10285.32315	2.6	20.203	2.0	0.1772	2.9	0.0260	2.1	0.72	165.3	3.4	165.7	4.4	171.5	46.62	165.3	3.4
RF16-23b2-49	189.74	5344.250703	2.2	17.226	2.8	0.2079	3.5	0.0260	2.1	0.61	165.4	3.5	191.8	6.2	531.8	61.56	165.4	3.5
RF16-23b2-60	129.4	1259918.108	2.2	19.351	1.8	0.1852	3.3	0.0260	2.8	0.83	165.5	4.6	172.5	5.3	271.2	42.43	165.5	4.6
RF16-23b2-52	303.78	140912.6485	2.0	19.644	1.4	0.1827	3.0	0.0260	2.6	0.88	165.7	4.2	170.3	4.6	236.5	32.96	165.7	4.2
RF16-23b2-54	151.12	15587.11703	2.3	19.539	1.4	0.1839	3.2	0.0261	2.9	0.90	165.9	4.7	171.4	5.0	248.9	32.23	165.9	4.7
RF16-23b2-46	97.608	7766.240834	2.3	20.218	1.9	0.1782	2.8	0.0261	2.1	0.75	166.4	3.5	166.5	4.4	169.7	44.1	166.4	3.5
RF16-23b2-58	136.79	9582.946854	2.8	20.774	1.8	0.1741	3.5	0.0262	3.1	0.86	167.0	5.1	162.9	5.3	105.9	42.15	167.0	5.1
RF16-23b2-38	195.73	6604.552636	2.0	20.625	1.6	0.1760	3.3	0.0263	2.9	0.87	167.6	4.8	164.6	5.1	123.0	38.15	167.6	4.8
RF16-23b2-43	167.94	7168.759208	2.8	20.181	2.1	0.1803	3.8	0.0264	3.2	0.84	168.0	5.3	168.3	5.9	174.0	48.7	168.0	5.3
RF16-23b2-65	96.076	3155.423455	2.4	20.351	4.3	0.1789	5.3	0.0264	3.2	0.59	168.1	5.2	167.1	8.2	154.4	100.3	168.1	5.2
RF16-23b2-47	126.09	13632.70379	2.0	19.873	1.7	0.1833	3.2	0.0264	2.8	0.85	168.2	4.6	170.9	5.1	209.8	39.87	168.2	4.6
RF16-23b2-63	126.36	10948.40106	2.5	20.502	1.6	0.1785	2.6	0.0265	2.0	0.78	168.9	3.4	166.7	4.0	137.1	37.89	168.9	3.4
RF16-23b2-42	287.5	48341.83111	2.3	19.489	1.4	0.1878	2.5	0.0266	2.1	0.83	169.0	3.5	174.8	4.1	254.8	32.47	169.0	3.5
RF16-23b2-55	212.18	167359.1242	2.5	19.350	1.6	0.1895	2.6	0.0266	2.0	0.79	169.2	3.4	176.2	4.2	271.3	36.72	169.2	3.4
RF16-23b2-61	618.88	17499.46059	1.6	20.245	1.1	0.1812	2.9	0.0266	2.7	0.93	169.4	4.6	169.1	4.6	166.6	25.67	169.4	4.6
RF16-23b2-50	125.94	7279.188413	3.5	19.557	2.1	0.1876	3.5	0.0266	2.8	0.81	169.4	4.7	174.6	5.6	246.9	47.31	169.4	4.7
RF16-23b2-41	147.45	15077.09155	2.4	20.247	2.1	0.1815	3.3	0.0267	2.6	0.78	169.7	4.4	169.4	5.2	166.4	48.13	169.7	4.4
RF16-23b2-59	963.66	1526902.444	2.0	19.591	1.2	0.1877	3.0	0.0267	2.7	0.91	169.7	4.6	174.6	4.8	242.7	27.83	169.7	4.6
RF16-23b2-44	153.44	2696.203316	2.3	11.494	8.3	0.3269	8.8	0.0273	3.0	0.34	173.4	5.1	287.2	22.0	1360.5	159.8	173.4	5.1
RF16-23b2-53	92.482	1348.593238	3.5	7.963	13.5	0.5339	14.3	0.0308	4.9	0.34	195.9	9.5	434.4	50.7	2037.0	239.3	195.9	9.5
RF16-23b2-62	125.61	413.5314478	3.3	3.335	43.1	1.6422	43.5	0.0397	5.1	0.12	251.2	12.7	986.6	281.2	3469.2	709.2	251.2	12.7
RF16-23b2-36	706.81	5063.791448	1.2	14.153	1.7	0.6032	3.4	0.0619	3.0	0.87	387.4	11.2	479.3	13.2	947.5	35.28	387.4	11.2
RF16-23b2-39	481.38	205127.4371	1.7	11.439	1.0	2.7198	3.3	0.2257	3.1	0.91	1312.1	36.9	1333.9	24.2	1369.8	18.87	1369.8	18.9
RF16-23b2-64	262.33	1011378.48	4.2	9.664	1.0	4.4010	3.8	0.3086	3.7	0.96	1733.8	55.7	1712.5	31.4	1687.4	18.42	1687.4	18.4
RF16-23b2-51	248.55	100638.6467	2.3	9.526	0.9	4.3111	2.3	0.2980	2.2	0.93	1681.3	32.3	1695.5	19.3	1713.8	15.98	1713.8	16.0

						Isotope ratios						Apparent ages (Ma)							
Analysis	U	206Pb	U/Th	206Pb*	±	207Pb*	±	206Pb*	±	error	206Pb*	±	207Pb*	±	206Pb*	±	Best age	±
	(ppm)	204Pb		207Pb*	(%)	235U*	(%)	238U	(%)	corr.	238U*	(Ma)	235U	(Ma)	207Pb*	(Ma)	(Ma)	(Ma)

Sample, RF16-16, Yakutat Group Flysch Facies, (59.93722°,139.39713°)

Analysis	U (ppm)	206Pb/204Pb	U/Th	206Pb*/207Pb*	± (%)	207Pb*/235U*	± (%)	206Pb*/238U	± (%)	error corr.	206Pb*/238U* (Ma)	± (Ma)	207Pb*/235U (Ma)	± (Ma)	206Pb*/207Pb* (Ma)	± (Ma)	Best age (Ma)	± (Ma)
RF16-16-7	46.911	34681.90739	3.3	20.129	2.3	0.1814	4.2	0.0265	3.5	0.83	168.6	5.8	169.3	6.5	180.0	54.79	168.6	5.8
RF16-16-42	44.945	84067.73086	3.8	19.341	2.0	0.1896	3.8	0.0266	3.2	0.86	169.2	5.4	176.3	6.1	272.4	44.73	169.2	5.4
RF16-16-35	90.557	20741.36069	2.6	20.204	1.9	0.1817	4.0	0.0266	3.5	0.88	169.5	5.9	169.5	6.2	171.3	44.31	169.5	5.9
RF16-16-27	147.21	6223.72366	2.4	20.135	1.8	0.1839	3.5	0.0269	3.0	0.86	170.9	5.0	171.4	5.5	179.3	41.38	170.9	5.0
RF16-16-6	87.498	37450.69806	3.1	19.168	1.5	0.1937	3.2	0.0269	2.8	0.88	171.4	4.8	179.8	5.3	292.9	35.01	171.4	4.8
RF16-16-41	50.459	8327.223602	4.0	20.202	3.1	0.1839	4.4	0.0270	3.1	0.70	171.5	5.2	171.4	6.9	171.6	72.51	171.5	5.2
RF16-16-13	82.254	8564.087747	2.8	21.115	2.6	0.1762	4.9	0.0270	4.1	0.85	171.7	7.0	164.8	7.4	67.3	61.87	171.7	7.0
RF16-16-17	57.629	8924.050288	1.9	19.269	2.5	0.1933	3.7	0.0270	2.7	0.74	171.9	4.6	179.4	6.1	280.8	56.29	171.9	4.6
RF16-16-20	58.364	10128.38462	3.9	20.280	2.2	0.1842	3.5	0.0271	2.7	0.77	172.4	4.5	171.7	5.5	162.6	52.02	172.4	4.5
RF16-16-21	59.564	3502.980002	3.0	20.436	4.8	0.1829	5.6	0.0271	3.0	0.53	172.5	5.1	170.5	8.9	144.6	112.4	172.5	5.1
RF16-16-22	119.89	39162.72404	3.4	19.354	1.6	0.1938	3.6	0.0272	3.3	0.90	173.1	5.6	179.8	6.0	270.7	35.72	173.1	5.6
RF16-16-8	98.043	13850.67377	4.2	20.311	1.7	0.1848	3.4	0.0272	3.0	0.86	173.2	5.1	172.2	5.5	159.0	40.6	173.2	5.1
RF16-16-14	51.896	26886.4063	5.1	19.452	1.8	0.1930	3.7	0.0272	3.3	0.88	173.3	5.6	179.2	6.1	259.1	41.53	173.3	5.6
RF16-16-39	122.1	291538.912	2.4	19.403	1.7	0.1937	3.6	0.0273	3.2	0.88	173.4	5.5	179.8	6.0	265.0	39.31	173.4	5.5
RF16-16-2	218.07	31327.54048	2.0	19.789	1.5	0.1900	2.9	0.0273	2.5	0.85	173.5	4.3	176.7	4.7	219.6	34.9	173.5	4.3
RF16-16-44	56.261	2731.7412	2.9	21.426	2.4	0.1755	3.9	0.0273	3.1	0.79	173.6	5.3	164.2	5.9	32.5	56.96	173.6	5.3
RF16-16-30	83.78	7923.222868	3.7	20.160	1.9	0.1866	3.5	0.0273	2.9	0.84	173.6	5.0	173.7	5.5	176.4	44.4	173.6	5.0
RF16-16-43	44.222	8958.626748	4.1	20.621	2.5	0.1825	4.1	0.0273	3.3	0.79	173.6	5.6	170.2	6.5	123.4	59.75	173.6	5.6
RF16-16-34	48.386	11569.41946	3.4	18.941	2.9	0.1989	4.3	0.0273	3.1	0.73	173.8	5.3	184.2	7.2	320.1	66.54	173.8	5.3
RF16-16-12	43.212	4062.357066	3.8	20.657	2.8	0.1826	3.8	0.0274	2.6	0.68	174.1	4.4	170.3	5.9	119.4	64.98	174.1	4.4
RF16-16-29	124.47	7346.57849	2.5	20.583	2.5	0.1833	3.5	0.0274	2.5	0.70	174.1	4.2	170.9	5.5	127.8	59.03	174.1	4.2
RF16-16-33	39.093	26536.52849	4.0	19.045	2.5	0.1984	3.6	0.0274	2.5	0.70	174.3	4.4	183.7	6.0	307.5	57.41	174.3	4.4
RF16-16-31	57.328	67294.69814	5.1	19.488	2.0	0.1940	3.3	0.0274	2.7	0.81	174.5	4.7	180.0	5.5	255.0	44.96	174.5	4.7
RF16-16-18	91.731	21716.26736	2.5	20.013	2.0	0.1889	3.5	0.0274	2.9	0.82	174.5	5.0	175.7	5.7	193.5	47.39	174.5	5.0
RF16-16-19	115.21	32475.64501	3.4	19.759	1.9	0.1916	3.2	0.0275	2.8	0.86	174.7	4.8	178.0	5.2	223.1	37.4	174.7	4.8
RF16-16-4	130.17	29387.30712	4.7	19.658	1.5	0.1929	3.9	0.0275	3.6	0.92	174.9	6.2	179.1	6.4	234.9	35.22	174.9	6.2
RF16-16-15	95.694	11886.66686	5.0	20.125	2.1	0.1886	3.9	0.0275	3.3	0.84	175.1	5.7	175.4	6.4	180.5	49.4	175.1	5.7
RF16-16-10	54.729	10648.29025	3.6	20.556	2.2	0.1855	3.4	0.0277	2.6	0.76	175.9	4.4	172.8	5.3	130.8	51.58	175.9	4.4
RF16-16-24	174.59	40238.6719	4.0	19.907	1.3	0.1915	2.9	0.0277	2.5	0.88	175.9	4.4	177.9	4.7	205.9	30.97	175.9	4.4
RF16-16-32	44.531	8113.320385	3.9	19.480	2.9	0.1959	5.1	0.0277	4.2	0.83	176.1	7.3	181.7	8.4	255.9	65.74	176.1	7.3
RF16-16-37	36.38	4565.965921	3.6	22.676	3.5	0.1687	4.7	0.0278	3.1	0.66	176.5	5.3	158.3	6.8	NA	NA	176.5	5.3
RF16-16-11	161.41	10229.9629	2.2	20.177	1.6	0.1897	3.8	0.0278	3.4	0.91	176.6	6.0	176.2	6.1	174.5	36.81	176.6	6.0
RF16-16-36	51.13	9088.166515	3.1	20.313	2.7	0.1886	4.2	0.0278	3.3	0.78	176.7	5.8	175.4	6.8	158.7	62.61	176.7	5.8
RF16-16-40	152.71	21893.76793	2.7	20.395	1.7	0.1879	3.2	0.0278	2.7	0.84	176.8	4.6	174.8	5.1	149.3	39.97	176.8	4.6
RF16-16-1	67.929	8023.948324	2.6	19.745	2.3	0.1948	3.7	0.0279	2.9	0.78	177.4	5.0	180.7	6.1	224.7	53.01	177.4	5.0
RF16-16-28	55.3	5255.23215	2.7	20.945	2.0	0.1837	3.5	0.0279	2.9	0.81	177.5	5.0	171.2	5.5	86.6	48.52	177.5	5.0
RF16-16-16	67.91	59699.78412	2.6	18.694	3.2	0.2066	3.5	0.0280	2.6	0.73	178.2	4.6	190.7	6.1	349.8	52.28	178.2	4.6
RF16-16-5	129.25	14612.66693	3.4	19.812	2.1	0.1958	3.9	0.0282	3.3	0.85	179.0	5.8	181.6	6.5	216.9	47.55	179.0	5.8
RF16-16-38	91.543	41924.32961	2.7	19.638	2.2	0.1977	4.3	0.0282	3.6	0.85	179.1	6.4	183.2	7.2	237.3	51.75	179.1	6.4
RF16-16-3	52.993	9077.943106	3.6	19.215	2.8	0.2037	4.6	0.0284	3.6	0.80	180.5	6.5	188.2	7.8	287.2	63.24	180.5	6.5

				Isotope ratios							Apparent ages (Ma)							
Analysis	U	206Pb	U/Th	206Pb*	±	207Pb*	±	206Pb*	±	error	206Pb*	±	207Pb*	±	206Pb*	±	Best age	±
	(ppm)	204Pb		207Pb*	(%)	235U*	(%)	238U	(%)	corr.	238U*	(Ma)	235U	(Ma)	207Pb*	(Ma)	(Ma)	(Ma)
RF16-16-9	40.361	14907.92228	3.2	18.240	2.6	0.2167	3.5	0.0287	2.2	0.65	182.3	4.0	199.2	6.3	405.0	58.95	182.3	4.0
RF16-16-23	47.777	14334.9981	3.9	20.425	2.4	0.1939	3.7	0.0287	2.8	0.76	182.6	5.0	179.9	6.1	146.0	56.87	182.6	5.0
RF16-16-26	52.449	7431.272688	4.0	13.625	5.3	0.2916	6.4	0.0288	3.7	0.58	183.2	6.7	259.9	14.8	1024.8	106.6	183.2	6.7
Sample, RF16-26, Yakutat Group Flysch Facies, (59.85071°,139.31404°)																		
RF16-26-74	75.584	5919.038946	2.7	20.165	2.3	0.1805	3.7	0.0264	2.9	0.78	168.1	4.8	168.5	5.8	175.8	54.64	168.1	4.8
RF16-26-59	79.303	18290.87626	3.0	19.860	1.9	0.1833	3.3	0.0264	2.7	0.82	168.1	4.5	170.9	5.2	211.3	43.82	168.1	4.5
RF16-26-71	28.562	1391.942439	3.5	22.610	4.1	0.1619	5.3	0.0266	3.4	0.64	169.0	5.7	152.4	7.5	NA	NA	169.0	5.7
RF16-26-85	52.687	8525.987785	2.9	19.297	2.7	0.1898	4.4	0.0266	3.4	0.78	169.1	5.7	176.5	7.1	277.6	62.88	169.1	5.7
RF16-26-57	97.252	4886.243841	3.2	20.840	2.0	0.1774	3.6	0.0268	3.1	0.76	170.7	5.2	165.8	5.6	98.5	46.76	170.7	5.2
RF16-26-72	78.926	8378.510736	2.6	20.046	2.5	0.1854	4.1	0.0270	3.3	0.79	171.5	5.5	172.7	6.5	189.6	58.29	171.5	5.5
RF16-26-60	49.68	2801.609341	2.6	21.789	3.1	0.1708	4.6	0.0270	3.4	0.74	171.7	5.7	160.1	6.8	NA	NA	171.7	5.7
RF16-26-75	100.29	14689.57158	3.3	19.359	1.9	0.1924	3.4	0.0270	2.8	0.83	171.9	4.8	178.6	5.6	270.2	43.77	171.9	4.8
RF16-26-68	76.464	5315.352512	2.5	20.111	2.3	0.1852	3.8	0.0270	3.0	0.80	171.9	5.2	172.5	6.1	182.1	53.59	171.9	5.2
RF16-26-63	117.05	11913.16044	5.1	19.632	1.5	0.1900	3.3	0.0271	2.9	0.89	172.1	4.9	176.6	5.3	238.0	34.55	172.1	4.9
RF16-26-77	41.24	3024.19623	2.8	20.531	2.1	0.1825	3.9	0.0272	3.3	0.84	172.9	5.6	170.2	6.1	133.8	49.56	172.9	5.6
RF16-26-56	61.762	5023.448534	2.9	20.583	2.6	0.1820	4.1	0.0272	3.1	0.77	172.9	5.3	169.8	6.4	127.8	61.29	172.9	5.3
RF16-26-62	82.21	14446.75124	3.1	20.144	2.3	0.1861	3.8	0.0272	3.0	0.79	173.0	5.1	173.3	6.0	178.3	53.8	173.0	5.1
RF16-26-76	31.206	17531.95551	3.5	18.094	3.1	0.2076	4.5	0.0273	3.2	0.72	173.4	5.5	191.5	7.9	423.1	70.22	173.4	5.5
RF16-26-83	59.564	6570.047604	2.9	19.803	2.3	0.1901	3.7	0.0273	2.9	0.79	173.7	4.9	176.9	5.9	217.9	52.26	173.7	4.9
RF16-26-58	76.137	275606.4112	4.5	19.544	1.8	0.1930	3.5	0.0274	3.1	0.86	174.1	5.2	179.2	5.8	248.3	41.37	174.1	5.2
RF16-26-81	61.794	33378.6193	2.9	19.084	1.8	0.1980	3.5	0.0274	3.0	0.85	174.3	5.1	183.4	5.8	302.9	41.15	174.3	5.1
RF16-26-70	43.08	2428.336962	2.7	21.125	2.7	0.1789	3.9	0.0274	2.8	0.71	174.4	4.8	167.2	6.0	66.3	65.13	174.4	4.8
RF16-26-67	53.523	7506.476901	3.8	19.847	2.4	0.1906	3.8	0.0275	3.0	0.78	174.6	5.1	177.2	6.2	212.8	56.12	174.6	5.1
RF16-26-54	55.106	87015.61213	2.7	19.470	2.2	0.1945	4.0	0.0275	3.3	0.83	174.7	5.7	180.5	6.6	257.1	51.07	174.7	5.7
RF16-26-73	59.043	5487.492361	2.8	20.251	2.4	0.1872	3.9	0.0275	3.1	0.79	174.9	5.3	174.2	6.3	165.9	56.5	174.9	5.3
RF16-26-64	80.344	9943.181664	2.7	20.229	1.9	0.1877	3.8	0.0275	3.3	0.86	175.2	5.6	174.7	6.1	168.4	45.5	175.2	5.6
RF16-26-78	27.733	2941.431882	5.0	20.653	3.7	0.1840	5.0	0.0276	3.4	0.68	175.3	5.8	171.5	7.9	119.8	86.66	175.3	5.8
RF16-26-66	66.655	25126.82162	2.6	19.982	2.2	0.1902	3.6	0.0276	2.9	0.79	175.4	5.0	176.8	5.9	197.1	51.18	175.4	5.0
RF16-26-65	77.689	11904.63505	4.9	20.588	2.0	0.1850	3.9	0.0276	3.4	0.85	175.7	5.8	172.3	6.2	127.2	48.2	175.7	5.8
RF16-26-52	57.523	28483.48431	2.8	19.597	1.8	0.1945	3.2	0.0277	2.7	0.82	175.9	4.6	180.5	5.3	242.1	42.09	175.9	4.6
RF16-26-61	79.666	21410.64109	3.1	20.035	1.8	0.1903	3.9	0.0277	3.5	0.88	175.9	6.0	176.9	6.4	190.9	42.79	175.9	6.0
RF16-26-55	64.796	15008.06524	3.0	19.726	2.2	0.1935	4.3	0.0277	3.8	0.87	176.1	6.5	179.6	7.2	227.0	50.37	176.1	6.5
RF16-26-69	94.156	8497.940775	2.9	20.258	1.9	0.1885	3.3	0.0277	3.2	0.87	176.2	5.6	175.3	6.0	165.1	43.26	176.2	5.6
RF16-26-53	47.168	69026.42236	2.6	18.773	2.1	0.2037	3.8	0.0277	3.2	0.83	176.4	5.5	188.2	6.5	340.2	47.94	176.4	5.5
RF16-26-79	67.163	15257.51351	2.9	20.615	2.2	0.1870	3.4	0.0280	2.6	0.76	177.9	4.5	174.1	5.5	124.1	52.4	177.9	4.5
RF16-26-80	32.731	20435.91835	4.2	20.025	2.8	0.1929	5.4	0.0280	4.2	0.77	178.2	7.4	179.1	8.9	192.1	78.9	178.2	7.4
RF16-26-51	58.892	7653.760799	2.6	20.910	2.8	0.1852	3.7	0.0281	2.4	0.65	178.7	4.2	172.6	5.8	90.5	65.81	178.7	4.2
RF16-26-84	29.63	2898.907167	4.4	21.812	2.9	0.1784	4.0	0.0282	2.9	0.71	179.4	5.1	166.6	6.2	NA	NA	179.4	5.1
Sample, RF16-04, Schist of Nunatak Fjord, (59.84210°, 139.09860°)																		
RF16-04-45	280.76	8091.56103	3.7	16.307	3.9	0.0901	4.7	0.0107	2.6	0.56	68.3	1.8	87.6	4.0	650.5	84.6	68.3	1.8
RF16-04-1	162.81	3942.19192	4.7	20.972	3.7	0.0707	4.5	0.0108	2.6	0.57	69.0	1.8	69.4	3.0	83.5	87.7	69.0	1.8
RF16-04-64	240.4	6286.03511	4.0	21.095	2.2	0.0705	3.2	0.0108	2.3	0.72	69.2	1.6	69.2	2.1	69.7	52.6	69.2	1.6
RF16-04-54	321.48	13109.2141	4.5	20.604	2.2	0.0724	3.5	0.0108	2.7	0.76	69.4	1.8	71.0	2.4	125.4	52.9	69.4	1.8
RF16-04-103	648.36	28056.2598	2.4	19.995	1.4	0.0748	2.9	0.0109	2.6	0.87	69.6	1.8	73.2	2.1	195.6	33.2	69.6	1.8
RF16-04-105	454.72	196165.577	2.5	20.270	2.0	0.0740	3.3	0.0109	2.6	0.79	69.8	1.8	72.5	2.3	163.7	47.1	69.8	1.8
RF16-04-44	769.43	17072.7614	1.8	20.775	1.4	0.0723	2.7	0.0109	2.3	0.85	69.8	1.6	70.8	1.8	105.9	33.8	69.8	1.6
RF16-04-21	660.11	49668.0371	3.2	20.122	1.3	0.0748	2.1	0.0109	1.6	0.78	70.0	1.1	73.2	1.5	180.8	31	70.0	1.1
RF16-04-53	295.93	17539.463	2.2	20.124	1.7	0.0750	3.1	0.0109	2.5	0.83	70.2	1.8	73.4	2.2	180.6	39.7	70.2	1.8
RF16-04-6	171.82	3080.31797	4.4	21.771	2.6	0.0693	4.1	0.0109	3.2	0.78	70.2	2.2	68.0	2.7	NA	NA	70.2	2.2
RF16-04-58	734.36	34628.751	1.8	20.081	1.6	0.0751	2.5	0.0109	2.0	0.79	70.2	1.4	73.6	1.8	185.6	36.2	70.2	1.4
RF16-04-97	557.05	33792.8849	2.9	20.381	1.8	0.0742	2.9	0.0110	2.3	0.79	70.4	1.6	72.7	2.1	151.0	42.5	70.4	1.6
RF16-04-25	480.04	16504.9601	2.4	20.572	1.6	0.0736	3.3	0.0110	2.9	0.88	70.4	2.1	72.1	2.3	129.1	36.5	70.4	2.1
RF16-04-3	396.66	52137.752	1.6	20.707	1.3	0.0731	2.7	0.0110	2.3	0.88	70.5	1.6	71.7	1.9	113.6	30.6	70.5	1.6
RF16-04-8	211.8	3053.04631	4.5	22.564	2.5	0.0671	3.5	0.0110	2.5	0.71	70.5	1.8	66.0	2.3	NA	NA	70.5	1.8
RF16-04-61	469.53	17888.214	3.7	20.379	1.5	0.0746	2.8	0.0110	2.4	0.84	70.7	1.7	73.1	2.0	151.2	35.4	70.7	1.7
RF16-04-65	559.2	10531.623	4.6	20.598	1.6	0.0740	2.9	0.0111	2.4	0.83	70.9	1.7	72.5	2.0	126.1	38	70.9	1.7
RF16-04-37	201.81	32373.9156	3.3	20.366	2.3	0.0751	3.3	0.0111	2.3	0.70	71.2	1.6	73.6	2.3	152.7	54.9	71.2	1.6
RF16-04-16	422.74	12776.4238	4.3	20.593	1.7	0.0743	3.0	0.0111	2.4	0.82	71.2	1.7	72.8	2.1	126.7	40.3	71.2	1.7
RF16-04-40	948.06	284640.353	3.3	20.472	1.1	0.0750	2.0	0.0111	1.7	0.85	71.4	1.2	73.4	1.4	140.4	24.8	71.4	1.2
RF16-04-23	145.03	2686.38451	4.4	21.589	2.6	0.0712	3.2	0.0111	1.9	0.59	71.5	1.4	69.8	2.2	14.3	62.5	71.5	1.4
RF16-04-89	225.98	24941.7871	2.4	19.584	2.3	0.0786	3.3	0.0112	2.3	0.72	71.6	1.7	76.8	2.4	243.7	52.5	71.6	1.7
RF16-04-43	393.5	6282.14833	2.2	21.127	1.6	0.0730	3.0	0.0112	2.5	0.85	71.7	1.8	71.5	2.1	66.1	37.8	71.7	1.8
RF16-04-14	269.45	9116.01477	4.6	20.904	2.2	0.0743	3.1	0.0113	2.2	0.71	72.2	1.6	72.8	2.2	91.3	51.4	72.2	1.6
RF16-04-39	416.74	119257.231	2.6	19.835	1.5	0.0784	2.8	0.0113	2.4	0.84	72.3	1.7	76.6	2.1	214.2	35.1	72.3	1.7
RF16-04-48	769.97	17726.6702	3.1	20.299	1.1	0.0768	1.9	0.0113	1.5	0.82	72.5	1.1	75.1	1.4	160.4	25.3	72.5	1.1
RF16-04-18	1823	58645.4892	3.4	20.554	0.8	0.0760	2.2	0.0113	2.1	0.94	72.6	1.5	74.3	1.6	131.1	17.7	72.6	1.5
RF16-04-101	1392	128242.346	2.2	20.328	1.1	0.0770	2.5	0.0114	2.2	0.89	72.8	1.6	75.3	1.8	157.1	26.4	72.8	1.6
RF16-04-59	1239.8	53218.702	3.8	20.252	1.2	0.0773	2.3	0.0114	2.0	0.86	72.8	1.5	75.6	1.7	165.8	27.9	72.8	1.5
RF16-04-31	496.95	61571.9074	3.5	20.173	1.8	0.0777	3.5	0.0114	3.0	0.86	72.9	2.2	76.0	2.6	174.9	42.5	72.9	2.2
RF16-04-92	3442.7	132575.205	2.0	21.255	1.0	0.0737	2.5	0.0114	2.3	0.91	72.9	1.7	72.2	1.8	51.6	24.8	72.9	1.7
RF16-04-96	46.999	847.698564	2.6	27.264	16.5	0.0577	16.8	0.0114	2.4	0.19	73.2	2.3	57.0	9.3	NA	NA	73.2	2.3
RF16-04-86	2746.9	161449.655	6.9	20.625	1.0	0.0765	2.6	0.0114	2.4	0.92	73.4	1.8	74.8	1.9	122.9	23.7	73.4	1.8
RF16-04-74	270.24	28983.5768	3.5	20.156	1.8	0.0784	3.6	0.0115	3.1	0.86	73.5	2.2	76.6	2.6	176.9	43.1	73.5	2.2
RF16-04-7	853.01	582187.815	1.9	20.157	1.3	0.0786	2.8	0.0115	2.5	0.88	73.7	1.8	76.8	2.1	176.7	30.5	73.7	1.8
RF16-04-75	1601.9	33388.304	3.8	20.083	1.4	0.0790	2.8	0.0115	2.5	0.88	73.8	1.8	77.2	2.1	185.3	31.9	73.8	1.8
RF16-04-17	828.59	30482.8983	3.9	21.028	1.4	0.0754	2.5	0.0115	2.1	0.84	73.8	1.6	73.8	1.8	77.2	32.5	73.8	1.6
RF16-04-88	1592.3	28429.3017	3.3	20.491	1.0	0.0775	2.6	0.0115	2.4	0.93	73.8	1.7	75.8	1.9	138.4	22.9	73.8	1.7
RF16-04-35	362.55	26327.2314	2.3	20.289	1.4	0.0784	2.8	0.0115	2.5	0.87	74.0	1.8	76.6	2.1	161.6	32.9	74.0	1.8
RF16-04-108	370.78	16941.4951	2.6	20.083	2.1	0.0796	3.1	0.0116	2.2	0.73	74.4	1.7	77.8	2.3	185.3	49.4	74.4	1.7
RF16-04-102	3027.9	119913.688	4.4	20.960	1.0	0.0763	2.5	0.0116	2.2	0.89	74.4	1.7	74.7	1.8	84.9	27.6	74.4	1.7
RF16-04-33	932.61	30194.9659	2.3	20.026	1.0	0.0800	2.4	0.0116	2.2	0.90	74.5	1.6	78.1	1.8	192.0	24.1	74.5	1.6
RF16-04-82	828.45	9428.82513	3.4	15.001	2.7	0.1069	3.6	0.0116	2.5	0.68	74.6	1.8	103.1	3.6	827.3	55.8	74.6	1.8
RF16-04-76	3098.8	52888.9736	4.2	20.731	0.9	0.0774	1.9	0.0116	1.6	0.88	74.7	1.2	75.7	1.4	110.9	21.3	74.7	1.2
RF16-04-107	893.41	160297.409	1.9	19.944	1.1	0.0805	2.2	0.0117	1.9	0.85	74.7	1.4	78.7	1.7	201.5	26.6	74.7	1.4
RF16-04-11	525.13	35254.5131	3.3	20.540	1.6	0.0790	2.9	0.0118	2.4	0.85	75.5	1.8	77.2	2.1	132.7	35.7	75.5	1.8
RF16-04-38	614.51	10901.0714	3.9	20.543	1.6	0.0791	2.8	0.0118	2.3	0.81	75.6	1.7	77.3	2.1	132.4	38.3	75.6	1.7
RF16-04-62	236.49	13197.3805	2.4	20.148	2.2	0.0809	3.1	0.0118	2.2	0.71	75.8	1.7	79.0	2.4	177.8	52	75.8	1.7
RF16-04-2	120.76	8928.80352	1.8	20.468	3.4	0.0798	4.2	0.0118	2.4	0.57	75.9	1.8	77.9	3.1	141.0	80.8	75.9	1.8
RF16-04-90	198.55	8963.73468	2.1	21.106	2.6	0.0774	3.7	0.0118	2.6	0.72	75.9	2.0	75.7	2.7	68.4	61.1	75.9	2.0
RF16-04-42	201.27	9956.67621	5.6	21.167	2.2	0.0773	3.2	0.0119	2.2	0.67	76.1	1.6	75.6	2.4	61.6	57.4	76.1	1.6
RF16-04-26	982.54	33204.8023	5.6	20.316	1.1	0.0806	2.9	0.0119	2.6	0.92	76.1	2.0	78.7	2.2	158.4	26.9	76.1	2.0
RF16-04-71	714.23	16182.8745	3.5	20.412	1.5	0.0804	2.7	0.0119	2.2	0.83	76.4	1.7	78.6	2.0	147.4	34.9	76.4	1.7
RF16-04-73	2505.3	80381.1526	3.1	20.652	1.0	0.0796	3.0	0.0119	2.9	0.95	76.4	2.2	77.7	2.3	119.9	22.7	76.4	2.2

					Isotope ratios						Apparent ages (Ma)							
Analysis	U	206Pb	U/Th	206Pb*	±	207Pb*	±	206Pb*	±	error	206Pb*	±	207Pb*	±	206Pb*	±	Best age	±
	(ppm)	204Pb		207Pb*	(%)	235U*	(%)	238U	(%)	corr.	238U*	(Ma)	235U	(Ma)	207Pb*	(Ma)	(Ma)	(Ma)
RF16-04-66	80.386	1796.81785	2.0	23.543	4.2	0.0700	4.9	0.0120	2.5	0.51	76.6	1.9	68.7	3.2	NA	NA	76.6	1.9
RF16-04-60	271.09	4834.59688	4.8	20.663	1.9	0.0798	3.1	0.0120	2.4	0.79	76.6	1.9	77.9	2.3	118.7	44.6	76.6	1.9
RF16-04-87	106.98	1730.19538	1.9	24.146	7.0	0.0683	7.4	0.0120	2.5	0.34	76.7	1.9	67.1	4.8	NA	NA	76.7	1.9
RF16-04-72	151.54	4084.52875	4.5	21.463	3.5	0.0773	4.5	0.0120	2.8	0.62	77.1	2.2	75.6	3.3	28.4	84.4	77.1	2.2
RF16-04-104	851.49	26822.7942	3.7	20.576	1.3	0.0822	2.6	0.0123	2.3	0.88	78.6	1.8	80.2	2.0	128.6	30.1	78.6	1.8
RF16-04-98	1737.3	127655.657	2.9	20.551	1.0	0.0827	2.4	0.0123	2.2	0.91	79.0	1.7	80.7	1.9	131.5	23	79.0	1.7
RF16-04-55	869.39	26013.9573	4.8	20.311	1.1	0.0838	2.2	0.0123	1.9	0.85	79.1	1.5	81.7	1.7	159.1	26.6	79.1	1.5
RF16-04-80	657.64	47319.5636	5.7	20.435	1.5	0.0835	2.7	0.0124	2.2	0.83	79.3	1.7	81.4	2.1	144.7	35.2	79.3	1.7
RF16-04-99	1377.4	67230.953	2.7	20.525	1.1	0.0834	2.6	0.0124	2.4	0.91	79.5	1.9	81.3	2.0	134.5	25.9	79.5	1.9
RF16-04-13	1859.3	68907.0581	3.0	20.605	0.9	0.0832	2.3	0.0124	2.1	0.92	79.7	1.7	81.1	1.8	125.2	21.6	79.7	1.7
RF16-04-27	321.16	4681.74384	2.1	10.985	10.2	0.1564	10.6	0.0125	2.9	0.27	79.9	2.3	147.6	14.6	1447.3	195	79.9	2.3
RF16-04-46	1387.6	34084.9329	5.1	20.716	1.0	0.0832	1.8	0.0125	1.4	0.80	80.1	1.1	81.1	1.4	112.6	24.7	80.1	1.1
RF16-04-56	356.45	58701.5723	2.9	21.029	1.6	0.0820	2.9	0.0125	2.5	0.85	80.2	2.0	80.0	2.3	77.1	36.9	80.2	2.0
RF16-04-52	1812	492164.352	2.2	20.575	1.0	0.0843	2.3	0.0126	2.1	0.90	80.7	1.7	82.2	1.8	128.8	23.4	80.7	1.7
RF16-04-34	829.3	21422.1866	3.7	20.683	1.3	0.0839	2.7	0.0126	2.4	0.88	80.7	1.9	81.8	2.1	116.4	30.2	80.7	1.9
RF16-04-84	278.97	21194.7436	1.8	20.990	2.1	0.0827	3.4	0.0126	2.7	0.80	80.7	2.2	80.7	2.7	81.5	49.2	80.7	2.2
RF16-04-29	1452.9	170231.745	5.5	20.489	1.0	0.0848	1.9	0.0126	1.6	0.85	80.8	1.3	82.7	1.5	138.6	23.6	80.8	1.3
RF16-04-19	587.89	8544.77535	3.6	20.678	1.9	0.0846	2.7	0.0127	2.0	0.72	81.3	1.6	82.4	2.1	117.0	43.8	81.3	1.6
RF16-04-30	931.06	32408.8301	3.6	20.554	1.0	0.0853	2.1	0.0127	1.9	0.89	81.5	1.5	83.1	1.7	131.1	22.5	81.5	1.5
RF16-04-36	1131.2	20480.3576	7.1	21.393	1.0	0.0824	2.6	0.0128	2.4	0.92	81.9	1.9	80.4	2.0	36.1	23.7	81.9	1.9
RF16-04-41	66.148	4049.86547	2.1	21.038	3.6	0.0838	4.4	0.0128	2.5	0.56	81.9	2.0	81.7	3.4	76.1	85.7	81.9	2.0
RF16-04-15	472.07	25788.6363	4.8	19.815	1.5	0.0906	3.2	0.0130	2.8	0.88	83.4	2.4	88.1	2.7	216.5	34.8	83.4	2.4
RF16-04-49	418.74	5585.52851	5.1	21.033	1.7	0.0854	3.5	0.0130	3.0	0.87	83.5	2.5	83.2	2.8	76.6	40.2	83.5	2.5
RF16-04-67	400.27	8901.23513	2.0	20.583	2.2	0.0874	3.2	0.0131	2.2	0.71	83.6	1.9	85.1	2.6	127.8	52.7	83.6	1.9
RF16-04-68	121.79	3000.12198	2.3	20.766	3.8	0.0867	4.5	0.0131	2.4	0.53	83.7	2.0	84.4	3.6	107.0	89.8	83.7	2.0
RF16-04-51	618.84	57972.83	1.3	19.532	1.7	0.0939	3.4	0.0133	3.0	0.88	85.2	2.6	91.1	3.0	249.7	38	85.2	2.6
RF16-04-70	281.73	7932.02814	2.0	19.953	2.7	0.0933	3.6	0.0135	2.4	0.67	86.5	2.1	90.5	3.1	200.5	62.6	86.5	2.1
RF16-04-50	596.74	72222.8959	2.2	20.064	1.3	0.0941	3.4	0.0137	2.8	0.90	87.7	2.5	91.3	2.7	187.5	31.2	87.7	2.5
RF16-04-9	41.517	1508.37668	3.0	23.683	12.1	0.0805	12.4	0.0138	2.6	0.21	88.5	2.3	78.6	9.3	NA	NA	88.5	2.3
RF16-04-77	341.38	11919.6694	1.1	20.374	1.6	0.0940	2.8	0.0139	2.3	0.27	89.0	2.0	91.2	2.4	151.7	38.4	89.0	2.0
RF16-04-32	491.5	12185.4831	9.7	20.239	1.6	0.0996	3.0	0.0146	2.5	0.85	93.6	2.4	96.4	2.7	167.2	36.9	93.6	2.4
RF16-04-47	73.977	9727.99628	3.9	18.457	2.6	0.1147	4.0	0.0154	3.1	0.77	98.3	3.0	110.3	4.2	378.5	57.5	98.3	3.0
RF16-04-5	293.95	7319.56191	1.4	20.535	1.5	0.1588	3.6	0.0237	3.2	0.91	150.7	4.8	149.6	5.0	133.2	34.9	150.7	4.8
RF16-04-69	73.07	7291.01498	1.9	19.672	1.9	0.1690	3.2	0.0241	2.6	0.81	153.7	4.0	158.6	4.8	233.4	44.3	153.7	4.0
RF16-04-100	437.68	16577.8131	1.8	19.755	1.4	0.1755	3.0	0.0252	2.6	0.88	160.2	4.2	164.2	4.6	223.5	33	160.2	4.2
RF16-04-83	259.94	28706.8459	3.4	19.773	1.6	0.1754	3.0	0.0252	2.6	0.86	160.2	4.1	164.1	4.6	221.4	35.9	160.2	4.1
RF16-04-22	97.199	85517.2082	4.2	18.519	2.0	0.1946	3.3	0.0262	2.6	0.80	166.4	4.3	180.6	5.4	370.9	44.3	166.4	4.3
RF16-04-28	365.38	15270.7845	2.6	19.820	1.2	0.2011	2.5	0.0289	2.2	0.89	183.8	4.1	186.1	4.3	216.0	27.1	183.8	4.1
RF16-04-12	390.95	62584.0121	2.4	19.918	1.4	0.2060	2.7	0.0298	2.3	0.86	189.1	4.3	190.2	4.6	204.5	31.5	189.1	4.3
RF16-04-95	771.31	69528.1292	2.0	19.775	0.8	0.2089	1.9	0.0300	1.8	0.92	190.4	3.3	192.6	3.4	221.2	17.8	190.4	3.3
RF16-04-85	1042.5	115129.371	3.0	19.498	1.1	0.2187	2.5	0.0309	2.2	0.90	196.4	4.3	200.8	4.5	253.7	25.5	196.4	4.3
RF16-04-93	516.47	24273.5941	2.5	19.372	0.9	0.2216	2.8	0.0311	2.7	0.95	197.7	5.2	203.2	5.1	268.7	19.7	197.7	5.2
RF16-04-63	503.75	177874.322	2.1	19.204	1.3	0.2271	2.5	0.0316	2.2	0.86	200.8	4.3	207.8	4.7	288.6	29	200.8	4.3
RF16-04-106	951.91	139434.199	3.5	18.768	1.0	0.2401	2.9	0.0327	2.7	0.94	207.4	5.6	218.5	5.7	340.9	22	207.4	5.6
RF16-04-94	765.25	176958.805	6.1	19.752	1.2	0.2286	3.0	0.0328	2.7	0.92	207.8	5.6	209.1	5.6	223.9	27.5	207.8	5.6
RF16-04-91	46.625	10191.8642	3.4	19.252	2.6	0.2525	3.7	0.0353	2.6	0.70	223.4	5.7	228.6	7.6	283.0	60.1	223.4	5.7
RF16-04-20	516.77	18668.9419	2.5	18.590	1.0	0.4118	2.3	0.0555	2.1	0.89	348.5	7.0	350.1	6.9	362.4	23.5	348.5	7.0
RF16-04-4	117.66	23113.5729	4.6	17.921	1.5	0.4364	2.9	0.0567	2.5	0.86	355.8	8.6	367.7	8.9	444.4	32.3	355.8	8.6
RF16-04-78	252.33	62260.6936	2.7	18.036	1.0	0.4730	2.8	0.0619	2.6	0.94	387.1	9.7	393.2	9.0	430.2	21.4	387.1	9.7
RF16-04-24	169.38	107183.769	2.0	6.249	0.8	8.6365	2.5	0.3916	2.4	0.97	2130.3	44.2	2300.4	22.9	2455.9	10.8	2455.9	10.8
RF16-04-81	313.97	273657.512	2.2	5.890	0.7	10.2167	2.3	0.4366	2.1	0.95	2335.5	42.1	2454.6	21.0	2555.5	12.3	2555.5	12.3
RF16-04-57	357.09	3522944.08	2.3	5.780	0.7	11.1010	2.6	0.4655	2.4	0.96	2464.0	50.1	2531.6	23.8	2587.0	12	2587.0	12.0

Yakutat Sample, RF16-26, Yakutat Group Melange Facies, (59.94009°,139.53526°)

					Isotope ratios						Apparent ages (Ma)							
Analysis	U	206Pb	U/Th	206Pb*	±	207Pb*	±	206Pb*	±	error	206Pb*	±	207Pb*	±	206Pb*	±	Best age	±
	(ppm)	204Pb		207Pb*	(%)	235U*	(%)	238U	(%)	corr.	238U*	(Ma)	235U	(Ma)	207Pb*	(Ma)	(Ma)	(Ma)
YB16-06-95	45.628	2998.26878	1.5	23.653	3.9	0.0577	5.1	0.0099	3.4	0.66	63.5	2.1	57.0	2.8	NA	NA	63.5	2.1
YB16-06-88	470.6	26153.9976	2.6	21.300	1.4	0.0666	2.3	0.0103	1.9	0.81	66.0	1.2	65.5	1.5	46.6	32.3	66.0	1.2
YB16-06-109	180.11	52616.4381	3.6	21.689	1.9	0.0686	3.1	0.0108	2.5	0.80	69.3	1.7	67.4	2.0	3.1	45.2	69.3	1.7
YB16-06-31	319.24	15046.8608	2.5	21.186	1.7	0.0707	2.6	0.0109	1.9	0.73	69.7	1.3	69.3	1.7	59.4	41.7	69.7	1.3
YB16-06-16	482.09	315256.267	2.4	20.713	0.9	0.0724	2.7	0.0109	2.5	0.94	69.8	1.8	71.0	1.8	112.9	20.9	69.8	1.8
YB16-06-5	303.1	13687.0412	1.4	21.767	1.5	0.0696	3.3	0.0110	3.0	0.89	70.4	2.1	68.3	2.2	NA	NA	70.4	2.1
YB16-06-65	415.83	102630.37	5.6	20.501	1.3	0.0739	2.6	0.0110	2.3	0.87	70.5	1.6	72.4	1.8	137.2	30.3	70.5	1.6
YB16-06-60	238.86	30067.1885	2.2	20.788	1.7	0.0735	3.2	0.0111	2.7	0.84	71.1	1.9	72.0	2.2	104.4	40.5	71.1	1.9
YB16-06-103	274.86	252064.395	2.5	20.391	1.1	0.0764	2.9	0.0113	2.7	0.91	72.4	1.9	74.7	2.1	149.8	24.8	72.4	1.9
YB16-06-66	113.1	16765.8218	1.1	21.351	1.5	0.0747	2.4	0.0116	1.9	0.78	74.1	1.4	73.1	1.7	40.9	36.3	74.1	1.4
YB16-06-42	295.36	83291.4845	1.7	21.008	1.5	0.0761	3.0	0.0116	2.6	0.87	74.3	1.9	74.4	2.2	79.4	36	74.3	1.9
YB16-06-59	293.07	21694.0565	3.8	21.432	1.3	0.0748	2.7	0.0116	2.4	0.88	74.5	1.8	73.2	1.9	31.9	30.1	74.5	1.8
YB16-06-94	1427.2	151857.417	1.0	20.529	1.1	0.0789	2.3	0.0117	2.1	0.89	75.3	1.6	77.1	1.7	134.0	24.8	75.3	1.6
YB16-06-104	88.903	5812.6331	1.3	21.376	3.2	0.0759	3.8	0.0118	1.9	0.51	75.5	1.4	74.3	2.7	38.0	77.5	75.5	1.4
YB16-06-77	67.356	3510.53295	1.3	23.285	2.4	0.0700	7.4	0.0118	6.9	0.94	75.8	5.2	68.7	4.9	NA	NA	75.8	5.2
YB16-06-3	51.99	766991.408	2.5	20.846	2.6	0.0791	4.6	0.0120	3.7	0.82	76.7	2.8	77.3	3.4	97.8	62.1	76.7	2.8
YB16-06-102	35.749	2513.70822	1.7	22.020	3.7	0.0756	4.7	0.0121	2.9	0.62	77.4	2.3	74.0	3.3	NA	NA	77.4	2.3
YB16-06-30	131.76	8665.60393	2.0	22.633	2.4	0.0737	3.6	0.0121	2.7	0.75	77.6	2.1	72.2	2.5	NA	NA	77.6	2.1
YB16-06-62	216.58	49058.8393	1.3	21.057	1.6	0.0800	2.9	0.0122	2.5	0.84	78.3	1.9	78.1	2.2	73.9	38.3	78.3	1.9
YB16-06-83	453.24	117751.908	6.0	20.504	1.1	0.0858	2.5	0.0128	2.3	0.90	81.8	1.8	83.6	2.0	136.8	26.2	81.8	1.8
YB16-06-4	90.338	4752.48262	3.0	18.796	3.2	0.0937	4.3	0.0128	2.9	0.67	81.9	2.3	91.0	3.8	337.5	72.6	81.9	2.3
YB16-06-15	246.89	103522.456	2.3	21.060	1.6	0.0895	3.7	0.0137	3.3	0.90	87.5	2.9	87.0	3.1	73.6	38.1	87.5	2.9
YB16-06-17	259.12	48948.522	2.1	20.531	1.7	0.0921	2.8	0.0137	2.2	0.79	87.8	2.0	89.5	2.4	133.7	40.4	87.8	2.0
YB16-06-82	201.33	8443.45073	3.1	21.402	1.6	0.0891	3.3	0.0138	2.9	0.88	88.5	2.5	86.6	2.7	35.2	37.2	88.5	2.5
YB16-06-69	282.53	21197.1545	2.0	20.764	1.5	0.0920	3.1	0.0139	2.7	0.88	88.8	2.4	89.4	2.7	107.2	34.4	88.8	2.4
YB16-06-20	116.89	17297.5996	3.0	22.163	2.1	0.0863	3.2	0.0139	2.4	0.76	88.9	2.1	84.1	2.6	NA	NA	88.9	2.1
YB16-06-81	207.5	16739.7946	2.7	16.523	3.2	0.1176	3.8	0.0141	2.1	0.54	90.2	1.9	112.9	4.1	622.2	69.8	90.2	1.9
YB16-06-101	1671.4	185051.044	5.1	20.806	0.9	0.0934	2.2	0.0141	2.0	0.92	90.3	1.8	90.7	1.9	102.4	20.2	90.3	1.8
YB16-06-44	138.09	8441.45381	3.2	21.402	2.7	0.0915	3.7	0.0142	2.5	0.68	91.0	2.3	88.9	3.1	35.1	64.7	91.0	2.3
YB16-06-52	136.49	27365.0493	4.0	20.962	1.4	0.0937	2.5	0.0143	1.9	0.76	91.3	1.9	91.0	2.2	84.7	34.3	91.3	1.9
YB16-06-107	1632.1	73441.0753	71.5	20.814	0.9	0.0946	2.1	0.0143	1.9	0.91	91.5	1.8	91.8	1.9	101.4	20.9	91.5	1.8
YB16-06-86	94.862	4190.61765	2.6	22.123	2.2	0.0896	3.2	0.0144	2.4	0.74	92.1	2.2	87.2	2.7	NA	NA	92.1	2.2
YB16-06-106	**179.51**	**14881.7559**	**2.4**	**20.819**	**1.8**	**0.0953**	**2.8**	**0.0144**	**2.1**	**0.76**	**92.1**	**1.9**	**92.4**	**2.4**	**100.9**	**42.6**	**92.1**	**1.9**
YB16-06-97	398.36	25052.2556	2.5	20.966	1.3	0.0947	2.9	0.0144	2.6	0.88	92.2	2.3	91.9	2.5	84.2	31.8	92.2	2.3
YB16-06-22	138.39	43710.6495	2.6	20.527	1.7	0.0973	3.6	0.0145	3.1	0.87	92.8	2.9	94.3	3.2	134.2	40.8	92.8	2.9
YB16-06-35	86.228	17357.8804	1.5	21.042	2.8	0.0951	3.7	0.0145	2.5	0.67	92.9	2.3	92.2	3.3	75.6	65.8	92.9	2.3
YB16-06-2	53.642	11715.5529	3.3	19.955	3.8	0.1008	4.5	0.0146	2.3	0.52	93.4	2.1	97.5	4.2	200.2	89.1	93.4	2.1
YB16-06-39	654.9	117739.825	4.6	20.714	1.3	0.0974	4.2	0.0146	4.0	0.95	93.7	3.7	94.4	3.8	112.8	30.4	93.7	3.7
YB16-06-43	191.52	19058.2873	2.8	21.078	1.6	0.0967	2.4	0.0148	1.9	0.74	94.7	1.7	93.7	2.2	71.6	38.7	94.7	1.7
YB16-06-67	164.69	49634.2003	2.1	20.719	1.8	0.0987	2.7	0.0148	2.1	0.76	94.9	1.9	95.5	2.5	112.3	41.7	94.9	1.9
YB16-06-53	372.36	395284.786	46.2	20.762	1.4	0.0986	2.3	0.0149	1.8	0.80	95.1	1.7	95.5	2.1	107.4	32.1	95.1	1.7

				Isotope ratios							Apparent ages (Ma)							
Analysis	U	206Pb	U/Th	206Pb*	±	207Pb*	±	206Pb*	±	error	206Pb*	±	207Pb*	±	206Pb*	±	Best age	±
	(ppm)	204Pb		207Pb*	(%)	235U*	(%)	238U	(%)	corr.	238U*	(Ma)	235U	(Ma)	207Pb*	(Ma)	(Ma)	(Ma)
YB16-06-68	1977.4	226877.48	1.5	20.674	1.0	0.0995	2.5	0.0149	2.3	0.92	95.5	2.1	96.3	2.3	117.5	23.5	95.5	2.1
YB16-06-45	157.01	17325.8095	1.8	21.713	1.8	0.0956	3.1	0.0151	2.5	0.81	96.4	2.4	92.7	2.7	NA	NA	96.4	2.4
YB16-06-37	108.83	10735.561	1.5	18.872	2.7	0.1104	3.5	0.0151	2.1	0.62	96.7	2.1	106.3	3.5	328.3	61.9	96.7	2.1
YB16-06-105	249.5	28924.7306	0.6	21.008	1.2	0.1000	2.3	0.0152	2.0	0.86	97.5	1.9	96.8	2.1	79.4	28	97.5	1.9
YB16-06-29	52.973	3012.31959	2.3	23.715	3.7	0.0901	4.4	0.0155	2.5	0.56	99.2	2.4	87.6	3.7	NA	NA	99.2	2.4
YB16-06-58	423.81	126536.637	3.0	20.679	1.5	0.1043	3.4	0.0157	3.1	0.89	100.1	3.0	100.8	3.3	116.8	36.4	100.1	3.0
YB16-06-54	426.24	57040.6405	62.6	21.032	1.1	0.1102	2.8	0.0168	2.6	0.92	107.5	2.7	106.1	2.8	76.7	25.4	107.5	2.7
YB16-06-48	315.85	16644.2819	1.5	20.553	1.4	0.1129	2.5	0.0168	2.1	0.84	107.7	2.2	108.7	2.6	131.2	32.3	107.7	2.2
YB16-06-47	713.44	67432.2199	25.3	18.656	2.1	0.1249	5.9	0.0169	5.5	0.93	108.1	5.9	119.5	6.6	354.4	48.5	108.1	5.9
YB16-06-8	15.36	6631.17886	2.7	20.385	4.6	0.1149	5.3	0.0170	2.5	0.48	108.6	2.7	110.4	5.5	150.5	108	108.6	2.7
YB16-06-85	72.237	4303.37972	2.8	22.383	2.7	0.1052	3.4	0.0171	2.1	0.60	109.2	2.2	101.6	3.3	NA	NA	109.2	2.2
YB16-06-91	72.519	4821.57218	3.8	20.486	2.0	0.1189	3.3	0.0177	2.6	0.79	113.0	3.0	114.1	3.6	138.9	47.6	113.0	3.0
YB16-06-49	200.79	42179.1351	2.3	20.564	1.2	0.1202	2.6	0.0179	2.3	0.89	114.6	2.6	115.3	2.8	130.0	27.4	114.6	2.6
YB16-06-93	79.178	4039.80461	3.1	21.440	1.9	0.1173	3.1	0.0182	2.4	0.78	116.6	2.8	112.6	3.3	31.0	46.3	116.6	2.8
YB16-06-61	42.046	7675.69695	2.2	21.053	2.0	0.1240	3.7	0.0189	3.1	0.84	121.0	3.7	118.7	4.1	74.4	47.7	121.0	3.7
YB16-06-98	123.66	36152.0269	1.9	20.358	1.5	0.1424	3.3	0.0210	2.9	0.90	134.2	3.9	135.2	4.1			134.2	3.9
YB16-06-51	51.812	56417.8032	3.9	19.434	2.1	0.1507	3.1	0.0212	2.2	0.72	135.5	3.0	142.5	4.1	261.3	49.3	135.5	3.0
YB16-06-71	127.05	24613.5906	2.5	20.811	1.0	0.1442	3.0	0.0218	2.4	0.80	138.9	3.3	136.8	3.8	101.8	42.1	138.9	3.3
YB16-06-34	457.73	107599.599	3.5	20.439	1.3	0.1490	3.0	0.0221	2.7	0.91	140.9	3.8	141.0	4.0	144.3	29.4	140.9	3.8
YB16-06-21	163.41	34829.9607	4.3	20.557	1.4	0.1519	3.0	0.0227	2.7	0.88	144.4	3.8	143.6	4.1	130.7	34	144.4	3.8
YB16-06-13	157.38	27727.6092	3.4	20.270	1.3	0.1639	3.2	0.0241	2.9	0.91	153.5	4.4	154.1	4.6	163.7	31.3	153.5	4.4
YB16-06-100	127.37	247442.713	3.4	19.706	1.1	0.1704	2.9	0.0244	2.7	0.92	155.2	4.1	159.8	4.3	229.3	26.2	155.2	4.1
YB16-06-90	54.456	6082.55619	3.2	21.130	3.2	0.1606	3.9	0.0246	2.2	0.56	156.8	3.4	151.2	5.5	65.7	77.2	156.8	3.4
YB16-06-87	65.365	9967.05805	3.3	20.653	2.1	0.1663	3.2	0.0249	2.4	0.74	158.7	3.7	156.2	4.6	119.8	50.6	158.7	3.7
YB16-06-6	170.06	32236.1375	3.9	20.378	1.3	0.1711	3.4	0.0253	3.1	0.92	161.0	5.0	160.3	5.1	151.4	31.5	161.0	5.0
YB16-06-56	60.099	9283.58056	4.2	21.085	2.1	0.1678	3.4	0.0257	2.7	0.79	163.4	4.4	157.5	5.0	70.8	49.5	163.4	4.4
YB16-06-36	122.02	67666.5046	2.8	19.395	1.6	0.1827	3.0	0.0257	2.5	0.85	163.6	4.1	170.3	4.7	266.0	37	163.6	4.1
YB16-06-92	444.57	264882.026	7.2	19.989	1.0	0.1793	2.4	0.0260	2.2	0.92	165.5	3.6	167.5	3.7	196.2	22.1	165.5	3.6
YB16-06-24	69.806	109180.647	2.1	19.310	1.8	0.1859	3.4	0.0260	2.8	0.84	165.7	4.6	173.1	5.3	276.0	41.9	165.7	4.6
YB16-06-64	256.22	37285.4627	2.2	20.384	1.0	0.1836	2.4	0.0272	2.1	0.90	172.7	3.6	171.2	3.7	150.5	23.6	172.7	3.6
YB16-06-14	258.61	24220.5048	2.1	20.048	1.2	0.1902	2.7	0.0277	2.4	0.89	175.9	4.1	176.8	4.4	189.4	28.5	175.9	4.1
YB16-06-99	126.75	658432.099	4.8	20.226	1.5	0.1917	3.0	0.0281	2.6	0.86	178.8	4.6	178.1	5.0	168.8	35.8	178.8	4.6
YB16-06-12	104.24	7706.12828	4.0	21.052	1.3	0.1869	2.5	0.0286	2.2	0.86	181.5	3.9	174.0	4.1	74.5	30.9	181.5	3.9
YB16-06-110	68.687	10194.7782	1.5	13.687	5.4	0.2948	7.8	0.0293	5.6	0.72	186.0	10.2	262.4	18.0	1015.6	110	186.0	10.2
YB16-06-7	258.13	67139.4196	2.0	19.995	1.3	0.2040	3.3	0.0296	3.1	0.92	188.0	5.7	188.5	5.8	195.6	31	188.0	5.7
YB16-06-80	79.159	15955.3684	2.0	20.618	1.6	0.2007	2.8	0.0300	2.3	0.81	190.7	4.3	185.7	4.7	123.8	38	190.7	4.3
YB16-06-50	109.81	10024.4016	2.1	20.760	1.6	0.1995	2.7	0.0301	2.3	0.82	190.9	4.3	184.7	4.6	107.6	36.9	190.9	4.3
YB16-06-11	118.8	13176.4929	1.5	20.425	1.2	0.2054	2.7	0.0304	2.4	0.89	193.3	4.6	189.7	4.7	145.9	28.9	193.3	4.6
YB16-06-41	247.65	125948.165	2.9	19.962	1.0	0.2112	2.6	0.0306	2.4	0.93	194.3	4.7	194.6	4.6	199.4	22.2	194.3	4.7
YB16-06-9	204.61	33354.3688	2.1	18.805	1.4	0.2340	3.3	0.0319	3.1	0.95	202.6	6.2	213.5	6.3	336.4	23.7	202.6	6.2
YB16-06-108	253.64	235697.545	3.2	18.856	0.8	0.4244	2.4	0.0581	2.3	0.95	363.8	8.0	359.2	7.2	330.2	17.3	363.8	8.0
YB16-06-55	198.27	88322.2243	0.9	16.140	0.8	0.8844	2.0	0.1036	1.8	0.91	635.3	11.1	643.4	9.5	672.7	17.5	635.3	11.1
YB16-06-23	440.51	887119.075	8.3	11.575	0.9	2.8074	2.6	0.2358	2.5	0.94	1364.8	30.1	1357.5	19.6	1346.9	17.8	1346.9	17.8
YB16-06-38	236.97	124994.873	3.1	11.547	1.0	2.2389	2.4	0.1876	2.2	0.91	1108.2	22.2	1193.3	16.9	1351.7	19.6	1351.7	19.6
YB16-06-73	201.49	96548.0991	4.0	11.490	0.8	2.7363	2.1	0.2281	1.9	0.93	1324.6	23.3	1338.4	15.5	1361.2	14.5	1361.2	14.5
YB16-06-19	254.33	109955.097	7.8	11.435	1.0	2.8491	2.8	0.2364	2.6	0.94	1367.9	31.8	1368.6	20.7	1370.5	18.4	1370.5	18.4
YB16-06-75	697.75	1048751.8	1.2	11.400	0.9	2.7244	2.3	0.2254	2.1	0.94	1310.1	25.2	1335.1	17.1	1376.4	17.3	1376.4	17.3
YB16-06-18	333.54	1753424.29	1.5	11.359	0.8	2.8680	2.5	0.2364	2.3	0.94	1367.9	28.5	1373.5	18.5	1383.2	16.1	1383.2	16.1
YB16-06-1	189.72	554048.579	2.2	11.333	0.9	2.8544	3.0	0.2347	2.9	0.96	1359.2	35.4	1370.0	22.7	1387.7	17	1387.7	17.0
YB16-06-32	60.864	74929.4922	2.9	11.268	1.1	2.9332	2.5	0.2398	2.2	0.89	1385.8	27.7	1390.5	19.0	1398.6	22	1398.6	22.0
YB16-06-40	185.37	1597335.43	6.5	11.198	1.0	2.9240	2.7	0.2376	2.5	0.93	1374.1	31.0	1388.2	20.4	1410.6	18.8	1410.6	18.8
YB16-06-57	269.07	216012.47	8.4	10.852	0.9	3.1755	3.0	0.2500	2.9	0.95	1438.7	37.3	1451.2	23.5	1470.4	17.6	1470.4	17.6
YB16-06-70	512.06	96113.9964	4.3	10.678	0.9	3.0000	2.9	0.2324	2.7	0.95	1347.3	33.0	1407.6	21.8	1501.0	16.8	1501.0	16.8
YB16-06-89	182.6	146917.883	3.4	10.112	0.9	3.8025	2.5	0.2790	2.4	0.96	1586.3	34.1	1593.3	20.3	1603.3	13.4	1603.3	13.4
YB16-06-46	297.02	485255.915	1.9	10.047	0.8	3.7179	3.0	0.2710	2.9	0.96	1546.0	39.9	1575.2	24.1	1615.4	15.4	1615.4	15.4
YB16-06-63	68.815	111153.867	2.0	9.926	0.7	3.9749	2.7	0.2863	2.6	0.97	1622.9	37.8	1629.1	22.1	1637.9	12.5	1637.9	12.5
YB16-06-25	148.42	100432.79	2.2	9.539	0.7	4.3875	2.6	0.3037	2.4	0.92	1709.4	38.0	1710.2	21.7	1711.4	12.6	1711.4	12.6
YB16-06-96	212.24	163700.885	4.5	9.060	0.7	4.6589	2.2	0.3063	2.1	0.94	1722.4	31.7	1759.9	18.6	1805.5	13.3	1805.5	13.3
YB16-06-79	56.204	82493.631	0.7	9.049	1.0	4.2800	3.7	0.2810	3.5	0.96	1596.4	50.0	1689.5	30.2	1807.8	18.1	1807.8	18.1
YB16-06-27	214.21	261827.966	2.2	8.279	0.7	5.3288	2.3	0.3201	2.1	0.95	1790.3	33.5	1873.5	19.2	1967.8	12.2	1967.8	12.2
YB16-06-28	95.195	166593.575	1.5	8.103	0.6	6.1740	2.2	0.3630	2.1	0.96	1996.4	36.8	2000.8	19.6	2006.0	11.2	2006.0	11.2
YB16-06-76	559.68	10654829.7	1.2	6.678	0.9	9.2233	2.4	0.4469	2.2	0.92	2381.5	43.6	2360.4	21.7	2343.0	15.6	2343.0	15.6
YB16-06-26	133.46	5361482.54	1.7	6.219	0.9	9.9874	2.5	0.4507	2.4	0.93	2398.3	47.5	2433.6	23.5	2464.0	15.8	2464.0	15.8

Notes

1. Analyses with >10% uncertainty (1-sigma) in $^{206}Pb/^{238}U$ age are not included.
2. Analyses with >10% uncertainty (1-sigma) in $^{206}Pb/^{207}Pb$ age are not included, unless $^{206}Pb/^{238}U$ age is <400 Ma.
3. Best age is determined from $^{206}Pb/^{238}U$ age for analyses with $^{206}Pb/^{238}U$ age <900 Ma and from $^{206}Pb/^{207}Pb$ age for analyses with $^{206}Pb/^{238}U$ age >900 Ma.
4. Concordance is based on $^{206}Pb/^{238}U$ age / $^{206}Pb/^{207}Pb$ age. Value is not reported for $^{206}Pb/^{238}U$ ages <400 Ma because of large uncertainty in $^{206}Pb/^{207}Pb$ age.
5. Analyses with $^{206}Pb/^{238}U$ age >400 Ma and with >20% discordance (<80% concordance) are not included.
6. Analyses with $^{206}Pb/^{238}U$ age >400 Ma and with >5% reverse discordance (<105% concordance) are not included.
7. All uncertainties are reported at the 1-sigma level, and include only measurement errors.
8. Systematic errors are as follows (at 2-sigma level): [sample 1: xxx% ($^{206}Pb/^{238}U$) & xxx% ($^{206}Pb/^{207}Pb$)] These values are reported on cells U1 and W1 of E2agecalc.
9. Analyses conducted by LA-ICPMS, as described by Gehrels and others (2008) and Gehrels and Pecha (2014).
10. U concentration and U/Th are calibrated relative to FC-1 zircon standard and are accurate to ~20%.
11. Common Pb correction is from measured ^{204}Pb with common Pb composition interpreted from Stacey and Kramers (1975).
12. Common Pb composition assigned uncertainties of 1.5 for $^{206}Pb/^{204}Pb$, 0.3 for $^{207}Pb/^{204}Pb$, and 2.0 for $^{208}Pb/^{204}Pb$.
13. U/Pb and $^{206}Pb/^{207}Pb$ fractionation is calibrated relative to fragments of large Sri Lanka zircons and individual crystals of FC-1, and R33.
14. U decay constants and composition as follows: ^{238}U = 9.8485 x 10-10, 235U = 1.55125 x 10-10, $^{238}U/^{235}U$ = 137.82.
15. U-Th disequilibrium correction is applied to $^{206}Pb/^{238}U$ ages assuming a value of 2.3 for the magma.
16. Weighted mean and concordia plots determined with Isoplot (Ludwig, 2008).

APPENDIX C:

Hafnium Data Table

Hf isotope data from Yakutat 2016

Sample	(176Yb + 176Lu) / 176Hf (%)	Volts Hf	176Hf/177Hf	± (1s)	176Lu/177Hf	176Hf/177Hf (E-Hf (0)	E-Hf (0)	E-Hf (T)	Age (Ma
RF16-23b2: Rounded igneous clast in conglomerate									
RF16-23B2-52	37.8	2.1	0.282969	0.000028	0.002185	0.282963	6.5	1.0	10.0	165.7
RF16-23B2-49	32.0	1.8	0.282981	0.000031	0.002020	0.282975	6.9	1.1	10.4	165.4
RF16-23B2-42	32.6	2.1	0.282995	0.000025	0.001931	0.282989	7.4	0.9	11.0	169.0
RF16-23B2-41	41.9	3.0	0.283010	0.000022	0.002801	0.283001	8.0	0.8	11.4	169.7
RF16-23B2-55	36.1	2.4	0.283028	0.000028	0.002141	0.283021	8.6	1.0	12.1	169.2
RF16-23B2-58	25.1	2.0	0.283043	0.000027	0.001483	0.283039	9.1	1.0	12.7	167.0
RF16-23B2-43	34.9	2.0	0.283063	0.000025	0.002144	0.283056	9.8	0.9	13.3	168.0
RF16-23B2-45	35.5	2.0	0.283068	0.000027	0.002074	0.283062	10.0	1.0	13.4	162.3
RF16-23B2-38	48.0	2.4	0.283095	0.000033	0.003394	0.283085	11.0	1.2	14.3	167.6
RF16-23B2-61	109.6	1.5	0.283166	0.000043	0.006693	0.283145	13.5	1.5	16.5	169.4
RF16-16: Diorite Knocker in Melange									
RF16-16-18	21.9	2.8	0.282957	0.000021	0.001263	0.282953	6.1	0.7	9.8	174.5
RF16-16-30	23.7	3.0	0.282960	0.000021	0.001345	0.282956	6.2	0.7	9.9	173.6
RF16-16-11	40.7	2.7	0.282963	0.000023	0.002133	0.282956	6.3	0.8	10.0	176.6
RF16-16-4	25.7	2.5	0.282966	0.000022	0.001560	0.282961	6.4	0.8	10.1	174.9
RF16-16-15	9.5	2.9	0.282967	0.000015	0.000702	0.282964	6.4	0.5	10.2	175.1
RF16-16-19	28.6	2.1	0.282982	0.000027	0.001642	0.282977	7.0	0.9	10.7	174.7
RF16-16-8	20.1	2.8	0.282984	0.000020	0.001158	0.282980	7.0	0.7	10.7	173.2
RF16-16-14	19.6	3.0	0.282993	0.000018	0.001069	0.282989	7.4	0.6	11.1	173.3
RF16-16-29	20.4	2.9	0.282998	0.000017	0.001227	0.282994	7.5	0.6	11.2	174.1
RF16-16-22	22.4	3.2	0.283010	0.000023	0.001295	0.283006	8.0	0.8	11.7	173.1
RF16-16-24	10.8	2.8	0.283010	0.000016	0.000794	0.283007	8.0	0.6	11.8	175.9
RF16-16-31	12.0	3.4	0.283015	0.000023	0.000715	0.283012	8.1	0.8	11.9	174.5
RF16-16-39	33.7	2.6	0.283020	0.000022	0.001860	0.283014	8.3	0.8	12.0	173.4
RF16-16-44	19.0	3.5	0.283058	0.000018	0.001130	0.283054	9.6	0.6	13.4	173.6
RF16-16-2	19.8	2.8	0.283081	0.000019	0.001154	0.283077	10.5	0.7	14.2	173.5

APPENDIX D:

Raman Spectroscopy Data Table

RF16-23a Yakutat Mélange sandstone - U-Pb and Raman															
	U	U/Th	Best age	±	Th	eU	Grain	V3SiO4	FWHM	V1SiO4	FWHM	StDevV3	StDev	StDevV	StDev
	(ppm)		(Ma)	(Ma)	(ppm)	ppm		(Cm-1)		(Cm-1)		V3SiO4	FWHM	V1SiO4	FWHM
Analysis															
RF16-23A PC-001	290	1.8	491.1	26.8	160.8	327.5	001a	1006.0	6.6	973.0	6.2	0.65	0.33	0.43	0.17
RF16-23A PC-005	118	1.6	1364.2	21.3	75.6	135.8	005a	1007.3	4.9	973.9	3.9	0.09	0.04	0.10	0.07
RF16-23A PC-006	784	0.7	1445.6	14.4	1062.8	1033.5	006a	1005.9	8.0	972.7	8.5	0.04	0.01	0.04	0.12
RF16-23A PC-009	629	3.4	1655.0	14.4	184.6	672.7	009a	1007.6	4.1	974.2	3.8	0.16	0.07	0.19	0.15
RF16-23A PC-010	220	2.3	1488.1	12.7	95.1	242.0	010a	1006.7	6.4	973.5	8.4	0.01	0.18	0.09	1.15
RF16-23A PC-011	332	3.4	1748.1	14.6	98.3	354.8	011a	1004.8	8.3	972.5	5.3	0.28	0.31	0.64	0.68
RF16-23A PC-017	412	2.9	1369.4	16.1	140.5	445.4	017a	1006.7	5.9	973.4	5.7	0.35	0.17	0.15	1.27
RF16-23A PC-018	162	2.8	1712.4	13.6	56.9	175.5	018a	1007.5	4.7	974.1	3.7	0.15	0.15	0.08	0.26
RF16-23A PC-020	511	1.4	1438.7	14.3	365.9	596.9	020a	1005.9	7.5	972.8	10.0	0.03	0.48	0.06	0.72
RF16-23A PC-021	568	1.8	1712.5	14.8	322.1	643.4	021a	1005.5	8.2	972.5	7.7	0.45	0.19	0.12	0.03
RF16-23A PC-024	1156	2.0	1330.8	17.2	590.1	1294.6	024a	1006.9	6.9	973.4	6.3	0.11	0.12	0.01	0.88
RF16-23A PC-027	259	1.9	1911.5	12.7	133.2	290.1	027a	1007.3	4.1	974.0	4.0	0.07	0.03	0.03	0.09
RF16-23A PC-029	352	2.2	1058.3	18.0	157.4	389.3	029a	1005.0	9.2	972.4	10.0	0.10	1.45	0.46	2.36
RF16-23A PC-030	203	3.6	1765.1	14.6	55.8	215.8	030a	1005.1	7.4	972.2	5.6	0.16	1.26	0.02	1.24
RF16-23A PC-032	275	0.8	1603.5	16.5	336.1	354.1	032a	1006.5	6.6	973.4	6.5	0.43	0.57	0.06	0.84
RF16-23A PC-033	357	1.8	2377.4	16.1	203.1	404.3	033a	1007.5	4.0	974.1	3.1	0.01	0.17	0.00	0.55
RF16-23A PC-037	300	1.9	1714.5	16.7	154.4	335.8	037a	1005.4	8.3	972.5	10.6	0.08	0.95	0.04	3.39
RF16-23A PC-039	329	3.0	1707.3	14.2	108.7	354.3	039a	1007.4	5.7	974.0	4.6	0.16	0.21	0.20	0.14
RF16-23A PC-041	968	5.5	1655.4	14.1	176.3	1009.7	041a	1007.1	5.1	973.8	5.4	0.33	0.23	0.41	0.38
RF16-23A PC-043	335	3.6	1757.9	15.9	94.1	357.6	043a	1005.4	8.5	972.6	13.5	0.28	0.17	0.11	0.11
RF16-23A PC-049	99	0.9	1933.3	20.1	110.6	125.1	049a	1005.8	7.5	972.6	7.0	0.27	0.06	0.00	0.07
RF16-23A PC-050	989	2.2	1733.5	20.7	458.6	1096.5	050a	1004.5	8.0	972.0	8.7	0.18	0.28	0.13	0.66
RF16-23A PC-053	703	4.5	1583.7	11.1	157.1	739.6	053a	1004.5	8.5	971.9	9.8	0.13	0.04	0.39	0.16
RF16-23A PC-054	322	1.9	2504.8	12.9	166.1	360.8	054a	1006.3	6.1	973.4	5.7	0.16	0.40	0.21	1.11
RF16-23A PC-059	290	3.1	2093.2	15.3	93.3	311.7	059a	1005.6	7.2	972.8	4.6	0.12	0.12	0.77	0.14
RF16-23A PC-064	440	2.1	1680.2	21.9	209.9	489.3	064a	1005.4	7.9	972.3	9.4	0.68	0.46	0.57	0.79
RF16-23A PC-065	448	2.3	1712.3	12.4	197.4	494.6	065a	1005.2	8.0	972.2	6.8	0.40	0.40	0.25	1.02
RF16-23A PC-070	98	1.2	1745.2	17.5	85.0	118.1	070a	1008.0	4.2	974.4	4.0	0.03	0.01	0.01	0.09
RF16-23A PC-076	321	1.1	1733.5	12.7	282.2	387.8	076a	1006.5	6.3	973.3	7.3	0.01	0.01	0.03	0.55
RF16-23A PC-085	3106	7.0	501.2	23.2	446.6	3211.2	085a	1004.1	8.8	971.2	11.3	0.25	0.19	0.17	0.21
RF16-23A PC-086	537	1.5	1686.3	14.1	361.5	621.8	086a	1006.1	7.7	973.1	9.3	0.38	0.26	0.25	0.46
RF16-23A PC-087	81	4.8	1743.0	14.7	16.8	84.7	087a	1006.9	5.1	973.9	5.9	0.12	0.07	0.13	0.10
RF16-23A PC-089	709	1.8	1383.3	13.9	385.0	799.2	089a	1004.5	10.7	971.5	14.3	0.27	0.65	0.40	2.17
RF16-23A PC-091	201	1.3	1780.4	14.3	158.6	238.5	091a	1007.0	5.6	973.8	7.6	0.05	0.25	0.05	0.79
RF16-23A PC-093	249	2.7	1712.8	16.7	93.3	270.7	093a	1005.7	8.1	972.5	9.5	0.35	0.28	0.32	0.58
RF16-23A PC-094	283	2.5	1468.5	13.1	114.0	309.9	094a	1005.5	8.0	972.8	9.1	0.47	0.08	0.28	0.62
RF16-23A PC-095	187	1.5	1792.3	14.1	125.9	216.3	095a	1005.4	9.3	972.5	13.0	0.02	0.59	0.01	1.12
RF16-23A PC-096	173	1.5	1682.5	17.7	118.0	200.8	096a	1007.3	5.0	974.0	4.9	0.34	0.16	0.21	0.26
RF16-23A PC-098	1125	2.9	1301.1	18.6	390.2	1216.4	098a	1005.8	8.3	972.5	7.1	0.14	0.00	0.10	0.60
RF16-23A-104	529	7.2	1387.0	11.9	73.9	546.6	104aa	1005.6	9.9	972.4	8.8	1.36	0.90	0.92	1.48
RF16-23A-107	723	17.2	1170.2	25.6	41.9	732.7	107a	1007.7	5.5	974.3	4.9	0.00	0.00	0.00	0.00
RF16-23A-108	978	10.9	1335.1	17.6	89.4	998.9	108a	1007.0	5.8	973.7	5.6	0.04	0.15	0.01	0.28
RF16-23A-112	569	3.4	1342.0	19.2	169.1	608.7	112a	1007.3	5.8	974.1	4.5	0.24	0.09	0.09	0.09
RF16-23A-114	181	1.5	1481.9	15.4	117.0	208.7	114a	1007.7	4.8	974.2	4.2	0.02	0.09	0.01	0.17
RF16-23A-118	784	1.2	1335.7	18.9	679.6	943.7	118a	1007.2	7.2	973.7	5.1	0.20	0.25	0.15	0.16
RF16-23A-120	146	1.2	1675.2	17.3	120.1	174.1	120a	1007.4	4.3	974.2	3.4	0.09	0.27	0.07	0.59

RF16-23A-121	938	7.4	1359.1	15.9	126.2	968.0	121a	1007.4	5.7	974.0	4.8	0.22	0.28	0.23	0.58
RF16-23A-127	676	5.0	1500.6	18.4	134.5	707.4	127a	1007.1	6.3	973.7	4.8	0.00	0.00	0.00	0.00
RF16-23A-136	157	3.0	1696.8	19.1	51.8	169.5	136a	1006.8	5.2	973.5	4.3	0.11	0.65	0.02	0.15
RF16-23A-138	274	1.4	1769.4	10.8	197.2	320.2	138a	1007.7	4.1	974.3	3.9	0.10	0.24	0.04	0.06
RF16-23A-139	293	2.1	1694.4	16.0	142.0	326.2	139a	1007.6	4.8	974.3	5.0	0.00	0.00	0.00	0.00
RF16-23A-143	270	3.7	1667.0	21.3	73.5	287.6	143a	1006.4	6.3	973.5	8.5	0.11	0.07	0.11	0.95
RF16-23A-144	336	4.3	1388.6	19.3	78.2	354.2	144a	1007.0	6.1	973.7	4.3	0.63	0.82	0.38	0.18
RF16-23A-153	162	2.1	1748.0	14.7	78.8	180.8	153a	1006.0	7.8	973.1	10.2	0.16	0.59	0.25	2.15
RF16-23A-163	893	15.0	1333.0	18.2	59.5	907.0	163a	1007.5	5.0	973.9	4.3	0.16	0.16	0.14	0.00
RF16-23A-176	430	4.1	1374.2	13.3	104.7	454.6	176a	1007.4	4.7	974.1	4.9	0.30	0.18	0.08	0.36
RF16-23A-179	474	5.1	1672.4	10.6	92.5	495.7	179a	1007.3	4.8	974.0	4.9	0.01	0.11	0.01	0.43
RF16-23A-180	1330	8.0	1308.9	16.4	167.0	1369.4	180a	1006.8	5.7	973.5	4.3	0.56	0.31	0.46	0.37
RF16-23A-184	760	2.4	1422.8	21.4	310.5	833.3	184a	1005.8	7.0	973.2	5.2	0.67	0.72	0.28	0.89
RF16-23A-189	382	4.5	1366.3	17.7	85.4	402.6	189a	1006.6	6.1	973.4	4.3	0.49	0.06	0.24	0.23
RF16-23A-196	725	1.5	1435.3	15.1	497.2	841.3	196a	1006.4	6.7	973.0	5.8	0.09	1.28	0.53	1.80
RF16-23A-197	337	2.8	1405.6	17.2	118.7	364.9	197a	1007.6	5.0	974.1	5.8	0.04	0.03	0.02	0.95
RF16-23A-198	257	3.5	1403.3	15.2	72.9	273.7	198a	1007.5	5.3	974.1	4.8	0.13	0.02	0.04	0.45
RF16-23A-213	436	4.3	1354.0	17.4	102.0	460.3	213a	1007.1	5.6	973.6	4.7	0.08	0.17	0.05	0.20
RF16-23A-214	609	7.0	1364.1	12.4	86.5	629.7	214a	1006.7	6.1	973.2	3.4	0.03	0.07	0.00	0.11
RF16-23A-217	389	1.2	1369.0	13.2	317.9	463.8	217a	1007.3	5.1	973.8	5.9	0.40	0.15	0.53	0.53
RF16-23A-218	340	5.3	1809.0	13.6	64.0	354.7	218a	1007.3	4.8	974.0	4.5	0.44	0.06	0.25	0.11

APPENDIX E:

Geochemistry Data Table

Major elements in wt% oxide

Sample	Time	Cal#	SiO2	TiO2	Al2O3	FeO*	MnO	MgO	CaO	Na2O	K2O	P2O5
RF16-23B1	6:22 8-11-16	2	70.5127	0.5070	13.4771	2.8267	0.1013	1.1208	3.4433	4.9442	0.5134	0.1381
RF16-23B2	8:32 8-11-16	2	72.8586	0.3149	13.1120	2.0900	0.0553	0.6832	1.5270	4.1072	3.0033	0.0713
RF16-23B7	10:42 8-11-16	2	58.9248	0.7661	17.0824	5.6447	0.1587	3.2646	4.4465	4.2295	2.3178	0.2838
RF16-16	4:07 7-11-16	2	54.4805	0.7808	16.9603	8.1319	0.1654	4.2302	5.8407	4.3979	1.2413	0.1478
RF16-26	23:01 8-11-16	2	56.5905	0.8097	17.3275	7.5555	0.1529	3.5233	5.7547	3.6886	1.4433	0.1370

Sample	LOI (wt%)	Maj+LOI	Sum All	Cl >= (wt%)	SO3 >= (wt%)	As >= (ppm)
RF16-23B1	1.2283	98.8131	98.9983	0.0000	0.0903	0.2024
RF16-23B2	2.0308	99.8537	100.1204	0.0000	0.1014	3.6432
RF16-23B7	2.1407	99.2595	99.6428	0.0205	0.1392	0.8096
RF16-16	2.6426	99.0193	99.2710	0.0107	0.0804	5.3636
RF16-26	2.4000	99.3831	99.7482	0.0112	0.0565	0.0000

Trace elements in ppm

Sample	Time	Cal#	Ni	Cr	V	Sc	Cu	Zn	Ga	Ba	Rb	Cs
RF16-23B1	6:22 8-11-16	2	4.6552	10.4236	51.7132	12.65	4.2504	57.9876	12.8524	147.8532	12.3464	2.9348
RF16-23B2	8:32 8-11-16	2	2.024	10.0188	19.6328	5.9708	1.7204	21.9604	12.8524	1020.5008	47.3616	0.8096
RF16-23B7	10:42 8-11-16	2	11.8404	25.5024	149.9784	16.7992	21.1508	70.7388	17.8112	948.5476	52.624	1.8216
RF16-16	4:07 7-11-16	2	14.5728	56.7732	209.4840	29.8540	82.8828	80.8588	16.3944	471.0860	30.8660	0.8096
RF16-26	23:01 8-11-16	2	6.8816	15.3824	179.9336	26.4132	46.2484	73.3700	17.4064	1933.1224	29.1456	1.7204

Trace elements in ppm

Sample	Time	Cal#	Sr	Y	Zr	Hf	Nb	Ta	Mo	La	Ce	Nd
RF16-23B1	6:22 8-11-16	2	345.6992	27.9312	152.9132	4.048	4.3516	0	0	13.3584	32.6876	17.0016
RF16-23B2	8:32 8-11-16	2	166.98	26.5144	183.9816	4.4528	6.7804	0.3036	0.506	17.6088	39.468	16.698
RF16-23B7	10:42 8-11-16	2	645.7572	20.746	134.4948	2.53	6.072	0	0.7084	19.3292	38.6584	19.1268
RF16-16	4:07 7-11-16	2	382.9408	21.8592	124.7796	3.4408	3.5420	0.2024	2.2264	10.8284	25.0976	12.1440
RF16-26	23:01 8-11-16	2	427.3676	27.7288	106.0576	2.2264	5.5660	0.0000	1.5180	7.5900	26.9192	13.6620

Trace elements in ppm

Sample	Time	Cal#	Sm	Dy	Yb	U	Th	Tl	Pb	Bi
RF16-23B1	6:22 8-11-16	2	4.2504	4.4528	3.1372	0.8096	2.53	1.4168	6.2744	0.8096
RF16-23B2	8:32 8-11-16	2	3.7444	4.2504	4.7564	1.7204	6.1732	0	1.6192	0

Trace elements in ppm

Sample	Time	Cal#	Sm	Dy	Yb	Th	U	Tl	Pb	Bi
RF16-23B7	10:42 8-11-16	2	3.7444	3.8456	2.3276	4.048	2.1252	0.1012	4.6552	0.3036
RF16-16	4:07 7-11-16	2	2.9348	3.3396	2.5300	0.4048	1.8216	0.7084	1.8216	1.6192
RF16-26	23:01 8-11-16	2	3.4408	4.3516	3.1372	0.0000	0.1012	2.9348	1.4168	1.1132

The following Spreadsheet is used for the calcuations of mineral norms and oxides

Input analysis	Units	RF16-23B1	RF16-23B2	RF16-23B7	RF16-16	RF16-26
SiO2	%	70.513	72.859	58.925	54.481	56.591
TiO2	%	0.507	0.315	0.777	0.781	0.810
Al2O3	%	13.477	13.112	17.082	16.960	17.327
Fe2O3	%					
FeO	%	2.827	2.090	5.645	8.132	7.555
MnO	%	0.101	0.055	0.159	0.165	0.153
MgO	%	1.121	0.683	3.265	4.230	3.523
CaO	%	3.443	1.527	4.447	5.841	5.755
Na2O	%	4.944	4.107	4.229	4.398	3.689
K2O	%	0.513	3.003	2.318	1.241	1.443
P2O5	%	0.138	0.071	0.284	0.148	0.137
CO2	%					
SO3	%	0.090	0.101	0.139	0.080	0.056
S	%					
F	%					
Cl	%	0.000	0.000	0.021	0.011	0.011
Sr	ppm	345.699	166.980	645.757	382.941	427.368
Ba	ppm	147.853	1020.501	948.548	471.086	1933.122
Ni	ppm	4.655	2.024	11.840	14.573	6.882
Cr	ppm	10.424	10.019	25.502	56.773	15.382
Zr	ppm	152.913	183.982	134.495	124.780	106.058

Norms		RF16-23B1	RF16-23B2	RF16-23B7	RF16-16	RF16-26
Quartz		30.362	32.253	8.786	1.770	7.632
Plagioclase		54.611	41.279	55.040	59.702	57.099
Orthoclase		3.095	18.174	14.096	7.531	9.325
Nepheline		0.000	0.000	0.000	0.000	0.000

Norms	RF16-23B1	RF16-23B2	RF16-23B7	RF16-16	RF16-26
Leucite	0.000	0.000	0.000	0.000	0.000
Kalsilite	0.000	0.000	0.000	0.000	0.000
Corundum	0.000	0.533	0.302	0.000	0.000
Diopside	2.460	0.000	0.000	4.149	1.199
Hypersthene	5.326	4.549	15.971	20.194	18.942
Wollastonite	0.000	0.000	0.000	0.000	0.000
Olivine	0.000	0.000	0.000	0.000	0.000
Larnite	0.000	0.000	0.000	0.000	0.000
Aegirine	0.000	0.000	0.000	0.000	0.000
K2SiO3	0.000	0.000	0.000	0.000	0.000
Na2SiO3	0.000	0.000	0.000	0.000	0.000
Rutile	0.000	0.000	0.000	0.000	0.000
Ilmenite	0.963	0.599	1.476	1.484	1.540
Magnetite	0.456	0.337	0.910	1.311	1.219
Hematite	0.000	0.000	0.000	0.000	0.000
Apatite	0.320	0.165	0.658	0.343	0.318
Zircon	0.031	0.037	0.027	0.025	0.021
Perovskite	0.000	0.000	0.000	0.000	0.000
Chromite	0.002	0.002	0.005	0.012	0.003
Titanite	0.000	0.000	0.000	0.000	0.000
Pyrite	0.000	0.000	0.000	0.000	0.000
Halite	0.000	0.000	0.039	0.020	0.021
Fluorite	0.000	0.000	0.000	0.000	0.000
Anhydrite	0.000	0.000	0.000	0.000	0.000
Na2SO4	0.160	0.180	0.247	0.143	0.100
Calcite	0.000	0.000	0.000	0.000	0.000
Na2CO3	0.000	0.000	0.000	0.000	0.000
Total	97.787	98.108	97.558	96.683	97.419
Fe3+/(Total Fe) in rock	10.000	10.000	10.000	10.000	10.000
Mg/(Mg+Total Fe) in rock	41.411	36.818	50.762	48.114	45.393
Mg/(Mg+Fe2+) in rock	43.988	39.301	53.391	50.747	48.015
Mg/(Mg+Fe2+) in silicates	49.366	44.019	57.735	54.187	51.780
Ca/(Ca+Na) in rock	27.790	17.043	36.747	42.326	46.298
Plagioclase An content	23.372	16.530	35.751	37.383	44.741
Differentiation Index	88.068	91.706	77.922	69.003	74.055

Norms

	RF16-23B1	RF16-23B2	RF16-23B7	RF16-16	RF16-26
Aluminum Saturation Index	0.922	1.040	1.012	0.900	0.975
Alkalinity Index	1.551	1.310	1.804	1.977	2.271
Calculated density, g/cc	2.662	2.630	2.731	2.782	2.777
Calculated liquid density, g/cc	2.436	2.393	2.526	2.589	2.574
Calculated viscosity, dry, Pas	0.909	1.018	0.491	0.372	0.433
Calculated viscosity, wet, Pas	0.683	0.728	0.436	0.345	0.395
Estimated liquidus temp., °C	808.247	768.743	1022.867	1097.114	1065.210
Estimated H2O content, wt. %	3.753	4.213	1.586	1.001	1.241
Anorthite as part of the norm	13.347	7.162	20.410	23.138	26.352
Albite as part of the norm	41.245	34.090	34.573	36.529	30.676

Normalized analysis

	RF16-23B1	RF16-23B2	RF16-23B7	RF16-16	RF16-26
SiO2	70.513	72.859	58.925	54.481	56.591
TiO2	0.507	0.315	0.777	0.781	0.810
Al2O3	13.477	13.112	17.082	16.960	17.327
Fe2O3	0.314	0.232	0.627	0.904	0.840
FeO	2.544	1.881	5.080	7.319	6.800
MnO	0.101	0.055	0.159	0.165	0.153
MgO	1.121	0.683	3.265	4.230	3.523
CaO	3.443	1.527	4.447	5.841	5.755
Na2O	4.944	4.107	4.229	4.398	3.689
K2O	0.513	3.003	2.318	1.241	1.443
P2O5	0.138	0.071	0.284	0.148	0.137
CO2	0.000	0.000	0.000	0.000	0.000
SO3	0.090	0.101	0.139	0.080	0.056
S	0.000	0.000	0.000	0.000	0.000
F	0.000	0.000	0.000	0.000	0.000
Cl	0.000	0.000	0.021	0.011	0.011

Normalized analysis

	RF16-23B1	RF16-23B2	RF16-23B7	RF16-16	RF16-26
Sr	0.041	0.020	0.076	0.045	0.051
Ba	0.017	0.114	0.106	0.053	0.216
Ni	0.001	0.000	0.002	0.002	0.001
Cr	0.002	0.001	0.004	0.008	0.002

	RF16-23B1	RF16-23B2	RF16-23B7	RF16-16	RF16-26
Normalized analysis					
Zr	0.021	0.025	0.018	0.017	0.014
Total	97.787	98.108	97.558	96.683	97.419
Ferric iron selection					
Normalized analysis total=100%?	n	n	n	n	n
User Fe3+/FeT	0.1	0.1	0.1	0.1	0.1

APPENDIX E:

Limestone Masses

Sample Number	Mass Total (g)	Mass Dissolved (g)
RF16-23C1	207	207
RF16-23C2	310	310
RF16-23C3	255	255
RF16-23C4	252	252
RF16-23C5	153	153
RF16-23C6	2600	1130
RF16-23C7	1450	720
RF16-23C*	3700	840
RF16-25C1	660	660
RF16-25C2	97	97
RF16-25C3	840	840
RF16-25D	189	189
RF16-12B	808	808
RF16-14A	2800	980

Notes:

1) Not all masses were dissolved due to large quantity of limestone clast. These clasts needed to be smashed with a rock hammer to fit inside the Chipmunk Crusher. Not all material was used.
2) This thesis is part of a larger collaborative project and not all samples are included within this thesis.